Chem Soc Rev

Cite this: *Chem. Soc. Rev.*, 2012, **41**, 1130–1172

www.rsc.org/csr

CRITICAL REVIEW

Fluorescent indicators based on BODIPY

Noël Boens,* Volker Leen and Wim Dehaen*

Received 17th May 2011
DOI: 10.1039/c1cs15132k

This *critical review* covers the advances made using the 4-bora-3*a*,4*a*-diaza-*s*-indacene (BODIPY) scaffold as a fluorophore in the design, synthesis and application of fluorescent indicators for pH, metal ions, anions, biomolecules, reactive oxygen species, reactive nitrogen species, redox potential, chemical reactions and various physical phenomena. The sections of the review describing the criteria for rational design of fluorescent indicators and the mathematical expressions for analyzing spectrophotometric and fluorometric titrations are applicable to all fluorescent probes (206 references).

1. Introduction

Fluorescence spectroscopy, fluorescence imaging and fluorescence indicators are nowadays indispensable tools in various fields of modern science and medicine, including clinical diagnostics, biotechnology, molecular biology and biochemistry, materials science, and analytical and environmental chemistry. The classic indicator is a molecule capable of transforming *chemical* information, such as the presence or concentration of a specific analyte, into an analytically useful signal. In this review, we shall use the words *indicator*, *detector*, *sensor*, *chemosensor* and *probe* indiscriminately, with the sole purpose of bringing more variation in the text. A typical fluorescent indicator combines an analyte recognition site (also called chelator, chelating group, coordination site, binding site, receptor or ligand) with a fluorescent reporter moiety (fluorophore) which translates the binding between the analyte and the recognition site into a fluorescence output signal. Fluorescent sensors that can detect, quantify and/or image specific molecules or ions have become essential, sensitive tools in science, medicine and technology and have contributed considerably to the understanding of chemical and biological systems. The design, development, spectroscopic/photophysical characterization and application of novel fluorescent indicators continue to be topics of a vibrant, highly multidisciplinary research area.

Especially for sensing and visualization of analytes inside living cells, fluorescence microscopy offers considerable advantages over other measurement methods, such as microelectrodes, NMR, atomic absorption spectroscopy and spectrophotometry. Besides the high sensitivity and specificity, fluorescence techniques applied to intracellular measurements have a great spatial and temporal sampling capability, they tend to be operationally simple, and they are generally minimally disruptive to cells. Fluorescence is an experimentally versatile spectroscopy: the fluorescence signals may be monitored as (excitation and emission) spectra, intensities, intensity ratios, lifetimes, and even as anisotropy. Because light can travel through and egress from biological environments, it is possible *via* microscopic imaging to simultaneously visualize concentrations in all regions of a living cell. The use of several probes which are responsive to different ions allows the simultaneous monitoring/visualization of these ions.

Among the numerous classes of highly fluorescent dyes, the set based on 4,4-difluoro-4-bora-3*a*,4*a*-diaza-*s*-indacene[1,2] (better known as BODIPY,[3] difluoro*bo*ron *dipy*rromethene, Fig. 1) shows perhaps the highest potential and has spectacularly risen in popularity. Although the first member of this set was reported as early as 1968 by Treibs and Kreuzer,[4] the possible uses of BODIPY-based dyes for biological labeling, for electroluminescent devices, as tunable laser dyes, as potential candidates for solid-state solar concentrators, as fluorescent switches, and fluorophores in sensors and labels were fully recognized only since the mid 1990s. As a result, since then the number of research papers and patents has increased spectacularly as more researchers enter the field. The many excellent features of BODIPY can explain its ever-growing success. The robustness against light and chemicals, the relatively high molar absorption coefficients $\varepsilon(\lambda)$ and fluorescence quantum yields Φ, negligible triplet-state formation, narrow emission bandwidths with high peak intensities, good solubility, resistance towards self-aggregation in solution, excitation/emission wavelengths in the visible spectral region ($\geq$ 500 nm), and fluorescence lifetimes τ in the nanosecond range all contribute to the appeal of these interesting compounds. Moreover, their spectroscopic and photophysical properties can be fine-tuned by attachment of ancillary residues at the appropriate positions of the difluoroboron dipyrromethene core. The wide versatility of synthetic pathways to the BODIPY class of

Department of Chemistry, Katholieke Universiteit Leuven, Celestijnenlaan 200f – bus 02404, 3001 Heverlee (Leuven), Belgium. E-mail: Noel.Boens@chem.kuleuven.be, Wim.Dehaen@chem.kuleuven.be; Fax: +32-16-327990; Tel: +32-16-327497, +32-16-327439

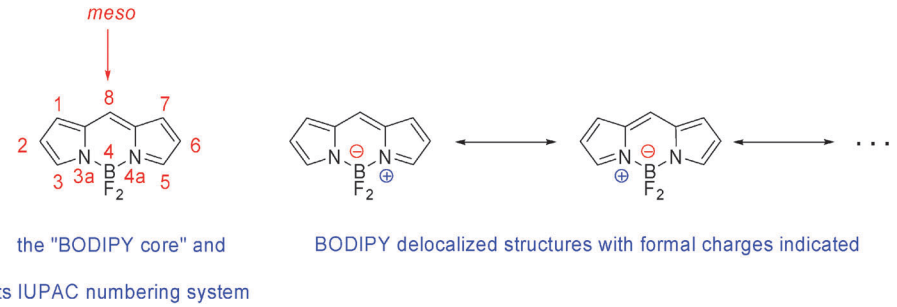

Fig. 1 (left panel) Representation of the BODIPY framework with the numbering scheme shown. The 8-position is often specified by *meso*. The 3,5-positions are sometimes referred to by α, while β is used to denote the 2,6-positions. All the positions of the BODIPY core are possible sites for functionalization. (right panel) A selection of dipolar, delocalized structures of BODIPY with the formal charges indicated.

fluorophores allows the creation of a perfect fit between the structure of the dye and its desired spectroscopic and photophysical characteristics.

Some earlier review articles cover the synthesis, spectroscopic properties and various applications of BODIPY compounds.[1,2,5] This critical review, however, is entirely dedicated to the advances made using the 4-bora-3*a*,4*a*-diaza-*s*-indacene scaffold as a fluorophore in the design, synthesis and application of fluorescent indicators in order to try to highlight the wide diversity and applicability of BODIPY derivatives. It gives an overview of the state-of-the-art of the chemistry involved in the synthesis of reported BODIPY sensors and of their relevant spectroscopic/photophysical properties, including fluorescence quantum yields Φ, wavelength of the absorption maximum λ_{abs}, wavelength of the fluorescence emission maximum λ_{em}, ground-state dissociation constants K_d of the formed complexes with the analytes, *etc*. The purpose of the present review is to provide a comprehensive account of developments in the area of probes with BODIPY as a fluorophore, covering the period since the beginning in 1997 till the end of 2010.

Theoretically, a sensor must respond to its analyte reversibly. Nevertheless, in many cases, reversibility has not been demonstrated, but can be expected based on the principles of coordination chemistry. A substantial number of indicators described here react irreversibly with the analyte and are therefore more appropriately designated as dosimeters. These irreversible sensors are also included in this review. BODIPY-derived fluorescent labels, tags and markers are not discussed, however. Readers interested in commercial BODIPY-based probes should consult the Life Technologies (formerly Invitrogen) web site.[6]

We begin this review with a short overview of the most important developments in the synthesis and functionalization of the BODIPY core. In Section 3, we describe the criteria to be considered in the rational design of functional fluorescent probes. Section 4 describes briefly the three most widely utilized photophysical mechanisms operative in fluorescent sensors. Section 5 focuses on the determination of the dissociation constant K_d of the analyte–probe complex. Spectrophotometric and fluorometric titrations, direct as well as ratiometric will be discussed. The probes reported in the literature since 1997 are described in Section 6. This section, which comprises the bulk of the review, is subdivided according to the analyte of interest (cation, anion, biomolecule, reactive oxygen and nitrogen species, other phenomena). We close this review with our view on which future developments might shape progress in the domain of BODIPY-based probes.

2. Synthesis

Starting from commercially available pyrrole-based starting materials, it is relatively easy to produce a multitude of boron dipyrromethene dyes, often in high yield and multi-gram quantity. Interestingly, their spectroscopic/photophysical properties can be 'fine-tuned' by introducing different electron releasing/withdrawing groups onto the BODIPY framework.

2.1. Synthesis of the BODIPY core

Synthetic approaches to the difluoroboron dipyrromethene core are largely based on chemistry well known from porphyrin research, leading to the parent BODIPY chromophore.[7]

The acid-catalyzed condensation of aldehydes **2** with pyrrole **1** affords dipyrromethanes **3** (Scheme 1). For unsubstituted pyrrole, this reaction is normally carried out in pyrrole as a solvent to prevent polymerization, although modifications allow the use of fewer equivalents of pyrrole.[8] On the other hand, for 2-substituted pyrroles, multiple condensations are not a competing side reaction, and an excess of pyrrole is not needed. Dipyrromethanes **3** are rather unstable compounds,

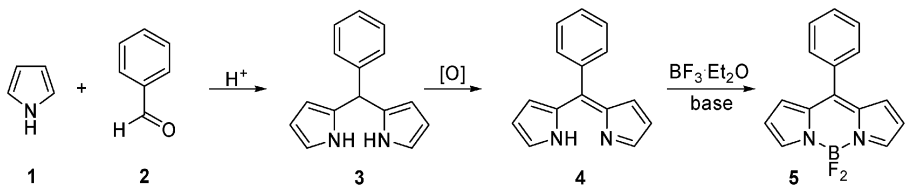

Scheme 1 Condensation of pyrrole with an aromatic aldehyde, yielding dipyrromethane **3** that is subsequently oxidized and complexed to BODIPY dye **5**.

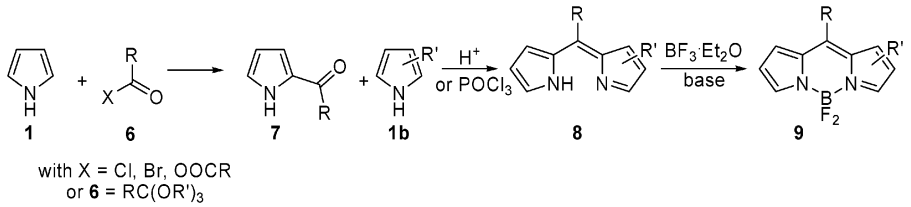

Scheme 2 Synthesis of BODIPY dyes through the acylation of pyrrole followed by condensation and complexation.

and because they are sensitive to light, air and acid, best used immediately after preparation. Oxidation of dipyrromethane **3** yields a dipyrromethene or dipyrrin **4**. This oxidation can be carried out with DDQ (2,3-dichloro-5,6-dicyano-*p*-benzoquinone) or *p*-chloranil (2,3,5,6-tetrachloro-*p*-benzoquinone), the latter providing milder reaction conditions. Moreover, there are only a few examples where the aldehyde is not an aromatic one, because oxidation tends to fail in other cases. Subjecting the dipyrrin to base and boron trifluoride etherate affords the borondifluoride complex **5** in high yield.

The chemical robustness of BODIPY dyes also allows many post-synthetic modifications on the *meso*-aryl substituent, such as oxidation, reduction and nucleophilic aromatic substitution (S_NAr), without significant decomposition of the dye.

A second route to BODIPY uses the condensation of pyrrole **1** with an acylium equivalent **6** (Scheme 2). The intermediate acylpyrrole **7** is usually not isolated, because it can react under acidic conditions with an excess of pyrrole to form a dipyrrinium salt **8**. The acylium equivalent can be an acid chloride,[9,10] an acid anhydride[11] or an orthoester.[12] A particular advantage of this approach lies in the synthesis of asymmetric dipyrrins, because the isolated acylpyrrole **7** can be combined with a second pyrrole moiety **1b** in an acidic condensation. Again, application of an excess of base and boron trifluoride etherate yields the BODIPY dye **9**.

A third route, described by Wu and Burgess, is an interesting alternative to the condensation of an acylated pyrrole.[13] Their serendipitous discovery that the second pyrrole equivalent is not always needed, and phosphorus oxychloride is capable of condensing pyrrole-2-carbaldehyde **10** with itself, deserves a closer look (Scheme 3). In the proposed mechanism, phosphorus oxychloride substitutes the aldehyde oxygen, resulting in a chlorinated azafulvene **11**, which is attacked by a second pyrrole aldehyde **12**. Subsequent nucleophilic attack by chloride, followed by decomposition of the unstable intermediate, yields dipyrrinium **15**. The dipyrromethene can undergo complexation in a standard fashion to symmetric BODIPY **16**. The products, arising from a one-pot procedure and requiring little purification, are generally obtained in exceptionally high yields. Similar mechanisms may account for scrambling that can occur in the preparation of asymmetric systems *via* the condensation of an acylpyrrole.

Likewise, the condensation of nitrosopyrroles leads to aza-dipyrrins, which in turn are complexed with boron-trifluoride etherate to the corresponding aza-BODIPY dyes. One-pot synthetic routes towards such deep blue aza-dipyrrins were established as early as 1943,[14–16] but the complexation to the aza-BODIPY **21** was not reported until 1994.[17] The one-pot sequence comprises condensation of the nitromethane adducts of chalcones **17** at elevated temperatures with a nitrogen source to form pyrroles **18**, which are partially nitrosated to **19** in the reaction mixture (Scheme 4). A cross-condensation of these two pyrrole moieties then results in the formation of aza-dipyrrin **20**. In more recent studies, optimized reaction conditions to the aza-dipyrrins were discovered, while also establishing a modular, asymmetric approach which includes isolation of the nitrosopyrrole.[18,19]

Unfortunately, these aza-BODIPY dyes can only be prepared from heavily substituted pyrroles, such as 2,4-diarylpyrroles or ring annelated pyrroles.[20,21] Several groups have put considerable effort in the synthesis of the alkyl analogues and less densely substituted structures, but without any success. Recent synthetic evidence confirms the instability of alkylated pyrroles and nitrosopyrroles under the previously established reaction conditions.[22]

Especially interesting about aza-BODIPY dyes is that the *meso*-nitrogen induces a large red shift of the absorption and fluorescence emission maxima, leading to dyes that fluoresce in

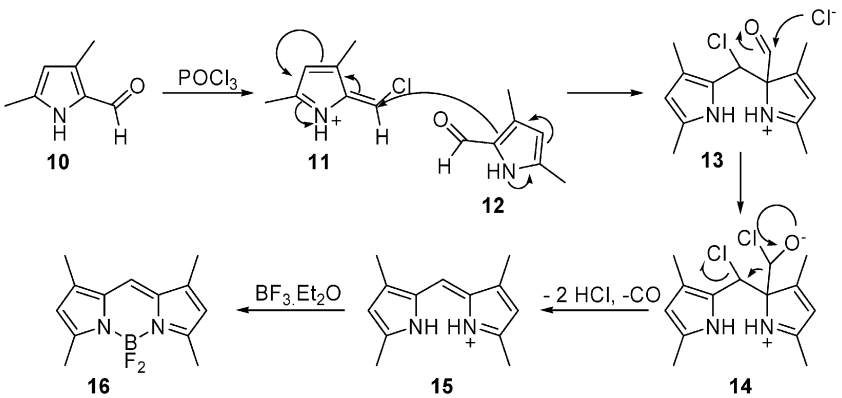

Scheme 3 One-pot condensation–decarbonylation of pyrrole-2-carbaldehydes to yield dipyrrins and BODIPY dyes.

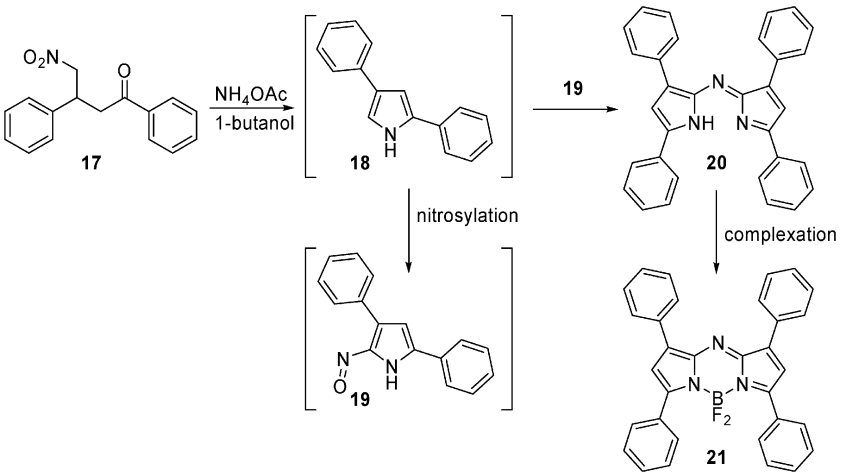

Scheme 4 Reaction of nitrosylated pyrrole to form an aza-dipyrrin **20** and aza-BODIPY **21**.

the near-infrared (NIR) spectral range with moderate to good fluorescence quantum yields Φ. However, recent work by Rurack and coworkers shows that it is not always possible to generalize this design, because a 1,7-constrained aza-BODIPY dye failed to show bathochromically shifted spectra in comparison with its standard BODIPY counterpart.[23]

2.2. Functionalization of the BODIPY scaffold

The increasing interest in difluoroboron dipyrromethene dyes has led to a closer examination of the chemistry of the BODIPY core itself, and an array of functionalization methods are now available. As most of this synthetic methodology has been described in recent reviews, and lies outside the scope of this review, only a few reactions that are highly relevant to the synthesis of fluorescent indicators will be briefly described.

Like other electron-deficient heteroaromatic systems,[24] the 3,5-methyl groups on *e.g.* BODIPY dye **22** are relatively acidic. This acidity allows the fluorophores to be condensed with aromatic aldehydes to form C=C double bonds in a Knoevenagel-type reaction (Scheme 5).[25,26] These reactions normally take place under basic conditions or in buffer, and removal of water from the mixture can be achieved by using a Dean–Stark apparatus or molecular sieves. Although the ease of these reactions has led to widespread use, yields are often low or not reported in the literature. Also, several electron-poor aldehydes have been found unreactive under these conditions.[27] The use of electron-donating substituents on the aromatic aldehyde (see *e.g.* **23**) shifts the absorbance and fluorescence spectra of the resulting BODIPY dyes to the red.[28,29] For example, *p*-dimethylaminostyryl substituted BODIPYs emit in the red (**24**)[30] to NIR (**25**)[26] spectral range.

The electron deficiency at the 3,5-positions renders halogen substituents at these positions highly reactive towards nucleophilic aromatic substitution (S_NAr) and palladium-catalyzed cross coupling. Originally introduced by Dehaen and Boens, 3,5-dichlorinated BODIPY dyes (as **26**) are prone to substitution with carbon, nitrogen, oxygen, sulfur, selenium, tellurium nucleophiles (Scheme 6).[31–34]

As for carbon and oxygen centered nucleophiles, the effects on the spectral properties of the parent dye are limited,[35,36] but nitrogen, sulfur, selenium and tellurium centered substituents induce large bathochromic shifts of the absorption and emission maxima.[34,37,38] Replacement of the *meso*-aryl with a trifluoromethyl moiety reduces the nonradiative decay through rotation, and thus leads to fluorophores with higher quantum yields.[39] Also, monohalogenated dyes have been prepared and were shown to exhibit similar reactivity, thus bypassing the necessity of a second substitution in order to avoid a remaining reactive chlorine substituent.[40]

Placing new substituents at the 3,5-positions has a large effect on the spectroscopic and photophysical properties, what

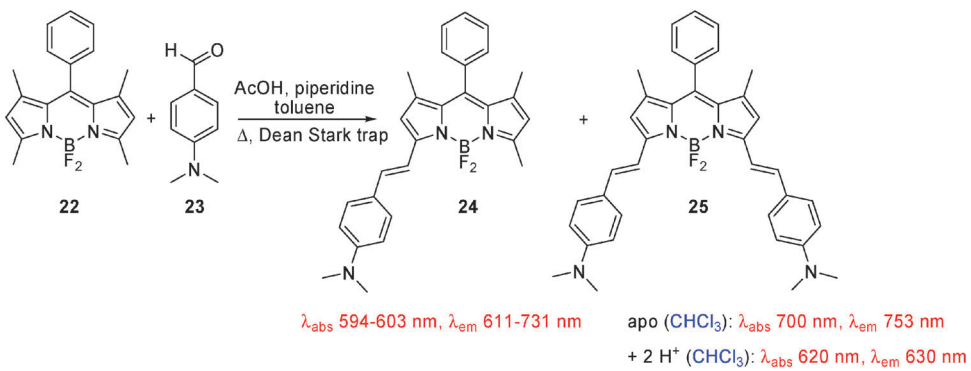

Scheme 5 Condensation of 3,5-dimethyl-BODIPY dyes with aromatic aldehydes can result in both mono- and distyrylated fluorophores.

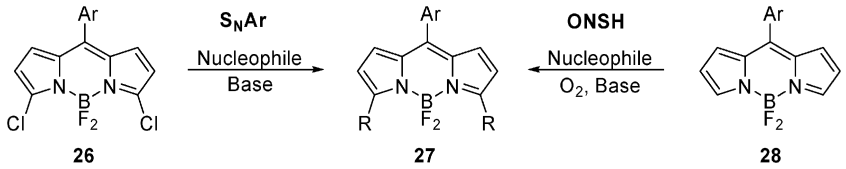

Scheme 6 Nucleophilic aromatic substitution (S_NAr) and oxidative nucleophilic substitution of hydrogen (ONSH) at the 3,5-positions of BODIPY.

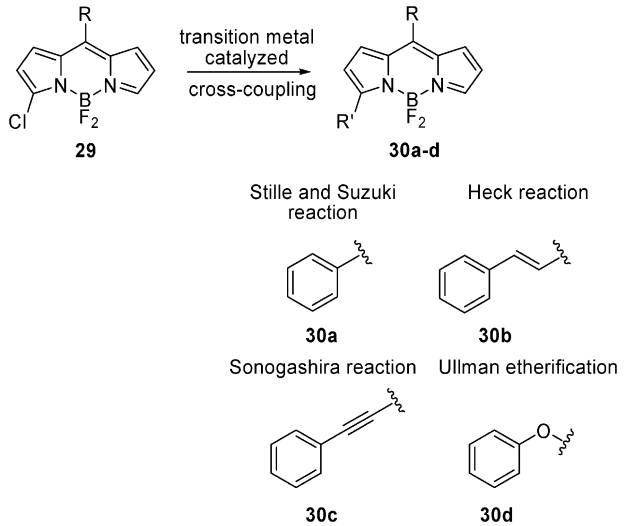

Scheme 7 Functionalization of 3-halogenated BODIPY dyes through transition metal catalysis. The R′ group is depicted for the various reaction types.

makes this strategy especially interesting for the design of novel fluorescent sensors and labels. In a recent development that is complementary to the chemistry of the 3- and 3,5-chlorinated structures, direct oxidative nucleophilic substitution of the 3- and 3,5-hydrogens allows the preparation of substituted BODIPYs **27** in a single step from 3,5-unsubstituted dyes **28** (Scheme 6).[41] For carbon centered nucleophiles, the products for double substitution can also be obtained.

The halogenated dyes **26** and **29** can also be reacted in various transition metal catalyzed cross-coupling reactions (Scheme 7).[42] As well as further fine-tuning of the maxima of absorption and fluorescence emission bands, such new substituents have a beneficial effect on the quantum yields of fluorescence. Suzuki and Stille arylations **30a**, Heck reactions **30b**, Sonogashira alkynations **30c** and, most recently, copper-catalyzed Ullman etherification **30d** can be used to introduce new functionality in mostly good yields.[43]Again, mono- and disubstituted systems are accessible.

Apart from their use in fluorescent sensors, such transition metal catalyzed reactions on 3,5-halogenated BODIPY derivatives have recently been used in the synthesis of novel fluorescent materials.[44,45]

3. Design criteria of fluorescent indicators

Fluorescent indicators for real-time sensing and fluorescence imaging are indispensable tools in life science and materials science.[46–48] Fluorescence sensing and imaging of analytes is critically dependent on the availability of the appropriate probes. The rest of this section discusses the criteria to be considered in the design of fluorescent probes, a research area of continually increasing importance.

For the rational design of useful fluorescent probes, the list of parameters that need to be optimized collectively and simultaneously is extensive. (i) First and foremost is the ability of the probe to elicit a highly selective fluorescence response to the analyte of interest without reaction with other competing analytes (*i.e.*, the preferred complex formation with the analyte of interest when other analytes are present). (ii) An obvious criterion is robustness of the indicator against chemicals and light. (iii) The fluorescence should be as bright as possible, requiring large $\varepsilon(\lambda)$ values at the excitation wavelength λ and high fluorescence quantum yields Φ, *i.e.*, a high dye brightness $\varepsilon(\lambda) \times \Phi$.[49] (iv) The ground-state dissociation constant (K_d) of the analyte–probe complex with 1 : 1 stoichiometry must be well-matched with the analyte concentration [X] one intends to monitor. Indeed, the fluorescence intensity originating from 1 : 1 analyte–probe complex formation is dependent upon the analyte concentration in the range from approximately $0.1K_d$ to $10K_d$ and is effectively invariant outside of this analyte concentration window. If the analyte concentration is too low ($[X] \ll 0.1K_d$), no fluorescence change is measured because no significant binding takes place. If the analyte concentration is too high ($[X] \gg 10K_d$), the sensor is saturated and cannot give any information about [X]. (v) If temporal resolution of changing analyte concentration is required, the reversible association–dissociation of a chelator and an analyte should be fast, so that real-time monitoring and visualization of changes in analyte concentration are possible. (vi) Fluorescence signaling by turn-on (*i.e.*, fluorescence enhancement) or shifts in excitation and/or emission wavelength is favored over turn-off response (*i.e.*, fluorescence quenching) with concomitant lower signal-to-noise ratios. For quantitative measurements, fluorescent indicators that respond to analyte binding by spectral shifts in the excitation and/or emission spectrum are superior. Ratiometric measurements at two excitation and/or emission wavelengths and the knowledge of K_d of the complex allow the determination of the unknown analyte concentration [X].[50] (vii) Indicators that absorb and emit light in the visible or NIR (650–900 nm) spectral range offer numerous advantages over UV light-excitable indicators [(a) availability of low-cost lasers as efficient excitation sources; (b) emission (observation) wavelengths compatible with affordable detectors; (c) no need for expensive quartz optical components; (d) less light scatter].

Some of the above properties are particularly important for fluorescent indicators functional inside live cells. (i) Selectivity for a specific analyte over other cellular analytes remains the

key criterion by which the usefulness of fluorescent indicators is ultimately judged. (ii) A bright fluorescent probe allows utilizing lower dye concentrations and, therefore, reduces phototoxicity to live cells. (iii) Ratiometric measurements are especially helpful for intracellular measurements because they cancel out most effects that are not related to changes in analyte concentration [X] (such as unequal dye loading, uneven cell thickness, altered excitation intensities, photobleaching, varied emission collection efficiencies and dye leakage). However, for certain applications, fluorescence turn-on indicators can be advantageous.[51] (iv) Long-wavelength (more specifically NIR: 650–900 nm) excitation and emission profiles minimize sample photodamage and cellular autofluorescence from endogenous chromophores. In the NIR range, biological samples have low fluorescence background, producing a high signal-to-noise ratio. Moreover, dramatically reduced Rayleigh and Raman scattering of NIR light allows this radiation to penetrate deeply into biological cells and tissues. For all these reasons, NIR fluorescent sensors have great potential for *in vivo* imaging applications.

Biological constraints require water solubility, membrane permeability and minimal toxicity to living samples. Ionic groups are preferable to ensure water solubility and to keep the probe within the cytosol (*i.e.*, intracellular retention). Minimally disruptive loading of indicators into cells requires cell membrane permeable dyes which are transformed inside the cell into their corresponding charged forms. This approach commonly involves import of membrane permeable dyes with attached esters into the cell where ubiquitous esterases liberate the charged and more hydrophilic form of these compounds. Since protons can sometimes compete with the analyte of interest, the pH dependence of any indicator developed for biological systems needs to be determined to assess the performance of the sensor within the pH range expected in the biological system studied. Finally, small molecular size probes are generally preferable over bulky ones because they penetrate the cells faster.

Although no fluorescent indicators are yet known that perfectly satisfy all these criteria at once, partial fulfillment is useful.

Owing to its beneficial properties, BODIPY is an excellent choice as a fluorescent building block for novel indicators. Good stability against chemicals and light, small molecular size, bright fluorescence due to high $\varepsilon(\lambda)$ and Φ, and fluorescence excitation and emission spectra in the visible region are all intrinsic to the BODIPY fluorophore. Moreover, one can attach practically any chelator at almost any position of the BODIPY core so that the spectroscopic and analyte binding properties can be custom-made.

4. Photophysical mechanisms

Many photophysical processes (quenching *via* collision, photoinduced electron transfer, exciplex formation, photoinduced proton transfer, energy transfer, ...) may be responsible for the fluorescence changes (excitation and emission spectra, quantum yield Φ, lifetime τ, anisotropy r) upon binding of the analyte by the indicator. The most widely utilized mechanisms in the design of indicators will be discussed briefly in this section. For a detailed treatment of these mechanisms, the reader is referred to textbooks in ref. 48 and 52.

4.1. Photoinduced electron transfer (PET)

Photoinduced electron transfer (PET) is often the cause of fluorescence quenching, when the PET process is followed by a nonluminescent process returning to the ground state. The Marcus theory[53] gives a quantitative description of the rate constant of electron transfer in solution if the interaction between the donor and acceptor in the encounter pair is weak. The PET process may be elucidated pictorially in terms of simple molecular orbital (MO) theory, which has become a powerful tool to discuss the fluorescence 'on–off' switching of fluorescent probes.

Fluorescent probes based on PET are often built as fluorophore–spacer–chelator constructs, in which the fluorophore and chelator are separated by a (short) aliphatic spacer, which electronically disconnects the π-electron systems of the fluorophore and the chelator. In many BODIPY-based probes, appending the chelator at the *meso*-position of the BODIPY fluorophore decouples the two subunits because of the almost perpendicular arrangement of the fluorophore and the chelator.

The reductive PET process according to eqn (1) is schematically illustrated in Fig. 2.

$$^1A^* + D \rightarrow A^{\bullet -} + D^{\bullet +} \quad (1)$$

where $^1A^*$ (A = electron acceptor) denotes the singlet-excited fluorophore and D (D = electron donor) stands for the electron-rich chelator (*e.g.*, ionophore for ion-sensitive probes). In reductive PET, the fluorophore is reduced whereas the chelator is oxidized. When the fluorophore serves as the electron acceptor, the HOMO (highest occupied molecular orbital) of the fluorophore should be lower than the HOMO of the chelator so that an electron can be transferred to the fluorophore and fill its singly occupied HOMO (see Fig. 2).

Reductive PET is used frequently in the design of BODIPY-based indicators. In these sensors, the chelator is the electron donor (*e.g.*, the amine group) and the BODIPY fluorophore acts as the electron acceptor. Photo-excitation promotes an electron from the HOMO of the BODIPY fluorophore to its LUMO (lowest unoccupied molecular orbital). Subsequently, an electron on the HOMO of the electron-rich chelator transfers to the HOMO of the BODIPY fluorophore. Since PET opens a nonluminescent deactivation channel to the excited fluorophore, fluorescence quenching will occur and the probe will be nonfluorescent or weakly fluorescent (*i.e.*, the sensor is in the fluorescence 'off' state). Generally, reductive PET occurs in the analyte-free form of the sensor when the chelator serves as an electron donor. Coordination of the analyte to the chelator lowers the HOMO of the chelator so that electron transfer to the attached fluorophore is slowed down (or even switched off) and fluorescence is turned on (illustrated in Fig. 3). The 'on' state displays fluorescence properties intrinsic to the BODIPY fluorophore.

Oxidative PET according to eqn (2) is schematically illustrated in Fig. 4.

$$^1D^* + A \rightarrow D^{\bullet +} + A^{\bullet -} \quad (2)$$

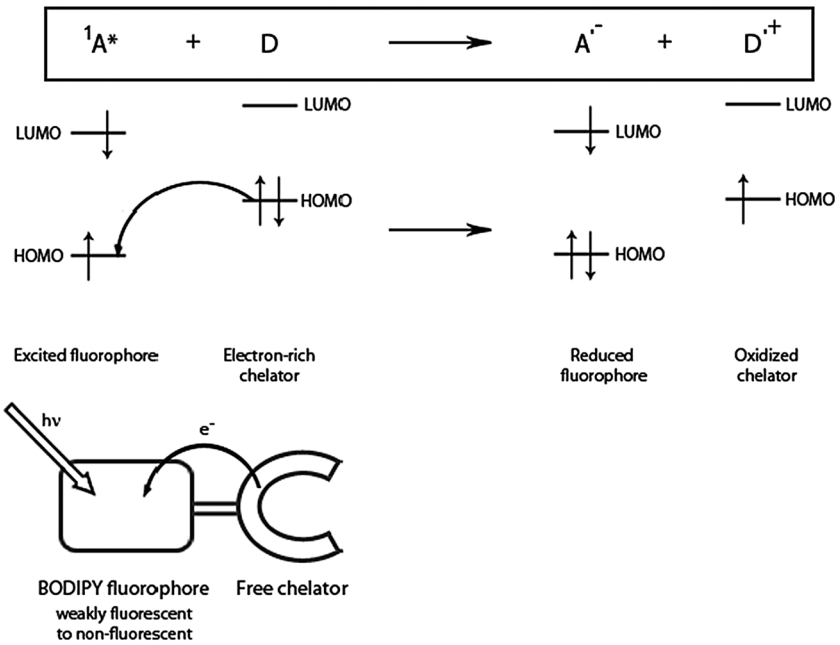

Fig. 2 Reductive PET for fluorescent indicator (A = electron acceptor, D = electron donor). The drawing at the bottom depicts an analyte-free fluorescent indicator in which the chelator is electron-rich (*e.g.*, amine electron donor). In that case the apo sensor will be in the fluorescence "off" state due to reductive PET. Complex formation will switch off PET and restore fluorescence, *i.e.*, the fluorescence 'on' state (this situation is depicted in Fig. 3).

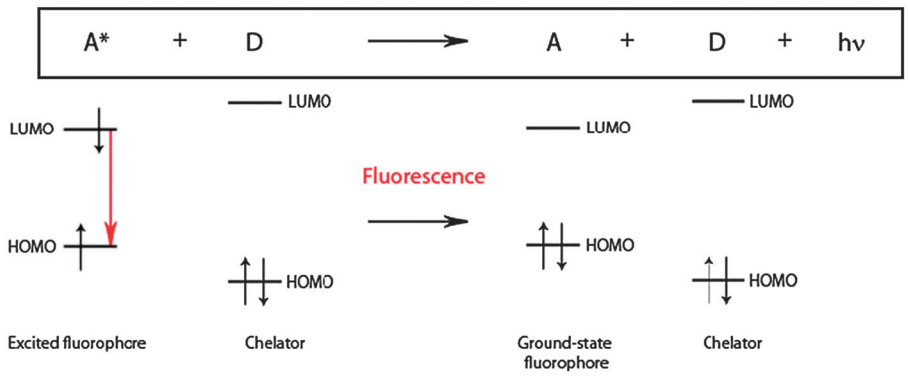

Fig. 3 Reductive and oxidative PETs are impossible and deactivation of the singlet-excited fluorophore *via* fluorescence becomes possible.

where ^{1}D* denotes the singlet-excited fluorophore and A stands for the electron-poor chelator. If the energy levels are such that the singlet excited state (LUMO) of BODIPY can donate electrons to the chelator's LUMO, then oxidative PET (*i.e.*, the fluorophore is oxidized while the chelator is reduced) occurs. When the fluorophore serves as the electron donor, the LUMO of the fluorophore should be higher than the LUMO of the chelator, which allows electron transfer from the LUMO of the fluorophore to that of the chelator.

A few fluorescent indicators shown in this review, which are based on oxidative PET, are in the fluorescence 'on' state when in the ion-free (apo) form.[54–56] This situation corresponds to that depicted in Fig. 3. Coordination of the ion with the ionophore makes the ionophore electron poor and lowers the LUMO of the ionophore, so that PET from the excited BODIPY fluorophore to the ionophore becomes possible (Fig. 4), leading to fluorescence quenching. The ion:indicator complex corresponds to the fluorescence 'off' state. The situation in which a BODIPY-based dosimeter or tag is in the 'off' (quenched) state (PET is operative) before reaction with thiol and fluorescence is turned on upon reaction also occurs (see ref. 57–60).

4.2. Photoinduced intramolecular charge transfer (ICT)

When the fluorophore possesses an electron-donating (*e.g.* amino, methoxy) group conjugated to an electron-withdrawing group, it undergoes intramolecular charge transfer from the donor to the acceptor upon photo-excitation and hence, the increase in dipole moment can be considerable. The excited state reached upon photo-excitation [Franck–Condon state or locally excited (LE) state] is not in thermodynamic equilibrium with the surrounding (polar) solvent molecules. A relaxed intramolecular charge transfer (ICT) state of minimal free energy is reached when the solvent cage is in thermodynamic equilibrium with the fluorophore. This solvent relaxation is

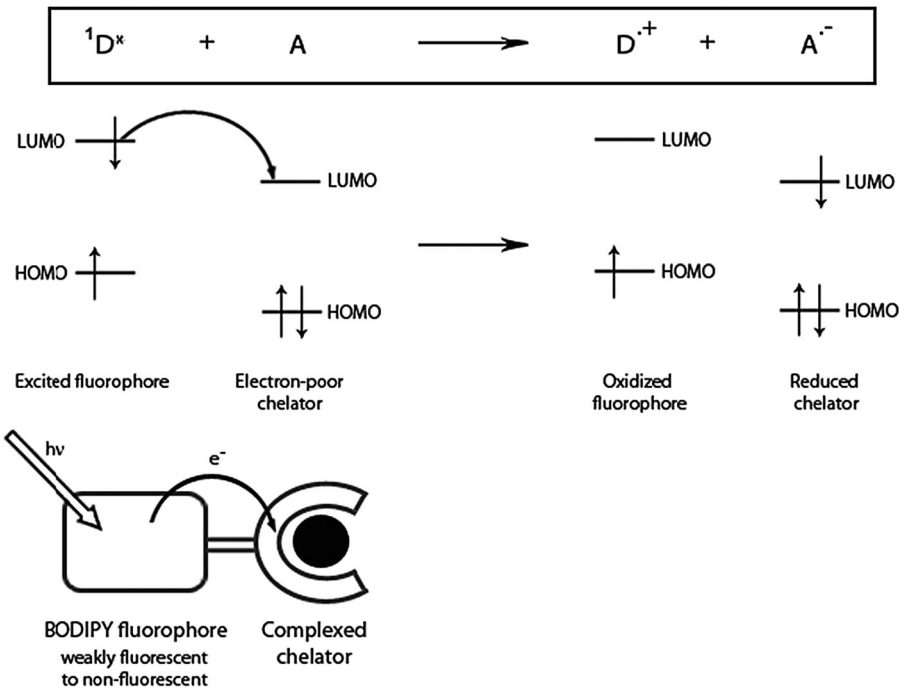

Fig. 4 Oxidative PET for fluorescent indicator (A = electron acceptor, D = electron donor). The drawing at the bottom depicts an analyte-bound fluorescent indicator in which the chelator is electron-poor. In that case the apo sensor will be in the fluorescence 'on' state (this situation is depicted in Fig. 3). Complex formation will turn on PET and quench the fluorescence, *i.e.*, the fluorescence 'off' state.

responsible for the red shift of the fluorescence spectra with increasing solvent polarity. The rate of charge recombination in the ICT state is slowed down if the donor and the acceptor are spatially separated so that conjugation is minimized. Typically, the absorption spectra of probes with an ICT state are rather narrow, while the fluorescence emission spectra are very dependent on solvent polarity. The fluorescence quantum yields Φ are low in polar solvents but not in apolar ones. It is expected that a cation, or a proton, closely interacting with the electron-rich donor will reduce the electron-donating capacity of this group and thus change the efficiency of ICT and consequently modulate Φ, τ and the absorption and fluorescence spectra. Conversely, a cation (or a proton) interacting with the electron acceptor enhances the electron-withdrawing character of this group. Therefore, changes in Φ and τ, and spectral shifts are expected.

The most prominent distinction between PET and ICT sensors lies in the different fluorescence response upon analyte recognition. PET probes display fluorescence enhancement or quenching without pronounced spectral shifts, so that the terms 'off–on' and 'on–off' fluorescent sensors are often used. The absence of shift of the spectra rules out ratiometric measurements at two wavelengths (see Sections 5.3 and 5.5). In contrast, indicators based on ICT show clear fluorescence band shifts upon analyte binding, making ratiometric measurements possible.

4.3. Resonance energy transfer (RET)

Two fluorophores may be joined in the same molecule. One of these, the *donor*, may collect radiation at the excitation wavelength and transfer this energy to the second fluorescent moiety, the *acceptor*, which emits it at a longer wavelength. This nonradiative transfer of excitation energy ($D^* + A \rightarrow D + A^*$) requires some interaction between donor and acceptor entities. It can occur if the emission spectrum of the donor overlaps the absorption spectrum of the acceptor, so that several vibronic transitions in the donor have nearly the same energy as the corresponding transitions in the acceptor. Such transitions are coupled: they are said to be in resonance and this type of nonradiative energy transfer is designated as *resonance energy transfer* (RET). Molecules in which RET is operative are typically used to artificially enhance the Stokes shift. RET can occur *via* different interaction mechanisms. If the mechanism of energy transfer is large-distance through space, the interactions between the donor and the acceptor consist of Coulombic dipole–dipole interactions. Förster derived the rate constant of such long-range, through-space dipole–dipole singlet–singlet energy transfer ($^1D^* + {}^1A \rightarrow {}^1D + {}^1A^*$) and could show that it depends on several factors:[61] (i) spectral overlap of the donor emission spectrum with the acceptor absorption spectrum; (ii) distance r_{DA} between the donor and acceptor; (iii) orientational factor κ^2; (iv) fluorescence quantum yield of the donor in the absence of RET; (v) refractive index of the medium. One important parameter is the critical distance or Förster radius R_0 which is defined as the distance at which the rate of RET and the decay of the singlet-excited donor (in the absence of RET) are equal. R_0 is generally in the range between 1.5 and 6.0 nm. Förster-type RET causes the fluorescence quantum yield of the donor to decrease while the acceptor fluorescence is enhanced. Time-resolved fluorescence of the donor and acceptor provides direct information on the transfer rate constant. A structure with donor–acceptor (through-space) energy transfer might be called an (through-space) energy transfer cassette or dyad.

5. Determination of K_d

5.1. The model

The most common model utilized for the determination of the ground-state dissociation constant K_d of the formed complex PX_n between probe P and analyte X is given by eqn (3).

$$P + nX \overset{K_d}{\rightleftharpoons} PX_n \quad (3)$$

K_d is given by eqn (4):

$$K_d = [P][X]^n/[PX_n] \quad (4)$$

where [ ] represent equilibrium molar concentrations. Strictly speaking, K_d should be defined in terms of activities, but, in practice, concentrations are almost always used. K_d defined in eqn (4) should be considered as an "apparent" constant, because it depends not only on temperature but also on ionic strength and the medium. Some of the references cited in this review quote values for the stability constant K_s (also referred to as equilibrium constant, association constant, formation constant or binding constant) of the complex PX_n instead of the dissociation constant K_d. There is a simple, reciprocal relationship between K_s and K_d: $K_d = 1/K_s$ and, hence, log K_d = −log K_s. For consistency, in this review, we have converted all the reported K_s values to K_d values. At least for 1 : 1 (analyte : probe) complexes, the K_d value estimated from the analysis of the fluorometric and/or spectrophotometric titrations should be somewhere in the range of the experimentally employed analyte concentrations [X]. A K_d value outside this [X] range should set off an alarm. The K_d value determines the range of analyte concentrations that can be probed by the sensor. The three simplest complex stoichiometries are 1 : 1 (PX), 2 : 1 (PX_2) and 1 : 2 (P_2X). Although equilibrium (association, binding, dissociation, ...) constants must be considered theoretically as dimensionless numbers, we will follow the common practice of expressing K_d for P : X complexes in mole per dm^3 (M); for 2 : 1 (analyte : indicator) complexes PX_2, K_d will be given in M^2; for 1 : 2 (analyte : indicator) complexes P_2X, K_d will be in $M^{0.5}$.

For the determination of the *ground-state* dissociation constant K_d of the complex PX_n *via* fluorometric titrations, the model becomes more elaborate because excited-state processes have to be taken into account (Scheme 8).

In this model, it is assumed that only the apo (free) probe P and the bound probe PX_n absorb light at the excitation wavelength (hence not the analyte X nor the intermediate complexes).

In Scheme 8, $h\nu$ denotes photo-excitation. The stars in P* and PX_n^* indicate that the respective free and bound probes are in the singlet-excited state. k_{ass}^* represents the rate constant of binding (association) of nX by the excited-state probe P*, while k_{diss}^* stands for the rate constant of dissociation of the excited-state complex PX_n^*. The kinetics of deactivation of P* and PX_n^* are expressed by the rate constants k_P and k_{PX_n}, respectively, which contain contributions of fluorescence and radiationless deactivation. n represents the number of analyte species bound per probe molecule (*i.e.*, stoichiometry of binding).

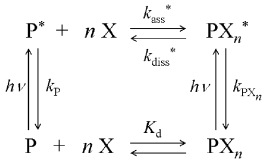

Scheme 8 Photophysical model used for the determination of K_d of the complex PX_n *via* fluorometric titration.

5.2. Determination of K_d *via direct* fluorometric titration

The correct expression of the steady-state fluorescence signal F as a function of analyte concentration [X] has been derived by Kowalczyk *et al.* for the simplest case of a 1 : 1 complex between fluorescent probe P and analyte X.[62] The plot of F as a function of [X] (*direct plot*) or F against −log [X] (*semilogarithmic plot*) is quite complicated, unless some simplifications are introduced. The simplified expression of F as a function of [X] has been extended for the case of a n : 1 complex between an analyte and an indicator [eqn (5)].[63] The ground-state dissociation constant K_d of the complex PX_n can be determined by *direct* fluorometric titration as a function of [X] using the fluorescence excitation or emission spectra. Nonlinear fitting of eqn (5) to the steady-state fluorescence data F recorded as a function of [X] yields values of K_d, F_{min}, F_{max}, and n.

$$F = \frac{F_{min}K_d + F_{max}[X]^n}{K_d + [X]^n} \quad (5)$$

In eqn (5), F stands for the fluorescence signal at [X], while F_{min} and F_{max} denote the fluorescence signals at minimal [X] (*i.e.*, in the absence of analyte X; apo form of the indicator; mathematically, $F_{min} = \lim_{[X]\to 0} F$) and maximal [X] (*i.e.*, in the presence of an excess of X; bound or saturated form of the indicator; mathematically, $F_{max} = \lim_{[X]\to\infty} F$), respectively. In eqn (5), F is the dependent variable, [X] is the independent variable, and F_{min}, F_{max}, n and K_d are adjustable parameters in the nonlinear fitting. Evidently, it is always possible to keep one or more parameters constant during the fitting. Note that [X] is the concentration of the free analyte, which may be different from the analytical (total) analyte concentration. For determining the stoichiometry of binding n, there is an additional way *via* the method of continuous variations, often called Job's plot.[64] One drawback of this method is that the sharpness of the maximum in the Job's plot depends on the magnitude of K_d: the smaller the K_d, the more accurate the maximum can be located and, hence, the more accurate the value of n will be.

The simplified eqn (5) assumes that (i) P and PX_n are excited with constant incident spectral radiant power; (ii) the absorbance of the sample is small (<0.1) and (iii) rate of binding of X to the probe in the excited state can be neglected (*i.e.*, $k_{ass}^*[X] \approx 0$). The latter condition can be checked by the invariance of the fluorescence decay times within the range of used [X].[65]

A graphical display of eqn (5) together with the experimental F-data against [X] or F against −log [X] is a powerful tool for detecting deviations and for judging the quality-of-fit. Ideally, one should use simultaneous (also referred to as global) nonlinear analysis of the fluorescence F-data surface collected

at multiple excitation and emission wavelengths (preferably the whole spectrum) as a function of [X] to estimate the global parameters n and K_d, and the local F_{min} and F_{max} parameters for each {excitation wavelength–emission wavelength} pair. Such global analysis provides parameter estimates with improved accuracy and precision compared to single curve analysis, in which F-data at a single pair of {excitation wavelength–emission wavelength} are analyzed in function of [X]. Moreover, global analysis is superior in discriminating among competing models. Unfortunately, global analysis of fluorometric titrations is not yet common.

Eqn (5) is often linearized. The objection to those linearizations is the transformation effect on the variables. Hence, proper weighting must be used in the linear least-squares regression to provide reliable parameter estimates. The difficulty of obtaining the correct weights for incorporation in the transformed linear equations complicates the regression analysis considerably and is a good reason for using the simpler nonlinear regression. The reader should consult ref. 66 for details. This reference gives a wealth of information on binding constants, statistical treatment of data, complex formation studied *via* UV–vis spectrophotometry, *etc*., but has an extremely limited discussion on fluorometric methods.

When eqn (5) is rewritten in the form of a *log–log plot*, it is known as the Hill plot [eqn (6)].[66]

$$\log\frac{F - F_{min}}{F_{max} - F} = -\log K_d + n\log[X] \qquad (6)$$

The plot of the left side of eqn (6) against log [X] is linear with slope = n and intersects the abscissa at the value corresponding to log K_d. Linear least-squares regression according to eqn (6) requires values of F_{min} and F_{max}.

There are also nonlogarithmic, linear plotting forms of eqn (5). Eqn (5) can be transformed into the linear Benesi–Hildebrand equation [eqn (7)].[66,67]

$$\frac{1}{F - F_{min}} = \frac{1}{F_{max} - F_{min}}\left[1 + \frac{K_d}{[X]^n}\right] \qquad (7)$$

The plot of the left side of eqn (7) against $1/[X]^n$ shows a linear relationship and K_d is given by the ratio of slope/intercept. This plot—sometimes referred to as the *double-reciprocal plot*—preserves the separation of independent (*i.e*., [X]) and dependent (*i.e*., F) variables. Linear least-squares regression analysis according to eqn (7) needs values of F_{min} and n.

Another linearization of eqn (5) is sometimes called the Scott equation [eqn (8)]:[66]

$$\frac{[X]^n}{F - F_{min}} = \frac{1}{F_{max} - F_{min}}(K_d + [X]^n) \qquad (8)$$

The plot of the left side of eqn (8) against $[X]^n$ shows a linear relationship and K_d is given by the ratio of intercept/slope. Linear least-squares regression according to eqn (8) necessitates values of F_{min} and n.

5.3. Determination of K_d *via ratiometric* fluorometric titration

If spectral shifts are observed in the excitation and/or emission spectra upon binding of the analyte X by the sensor, then *ratiometric* fluorometric titrations as a function of [X]—using ratios of the fluorescence excitation or emission spectral data—can be used to determine K_d and n of the analyte–probe complex. Ratiometric fluorometric measurements were introduced by R. Y. Tsien and coworkers.[50] Nonlinear fitting of eqn (9)[68] to the steady-state fluorescence ratios R recorded as a function of [X] yields values of $K_d\xi$, R_{min}, R_{max}, and n.

$$R = \frac{R_{min}K_d\xi + R_{max}[X]^n}{K_d\xi + [X]^n} \qquad (9)$$

In the *excitation* ratiometric method, one measures $R = F(\lambda_{em}, \lambda_{ex}^1)/F(\lambda_{em}, \lambda_{ex}^2)$ at a common emission wavelength, λ_{em}, and two different excitation wavelengths, λ_{ex}^1 and λ_{ex}^2. R_{min} is the ratio of the fluorescence intensities at two distinct excitation wavelengths and one emission wavelength of the apo (or free) form of the indicator (minimum [X]; mathematically $R_{min} = \lim_{[X]\to 0} R$), R_{max} represents the ratio of the fluorescence intensities of the bound form of the indicator (saturating [X]; mathematically $R_{max} = \lim_{[X]\to\infty} R$), R denotes the ratio of the fluorescence intensities corresponding to intermediate [X] and $\xi = F_{min}(\lambda_{em}, \lambda_{ex}^2)/F_{max}(\lambda_{em}, \lambda_{ex}^1)$. Choosing the wavelength of the pseudo-isoemissive point as λ_{ex}^2 simplifies the analysis. Then $\xi = 1$ and the expression for R [eqn (9)] reduces to that of F [eqn (5)].

Fitting eqn (9) to excitation ratiometric values R as a function of [X] yields values for $K_d\xi(\lambda_{em}, \lambda_{ex}^2)$, R_{min}, R_{max}, and n. Because $\xi(\lambda_{em}, \lambda_{ex}^2)$—the ratio of the fluorescence signal of the apo form of the indicator over that of the bound form at the given wavelengths—is experimentally accessible, a value for K_d can be recovered from ratiometric excitation fluorescence data.

In the *emission* ratiometric method, one determines $R = F(\lambda_{em}^1, \lambda_{ex})/F(\lambda_{em}^2, \lambda_{ex})$ at the given wavelengths as a function of [X]. In this case, ξ is defined as $\xi = F_{min}(\lambda_{em}^2, \lambda_{ex})/F_{max}(\lambda_{em}^2, \lambda_{ex})$. $\xi = 1$ when λ_{ex}^2 is chosen as the wavelength corresponding to the pseudo-isoemissive point and, in that case, the expression for R [eqn (9)] simplifies to that of F [eqn (5)].

Fitting eqn (9) to the emission ratiometric fluorescence data R as a function of [X] yields values for $K_d\xi(\lambda_{em}^2, \lambda_{ex})$, R_{min}, R_{max}, and n. Because $\xi(\lambda_{em}^2, \lambda_{ex})$ can be determined from the fluorescence signals of the apo and bound forms of the indicator at the given wavelengths, a value for K_d can be obtained.

As for F [eqn (5)], linear transformations of eqn (9) are also possible. However, the recommended parameter estimation method is *via* global nonlinear fitting.

5.4. Determination of K_d *via direct* spectrophotometric titration

The ground-state dissociation constant K_d of the complex PX_n can also be determined by *direct* spectrophotometric titration as a function of [X], using the UV-vis absorption spectra [eqn (10)]. Nonlinear fitting of eqn (10) to the absorbance data A recorded as a function of [X] yields values of K_d, A_{min}, A_{max}, and n.

$$A = \frac{A_{min}K_d + A_{max}[X]^n}{K_d + [X]^n} \qquad (10)$$

In eqn (10), A denotes the absorbance at [X], whereas A_{min} and A_{max} stand for the absorbances at minimal and

maximal [X], respectively. Hence A_{min} and A_{max} correspond to the absorbances of a free (minimal [X]) and a bound (saturating [X]) indicator, respectively.

Analogous linear plotting forms can be derived for eqn (10) as for F [eqn (5)]. However, global nonlinear least-squares fitting of the whole UV-vis absorption spectrum as a function of [X] is the preferred method for the accurate estimation of the global parameters K_d and n.

5.5. Determination of K_d *via ratiometric* spectrophotometric titration

If (large) spectral shifts are observed in the absorption spectra upon binding of the analyte X, the *ratiometric* method can be used to estimate K_d.[69] In eqn (9), $R = A(\lambda^1_{abs})/A(\lambda^2_{abs})$ is the ratio of the absorbances A at the two given wavelengths. Nonlinear fitting of eqn (9) to the ratiometric absorbance data R recorded as a function of [X] yields values of $K_d\xi$, the ratios R_{min} and R_{max}, and n. R_{min} is the ratio of the absorbances at the indicated wavelengths for the apo (or free) form of the indicator (minimum [X]), R_{max} represents the analogous ratio for the bound form of the indicator (maximum [X]), R denotes the ratio corresponding to intermediate [X] and $\xi = A_{min}(\lambda^2_{abs})/A_{max}(\lambda^2_{abs})$. Since ξ—the ratio of the absorbances at λ^2_{abs}—is experimentally accessible, a value for K_d can be extracted from ratiometric absorption data. Note that $\xi = 1$ if the wavelength corresponding to the isosbestic point is taken as λ^2_{abs}. In that case, the expression of R [eqn (9)] reduces formally to that of A [eqn (10)].

As for the previous cases, linear transformations are possible. However, the recommended parameter estimation method is *via* global nonlinear fitting.

6. Indicators

6.1. Indicators for cations

6.1.1. pH. Intracellular pH (pH_i) plays numerous crucial roles in living cells and hence a lot of effort has gone into the design and construction of probes for sensing and imaging pH inside live cells.[70] The most valuable probes are perhaps those responsive to near-neutral, cytosolic pH (6.8–7.4), although sensors which are sensitive to more acidic (*e.g.* probes **33**) or more basic environments are also useful.

Up to now, despite the valuable properties of BODIPY, no functional, BODIPY-derived probe for cytosolic pH has been built. However, a series of fluorescent BODIPY-based chemical sensors for protons in organic, aqueous, and mixed aqueous–organic media has been reported. Actually, the high potential for BODIPY dyes as building blocks in fluorescent indicators was first demonstrated in pH indicators, and has been followed by numerous examples of molecular sensors that incorporate BODIPY.

Dissociation constants for pH indicators will be expressed as $pK_a = -\log K_d$. For quantitative pH measurements, it is crucial to match the indicator's pK_a to the pH of the system of interest. pH sensors with 1 : 1 binding stoichiometry have a usable pH response in the range from approximately $pK_a - 1$ to $pK_a + 1$.

Many pH indicators contain a *p*-(*N*,*N*-dialkyl)aniline subunit as a pH sensitive group. The neutral form of **31** is nonfluorescent, attributed to reductive PET from the *meso* *p*-*N*,*N*-dimethylaminophenyl group to BODIPY.[71,72] Protonation prevents PET so that the protonated form displays strong emission. The twisting of the *meso*-aryl substituent out of the plane of the boradiazaindacene chromophore leads to nonconjugated π-systems and contributes to the efficiency of the 'off–on' switching.

Compound **32** with 3,5-distyryl substituents has red-shifted absorption and fluorescence emission maxima in comparison to **31**.[25] In apolar solvents the strong fluorescence emission of **32** occurs from the BODIPY locally excited (LE) state. As the solvent polarity increases, photo-excitation of **32** leads to population of a nonemissive ICT state, causing a drastic quenching of the characteristic BODIPY LE fluorescence (Φ decreases from 0.92 in hexane to 4×10^{-4} in MeCN). In polar solvents stabilization of the ICT state opens up a deactivation path for the LE state that occurs totally non-radiatively. Protonation of **32** completely suppresses the quenching ICT process and leads to strong fluorescence enhancement.

A series of fluorescent pH probes **33a–d** were recently reported for imaging acidic endosomes in cancer cells.[51] Compounds **33** are almost nonfluorescent in the nonprotonated form ($\Phi < 0.002$) attributed to reductive PET quenching by the *meso*-anilino substituent and they become highly fluorescent (Φ 0.55–0.60) when the aniline nitrogen is protonated. A new, highly selective strategy for *in vivo* tumor visualization was developed in which the pH-triggerable (*i.e.*, fluorescence switch-on) fluorescent probes **33** were conjugated to a cancer-targeting monoclonal antibody (trastuzumab). Confocal spectroscopy revealed that the probe–antibody conjugates are not fluorescent outside tumor cells at neutral pH. After internalization by endocytosis, the probe–antibody conjugates accumulate in late (after 4 h) endosomes or lysosomes (pH 5–6) where the acidic pH makes them highly fluorescent (Fig. 5).

Compound **24** is the first example of an unsymmetrically substituted BODIPY sensor with the pH sensitive *p*-*N*,*N*-dimethylaminostyryl group conjugated *via* the 3-position.[30] In contrast to compounds **31–33**, there is direct electronic conjugation in **24** between the *N*,*N*-dimethylaniline and BODIPY subunits by the introduction of an ethenyl linker at the 3-position. In polar solvents, photo-excitation of **24** leads to population of a highly polar ICT state, which is deactivated by an increase of the rate of internal conversion as the energy gap between the excited and the ground state decreases (Φ decreases from 0.97 in hexane to 0.13 in MeCN). Protonation of the dimethylanilino group of **24** switches off any ICT interaction and this leads to the typical BODIPY-like narrow, structured and solvent-polarity independent absorption and emission bands. It is not surprising that related compound **34** with a *p*-iodophenyl substituent at the *meso*-position shows similar spectroscopic and photophysical behavior.[73]

Also pH sensor **35** is very similar to **24** but now there is a *p*-anisyl group at the *meso*-position.[29] Its fluorescence properties (λ_{em}, Φ and lifetimes τ) were found to be strongly solvent dependent, indicative of the ICT nature of the emitting state. In MeCN solution, protonation of the tertiary amine function of **35** switches off ICT and this gives a large fluorescence enhancement in conjunction with hypsochromic shifts of the

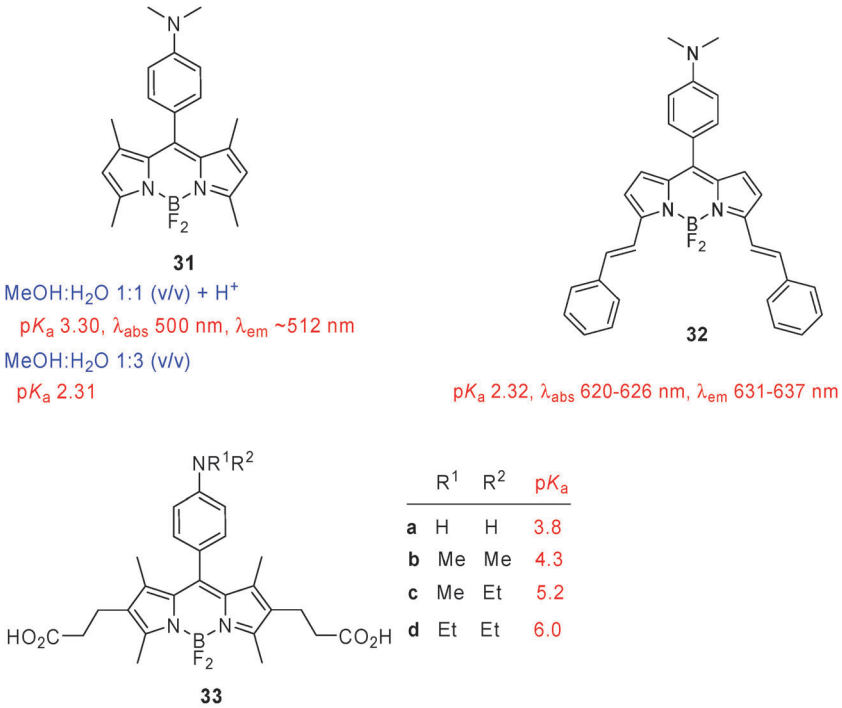

Fig. 5 pH-responsive BODIPY dyes with a 8-amino phenyl substituent.

absorption and emission maxima, in analogy to what was found for **34**.

Compounds **25**[26] and **36**[73] are 3,5-distyryl-boradiazaindacene dyes which differ only in the *p*-substituent (H in **25** *versus* I in **36**) on the *meso*-phenyl group. Upon protonation in chloroform solution, the absorption and emission spectra of **25** display a blue shift while those of comparable dye **37**[26] show a red shift. The difference was attributed to the ICT electron donor (in **25**) and acceptor (in **37**) properties of the 3,5-substituents on the BODIPY core. Upon protonation, compound **36** shows hypsochromically shifted absorption and emission bands as found for dye **25**. Simultaneously, Φ of **36** increases from 0.18 to 0.68. Analysis of the spectrophotometric and fluorometric titrations in terms of two successive protonation steps gave pK_a values of 3.0 and 5.1–5.2. Probe **36** was covalently anchored to inert, porous polyacrylate beads to form a solid-state colorimetric and fluorescent sensor for analysis of HCl in a gas stream and aqueous solution (Fig. 6).

Although phenol itself has a pK_a value of 10.0,[74–76] electron-withdrawing substituents can lower the pK_a so that the near-neutral pH range can be sensed. BODIPY analogues **38a–b** use *meso*-phenol–phenolate couples as pH-sensitive subunits and show fluorescence 'off–on' switching upon deprotonation–protonation.[77] Derivatives **38a–b** are twisted and conjugatively uncoupled, which is corroborated by the pK_a value of 10.4 in a MeOH : H_2O mixture (1 : 1), close to pK_a of phenol itself. The absence of emission of the phenolate forms can be attributed to reductive PET from phenolate to the BODIPY core.

BODIPY appended calix[4]arene **39** with four phenolic groups has a pK_a value of 6.5 and, hence, can signal near-neutral pH changes.[78] This indicator is based on PET mediated fluorescence: reductive PET renders it virtually nonfluorescent at high pH while protonation blocks PET and restores the typical BODIPY fluorescence.

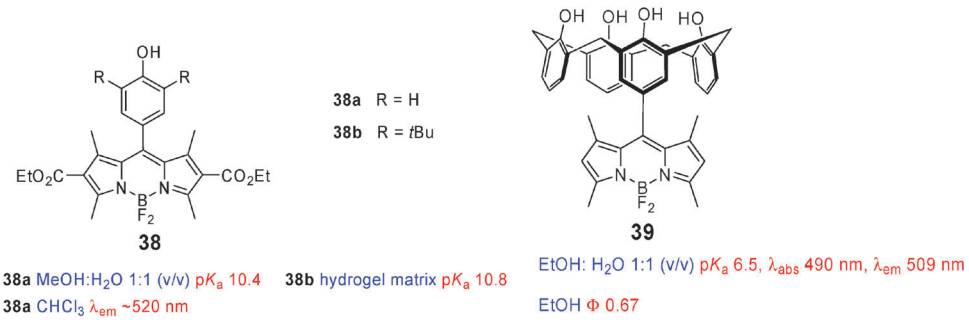

BODIPY dyes with phenolic (**40–41**) or naphtholic (**42**) subunits on the 8-position and with substituents having different electron driving forces on positions 3 and 5 have pK_a values between 7.5 and 9.3.[31,79] Compounds **40–42** have very similar BODIPY-based spectra, with λ_{abs} and λ_{em} which are hardly dependent on the solvent. In aqueous solution, the

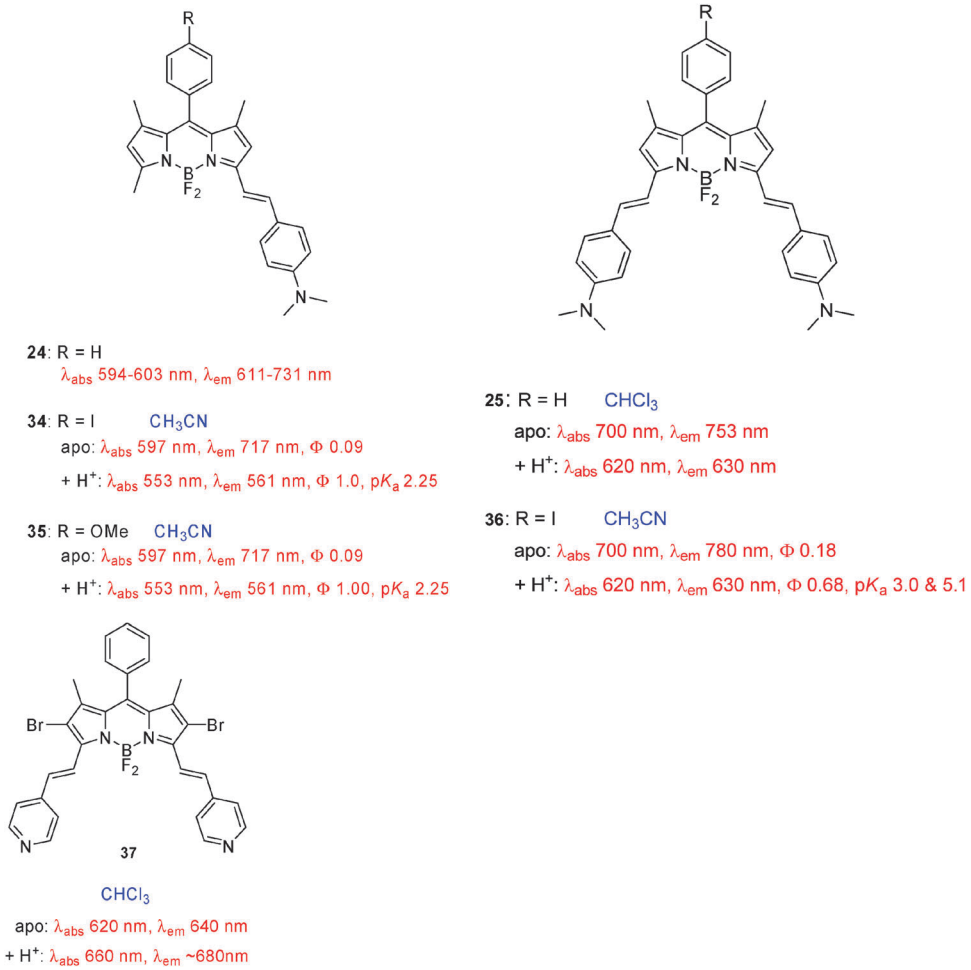

Fig. 6 Indicators with protonatable groups at the 3- and 3,5-positions.

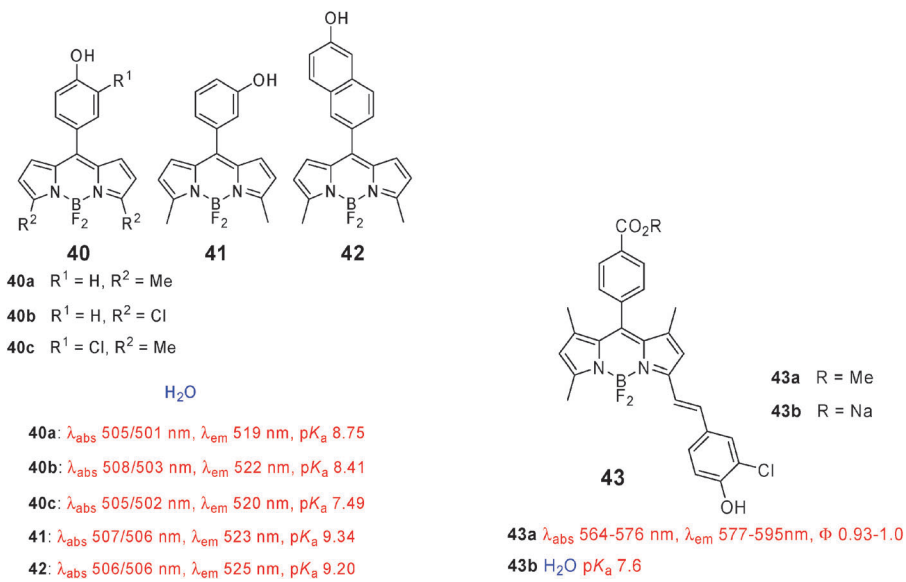

Fig. 7 pH indicators based on hydroxyaryl BODIPY derivatives.

absorption maxima λ_{abs} of these dyes undergo small blue shifts (up to 5 nm) upon increasing the pH, while the corresponding emission is quenched without spectral shifts. λ_{abs} at the lowest (left) and highest (right) pH are given in Fig. 7 (compounds **40–42**).

Ester **43a** has high quantum yields (0.93–1.0) in organic solvents and displays single exponential fluorescence decay kinetics with lifetimes τ in the 3.5–4.2 ns range.[69] The absorption maxima λ_{abs} are in the 564–576 nm range while the

emission maxima λ_{em} lie between 577 and 595 nm. Compound **43b** is a water-soluble pH sensor with a pK_a of 7.6 and Φ of 0.75 in its phenolic form. The phenolate form of **43b** is non-emissive.

6.1.2. Metal ions. Many metal ions play very diverse and crucial roles in several biological processes, while others are associated with toxicity and disease.[80] These functions have sparked the interest in the accurate measurement of such metal ions, and progress in this field has been thoroughly reviewed in recent years.

In the past decade, fluorescent probes for Zn^{2+} have attracted a great deal of attention and many probes have been proposed based on numerous fluorophores. Di(2-picolyl)-amine is the most widely used ionophore for Zn^{2+}. Sensors for the detection and imaging of Zn^{2+}, especially in biological systems, have been extensively reviewed.[81–85] A recent review describes the tools and tactics for the optical detection of Hg^{2+}.[86] Another recent review paper deals with the chemistry and biology of zinc, iron and copper in neurobiology.[87]

The ratiometric BODIPY-linked azacrown ether sensor **44** with high selectivity for potassium over other alkali ions in MeCN is the first example of a probe synthesized using S_NAr of 3,5-dichloroBODIPY (Fig. 8).[32] A large conformational change of the sensor upon K^+ binding (K_d of the 1 : 1 complex K^+–**44** equals 0.5 mM) was invoked to explain the blue shifts in absorption and emission. Later research[88] confirmed these findings and showed that some alkaline-earth metal ions (Ca^{2+}) and HTM ions (Pb^{2+}, Hg^{2+}) also produced comparable spectral hypsochromic shifts and increases of Φ.

Sensor **45** with a 1,3-alternate calix[4]bisazacrown-5 linked to two BODIPYs at the *meso*-position shows a high sensitivity and selectivity for K^+ ions over other alkali and alkaline-earth metal ions (Na^+, Cs^+, Ca^{2+}, Ba^{2+}) in acetonitrile, ethanol, and ethanol–water mixtures.[89] In medium to high polarity solvents, an efficient ICT process occurs in the excited state leading to a dual emission and a strong fluorescence quenching. Upon K^+ coordination, this ICT process is hindered and a large fluorescence enhancement is observed. The inhibition of the ICT process is more efficient when two K^+ ions are coordinated. The global K_d values of the 2 : 1 (metal : indicator) K^+–**45** complexes are dependent on the solvent and they were found to be 0.9×10^{-6} M^2, 5.5×10^{-6} M^2 and 3.2×10^{-4} M^2 in MeCN, EtOH, and EtOH : H_2O 3 : 1 (v/v), respectively.

Reaction of **46** with aminodextran gave a water-soluble, dextran-conjugated, triazacryptand-based, BODIPY-derived K^+ sensor. This compound shows a strong fluorescence emission increase upon K^+ binding, without observable spectral shift.[90] The dextran-conjugated indicator was used as an extracellular K^+ sensor to detect cellular K^+ efflux. A ratiometric, dual-color fluorescent dextran conjugate was synthesized by coupling dextran to green fluorescent, K^+-sensitive BODIPY derivative **46** and tetramethylrhodamine, a reference chromophore with K^+-insensitive red fluorescence.[91] The dextran backbone confers high water solubility and membrane impermeability. Upon K^+ binding, fluorescence quenching *via* reductive PET from the triazacryptand to BODIPY is hindered, resulting in increased BODIPY fluorescence of this conjugate. It was used to measure noninvasively [K^+] in the airway surface liquid (ASL) and to establish the major determinants of ASL [K^+] regulation.

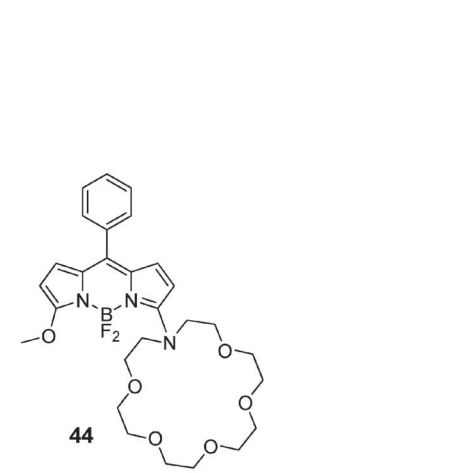

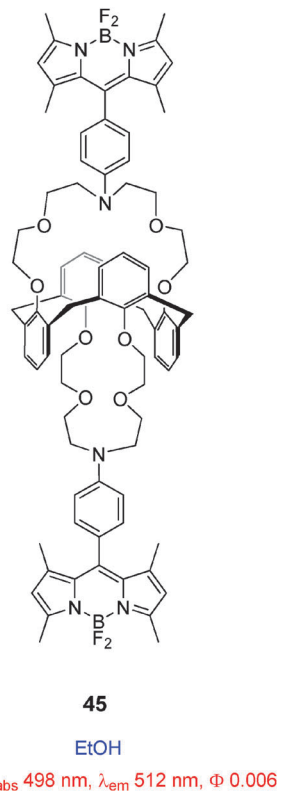

Fig. 8 Sensors with a selective response to K^+.

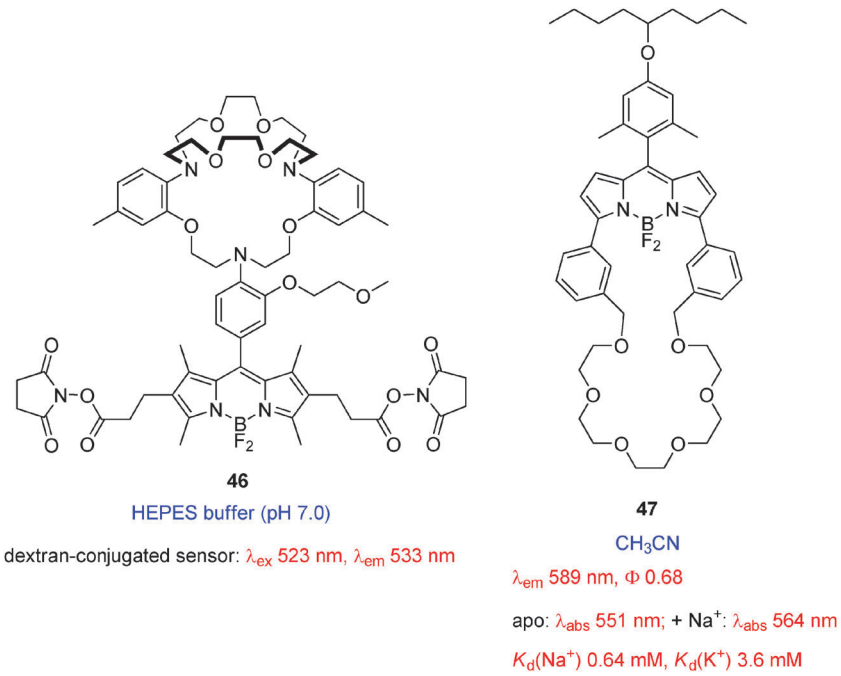

Fig. 9 BODIPY chemosensors for alkali metal ions.

Sodium-selective indicator **47** with an oligo-ethyleneglycol bridge between the *m*-positions of the 3- and 5-phenyl rings of BODIPY is based on conformational restriction triggered by cation recognition at this bridge.[92] Of the alkali metal ions (Li^+, Na^+, K^+, Rb^+, Cs^+), binding of Na^+ leads to the largest bathochromic shift of the absorption maximum, while no clear shift was found for the emission maximum. Determination of the K_d values of the 1 : 1 complexes of **47** with Na^+ and K^+ indicates that the selectivity of **47** for Na^+ (K_d 0.64 mM) over K^+ (K_d 3.6 mM) is low. Φ for the ion-free and Na^+ bound forms of **47** are the same (0.68), implying that PET is not operative (Fig. 9).

BODIPY derivative **48** with an aza-15-benzocrown-5 chelator is a Na^+-sensitive indicator.[93] The selectivity for Na^+ over K^+ is less than 2. The fluorescence emission intensity increased *ca.* 7-fold upon Na^+ binding and *ca.* 3-fold upon K^+ binding.

Chemosensors **49** represent 15-benzocrown-5 ether appended BODIPY analogues with different electron acceptor strengths.[94] In the polar solvents acetonitrile and methanol, apo **49a** is virtually nonfluorescent due to reductive PET from the weak benzocrown electron donor to BODIPY. Upon binding of Na^+ and K^+ to the benzocrown ether, the electron donor properties of the latter are further reduced, thus suppressing PET and leading to large cation-induced fluorescence increases without spectral shifts. Fluorometric titrations yielded K_d values of 3 mM and 1 mM for the 1 : 1 Na^+–**49a** and K^+–**49a** complexes, respectively. The higher K_d value for the Na^+ complex is unexpected, because 15-crown-5 is supposed to provide a tighter fit for Na^+ than for K^+. In compound **49b**, excited-state deactivation occurs mainly by fluorescence from the initially formed LE state of BODIPY and conversion to an ICT state does not occur. No red-shifted (broad and unstructured) emission from an energetically lower lying ICT

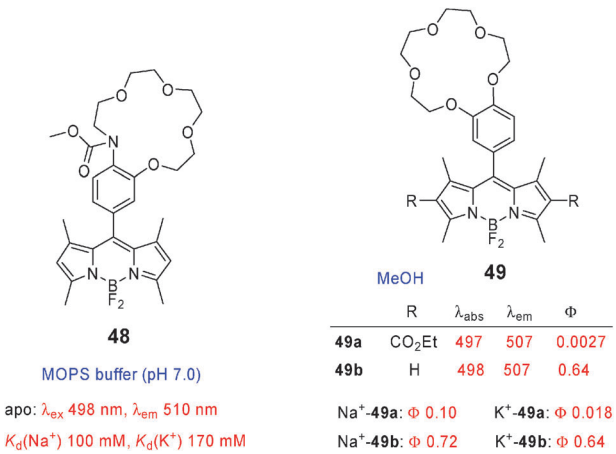

Fig. 10 Fluorescent chemosensors for Na^+ and K^+.

in acetonitrile, methanol, or any other polar solvents could be detected. Binding of Na^+ or K^+ to **49b** was only accompanied by a small increase of Φ. K_d for the 1 : 1 Na^+–**49b** complex was found to be 3 mM (Fig. 10).

In solvents more polar than hexane, BODIPY sensor **50** having a 13-phenyl-1,4,7,10-tetraoxa-13-azacyclopentadecane chelator shows dual emission from the LE and ICT state, both fluorescence quantum yields being low.[95,96] In acetonitrile solution, only emission from the LE state of **50** was observed (Φ 0.0002). Crowned compound **50** forms 1 : 1 complexes with various alkali (Li^+, Na^+) and alkaline-earth (Mg^{2+}, Ca^{2+}, Sr^{2+}, Ba^{2+}) metal ions, the latter being the stronger (K_d measured for the cation complexes of **50** are in the order $Na^+ > Li^+ > Mg^{2+} > Ba^{2+} > Sr^{2+} > Ca^{2+}$). Coordination of the cation to the nitrogen of the aza crown leads to cation-dependent enhancement of the LE fluorescence quantum yield

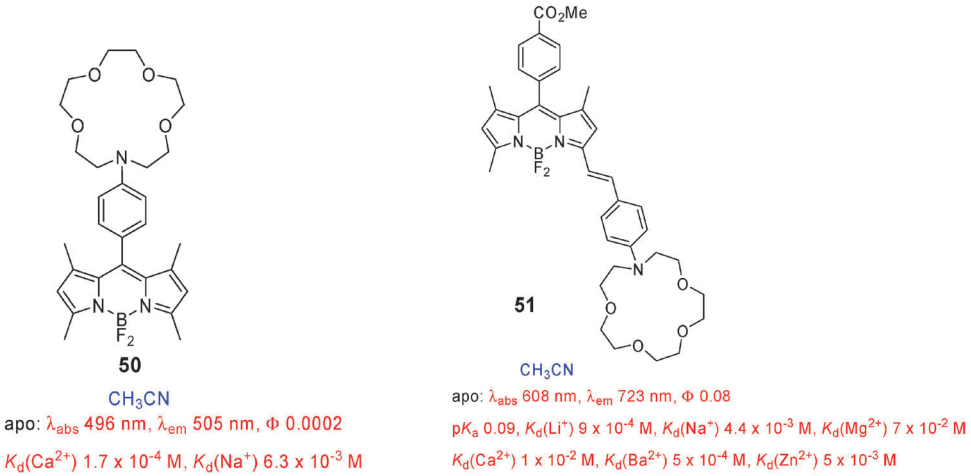

Fig. 11 Sensors with aza-15-crown-5 chelator at different locations.

and cation-independent slight (2–3 nm) red shifts of λ_{abs} and λ_{em}. The stability of the 1 : 1 complex between Na^+ and **50** is solvent dependent: K_d of Na^+–**50** equals 6 mM in acetonitrile and 23 mM in methanol.

The same aza-15-crown-5 chelator as in **50** was attached *via* a styryl linker to the 3-position of the BODIPY core to produce compound **51**.[97] Apo **51** in acetonitrile solution has a low fluorescence quantum yield which was attributed to the ICT character of the excited state. Also this sensor was not selective because it forms 1 : 1 complexes with several alkali (Li^+, Na^+), alkaline-earth (Mg^{2+}, Ca^{2+}, Ba^{2+}) and transition (Zn^{2+}) metal ions and protons, producing large blue shifts and significant cation-induced fluorescence amplifications. The stability of the metal-ion complexes with **51** decreases in the order $Ba^{2+} > Li^+ > Na^+ \approx Zn^{2+} > Ca^{2+} > Mg^{2+}$ (Fig. 11).

Two 'off–on' indicators with *meso*-APTRA substituents as low-affinity chelators for calcium but with different groups (methyl in **52a** *versus* *p*-anisyl in **52b**) at the 3,5-positions have very similar dissociation constants K_d of the 1 : 1 **52**–Ca^{2+} complexes and quantum yields Φ.[98] The absorption and

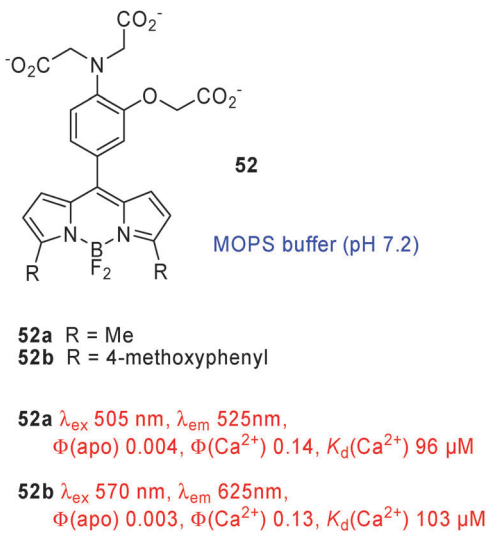

Fig. 12 BODIPY dyes with APTRA chelator at the *meso*-position.

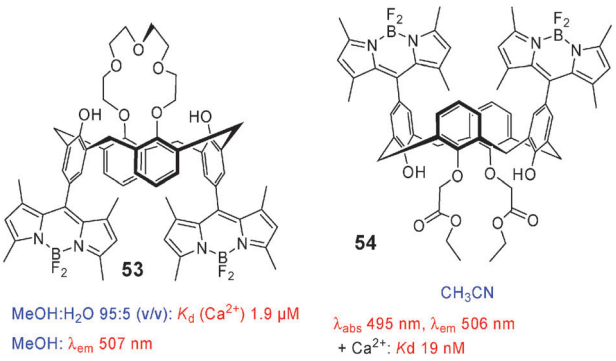

Fig. 13 Calixarenes with pending BODIPY fluorophores as Ca^{2+} sensors.

fluorescence emission spectra of **52b** are red-shifted by 65 and 100 nm, respectively, compared to those of **52a**. Reductive PET from APTRA to BODIPY is shut down upon Ca^{2+} complex formation so that a large fluorescence enhancement is observed without any spectral shifts (Fig. 12).

Sensor **53** was synthesized by appending BODIPY entities on a calix[4]arene-crown-5 ether.[99] In pure MeOH and in aqueous MeOH solution (up to 5% water), this indicator exhibits pronounced, selective fluorescence quenching in the presence of Ca^{2+}. Other physiologically important ions (Na^+, K^+, Mg^{2+}) did not quench the fluorescence.

BODIPY appended calix[4]arene diethyl ester **54** shows Ca^{2+} selectivity over other metal ions.[54] Upon Ca^{2+} binding, fluorescence quenching of **54** occurs, which was attributed to oxidative PET from the BODIPY donor to the electron-deficient Ca^{2+}-bound carbonyl groups of the esters. A value of 19 nM was determined for K_d of the 1 : 1 Ca^{2+}–**54** complex (Fig. 13).

BAPTA is very selective for Ca^{2+} over Mg^{2+} and was used as a high affinity Ca^{2+} chelator in the construction of a series of long-wavelength sensors **55**.[100] Attachment of the BAPTA moiety to the BODIPY scaffold *via* a 3-propanamide side chain results in strong fluorescence quenching due to reductive PET. This PET process is switched off upon addition of aqueous Ca^{2+}, resulting in significant fluorescence enhancements without spectral shifts. Measured K_d values for the Ca^{2+}–**55** complexes are around 200 nM (Fig. 14).

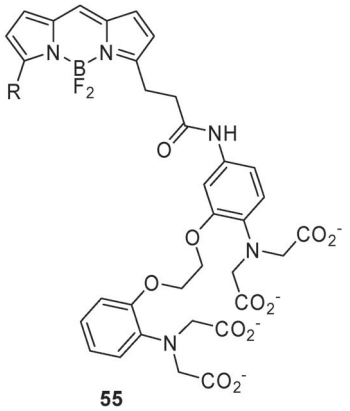

55

MOPS buffer (pH 7.2)

	R	K_d (Ca^{2+}-**43**)
55a	-CH=CH-Ph	175 nM
55b	-(CH=CH)$_2$-Ph	190 nM
55c	2-pyrrolyl	260 nM
55d	-$CH_2CH_2CO_2Na$	220 nM

Fig. 14 BAPTA–BODIPY dyad for Ca^{2+} sensing.

In chemosensor **56**, the high-affinity Ca^{2+} chelator BAPTA is connected to the BODIPY chromophore at the *meso*-position.[101] Upon Ca^{2+} binding, a *ca.* 250-fold fluorescence intensity increase was observed, without noteworthy spectral shifts. Derivative **57** with an O^6-benzylguanine residue can be covalently and selectively coupled to SNAP-tag fusion proteins in living cells to produce conjugate **58**, in which X represents a protein with defined localization. [SNAP-tag is a 20 kDa mutant of the human DNA repair protein O^6-alkylguanine-DNA alkyltransferase that reacts specifically and rapidly with benzylguanine and benzylchloropyrimidine derivatives, leading to covalent labeling of the SNAP-tag with a probe such as **57**. SNAP-tag can be localized in living cells through its fusion with targeted proteins and hence allows the precise localization of the conjugate **58**.] The indicator in **58** retains its high affinity for Ca^{2+} after conjugation to proteins, displaying a 180-fold fluorescence intensity amplification upon Ca^{2+} binding with 2 nm red shifts. Measured K_d values for the 1 : 1 complexes of Ca^{2+} with **56**, **57** and **58** in MOPS buffer (pH 7.2) were 300 nM, 210 nM and 200 nM, respectively. The high sensitivity of probe **57** in addition to the possibility of coupling it to specific proteins makes it a powerful tool for measuring/visualizing changes of Ca^{2+} levels with high spatiotemporal resolution in live cells (Fig. 15).

BODIPY linked aza-18-crown-6 ether indicators **59a** and **59b** are enantiopure derivatives of achiral dye **44**, having methyl and isobutyl groups on their stereogenic centers, respectively.[88] The Φ values of apo **59** were very low (0.005). Addition of metal ions, in particular Ca^{2+}, Pb^{2+}, Mg^{2+}, Zn^{2+} and Hg^{2+} ions, produces fluorescence enhancements and blue shifts of λ_{abs} and λ_{em} of **59**. The most stable complexes were formed with Ca^{2+} and Pb^{2+} and indicated 1 : 2 (metal : indicator) stoichiometries.

BODIPY bearing benzocrown ethers of various cavity sizes (15-crown-5, 18-crown-6 and 21-crown-7) at the *meso*-position (**60**) have been employed as multi-cation sensors.[102] Compound **60a** with 15-benzocrown-5 is similar to sensors **49** described in ref. 94. The selectivity afforded by the various crown ether sizes was investigated in a systematic way. In methanol solution, all sensors **60** are virtually nonfluorescent in their ion-free forms (Φ 0.004). Addition of metal ions does not induce any observable spectral changes but leads to fluorescence enhancement for ions that coordinate to the crown ether. For **60a** with the smallest cavity, only coordination to Na^+ (K_d 1.2×10^{-5} M) was found. Greater K_d values were determined for the analogous 1 : 1 Na^+–**49a** and Na^+–**49b**

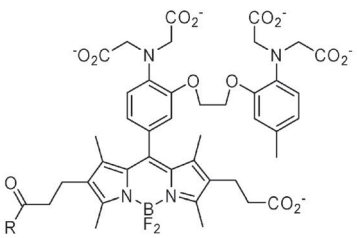

56-58

56: R =

apo: λ_{ex} 521 nm, λ_{em} 537 nm, Φ 0.001

+ Ca^{2+}: λ_{ex} 522 nm, λ_{em} 536 nm, Φ 0.26, K_d 0.3 μM

57: R =

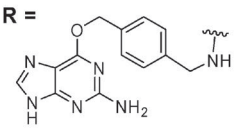

apo: λ_{ex} 522 nm, λ_{em} 532 nm, Φ 0.001

+ Ca^{2+}: λ_{ex} 523 nm, λ_{em} 535 nm, Φ 0.22, K_d 0.21 μM

58: R =

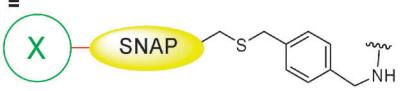

apo: λ_{ex} 527 nm, λ_{em} 537 nm, Φ 0.002

+ Ca^{2+}: λ_{ex} 529 nm, λ_{em} 539 nm, Φ 0.39, K_d 0.2 μM

MOPS buffer (pH 7.2)

Fig. 15 Functionalized BAPTA-based chemosensors.

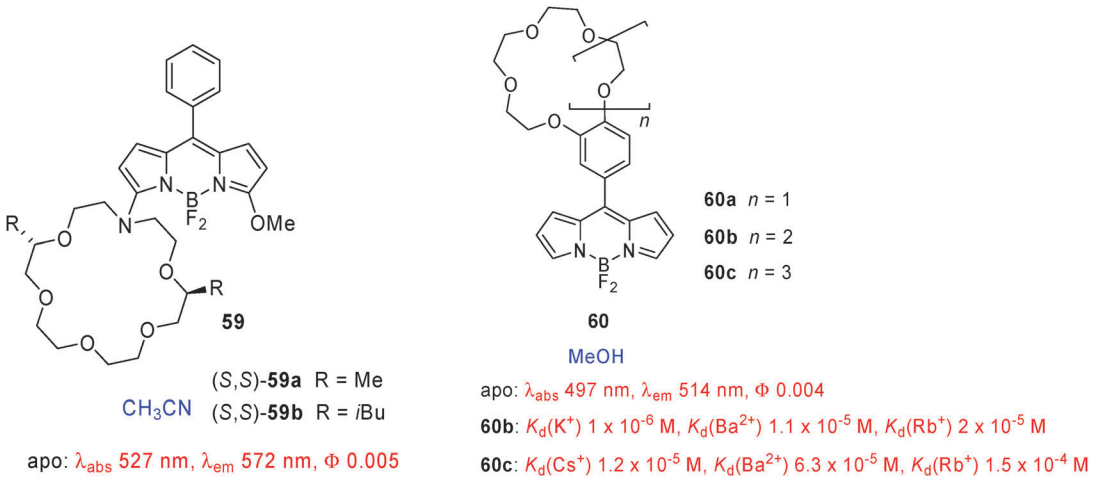

Fig. 16 Crown-ether containing derivatives as metal ion indicators.

complexes in methanol, namely 3×10^{-3} M. Indicator **60b** with a larger cavity than **60a** showed the maximum fluorescence enhancement upon K^+ binding. The stability of the 1 : 1 metal ion complexes with **60b** decreased in the order $K^+ > Ba^{2+} > Rb^+$. For **60c** with the largest cavity, the most stable complex was formed with Cs^+ (Fig. 16).

The two azacrown ether appended BODIPY analogues **61** are practically nonfluorescent in their ion-free forms.[103] Coordination of the alkali metal ions Li^+, Na^+, and K^+ with **61a** produces small red shifts of λ_{abs} and λ_{em} and large Φ increases (0.082 with Li^+, 0.073 with Na^+, 0.003 with K^+). Larger spectral red shifts were observed upon addition of Ca^{2+} and Mg^{2+}, while Φ also increased (to 0.017 with Ca^{2+} and 0.108 with Mg^{2+}). K_d of the 1 : 1 Li^+–**61a** and 1 : 1 Mg^{2+}–**61a** complexes were 3.2×10^{-4} M and 2.3×10^{-3} M, respectively. In contrast to **61a**, compound **61b** with the aza-18-crown-6 chelator shows a good selectivity toward K^+ with an estimated K_d of 1.5×10^{-4} M for the complex. Both probes are also pH sensitive, but no pK_a values were given.

Compound **62** has a selective fluorescence turn-on response to Ni^{2+} compared to other biologically relevant metal ions in water (Na^+, K^+, Mg^{2+}, Ca^{2+}, Mn^{2+}, Fe^{2+}, Co^{2+}, Cu^{2+}, Zn^{2+}).[104] Addition of 50 equiv. of Ni^{2+} switches off PET and triggers a *ca.* 25-fold fluorescence turn-on with no shifts of λ_{abs} and λ_{em} compared to the apo probe. Confocal microscopy showed that **62** can respond to changes in Ni^{2+} levels within live cells (Fig. 17).

Two BODIPY fluorophores and a noncyclic azatetrathia (NS_4) chelator were combined in sensor **63**.[105] The absorption spectrum of apo **63** shows two distinct maxima at 528 and 624 nm, corresponding to unmodified BODIPY (green) and extended conjugation BODIPY (red), respectively. Ag^+ binding only affects the long wavelength absorption peak (hypsochromic shift and intensity changes). Upon excitation of apo **63** at 480 nm, RET occurs, which leads to weak residual emission from the green emitting dye ($\lambda_{em} \approx 550$ nm, Φ 4.1 $\times 10^{-3}$) and strong emission from the red emitting dye (λ_{em} 680 nm, Φ 0.49). Binding of Ag^+ causes blue-shifted emission spectra, whereas all the other metal ions tested (Pb^{2+}, Mn^{2+}, Fe^{2+}, Hg^{2+}, Co^{2+}, ...) cause insignificant spectral changes. K_d of the Ag^+–**63** complex was determined to be 6 μM.

Compound **64** is a BODIPY-derived, water-soluble, membrane-permeable, fluorescence turn-on sensor with the same azatetrathia (NS_4) receptor as in **63**, but at the *meso*-position, exhibiting high selectivity and sensitivity for Cu^+.[106] Also probe **65** has the same Cu^+ chelating subunit but now at

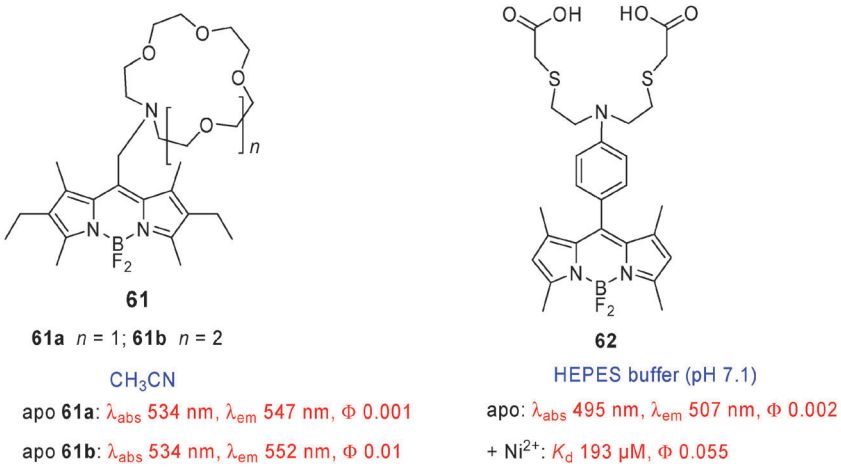

Fig. 17 Metal ion sensing dyes **61** and **62**.

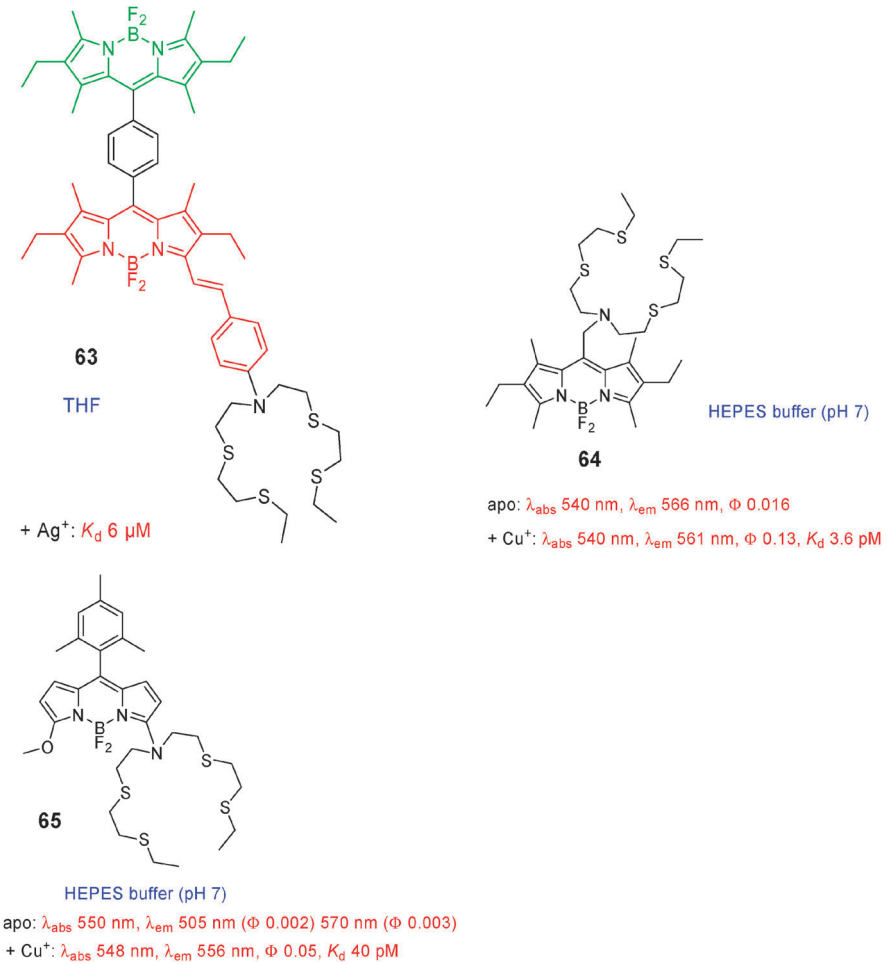

Fig. 18 Azatetrathia chelators in detectors for Ag^+ (**63**) and Cu^+ (**64**, **65**).

the 3-position of BODIPY.[107] Sensor **64** displays weak fluorescence in its apo form due to reductive PET from the azatetrathia chelator. Upon Cu^+ complexation (K_d 3.6 pM), PET is turned off and the fluorescence is enhanced *ca.* 10-fold, with a small blue shift of λ_{em}. Addition of Cu^+ to **65** induces small blue shifts of λ_{abs} (550 nm) and λ_{em} (570 nm) to 548 nm and 556 nm, respectively, with a concomitant 20-fold fluorescence increase. The emission band of **65** at 505 nm remains unchanged, rendering the probe useful for ratiometric applications. Compounds **64** and **65** both form 1 : 1 complexes with Cu^+ and feature excellent selectivity for Cu^+ over various biologically relevant metal ions, including Cu^{2+}. Both indicators are membrane-permeable and respond to changes in the levels of labile intracellular Cu^+ (Fig. 18).

Compound **66** is a membrane-permeable, water-soluble, Cu^{2+}-selective sensor with *N*,*N*-bis(2-hydroxyethyl)amine coordination sites at the 3,5-positions of BODIPY.[108] In the presence of 400 μM Cu^{2+}, the fluorescence emission of **66** was completely quenched, while under identical conditions, other biologically relevant metal ions, such as Na^+, K^+, Mg^{2+}, Mn^{2+}, Cd^{2+}, Co^{2+}, Zn^{2+}, Hg^{2+} and Pb^{2+}, produced only slight changes of the fluorescence emission of **66**. A 2 : 1 Cu^{2+}–**66** complex (K_d 9.7 × 10^{-8} M^2) was formed, indicating that each Cu^{2+} ion binds to one *N*,*N*-bis(2-hydroxyethyl)amine subunit. Indicator **66** can monitor intracellular Cu^{2+} (Fig. 19).

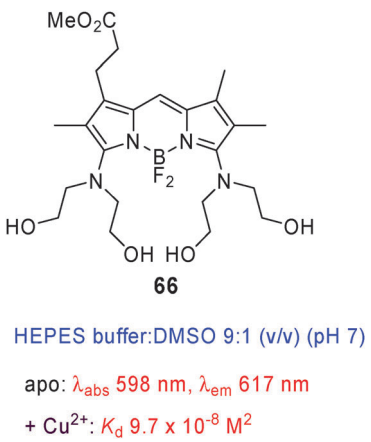

Fig. 19 Cu^{2+}-selective sensor **66** has ligands at the 3,5-positions.

In MeCN, compound **67a** is a selective 'off–on' fluorescent indicator for Pb^{2+}.[109] Dye **67a** is nonfluorescent due to reductive PET, but displays a large fluorescence enhancement with Pb^{2+} and to a lesser degree with Cu^{2+} and Zn^{2+}. Compound **67a** forms 1 : 1 complexes with Pb^{2+} and Cu^{2+} and exhibits a more than 15-times higher selectivity for Pb^{2+} over Cu^{2+}. Conversely, compound **67b** is a fluorescent dosimeter which shows a highly selective fluorescence increase in acetonitrile only with Cu^{2+}.

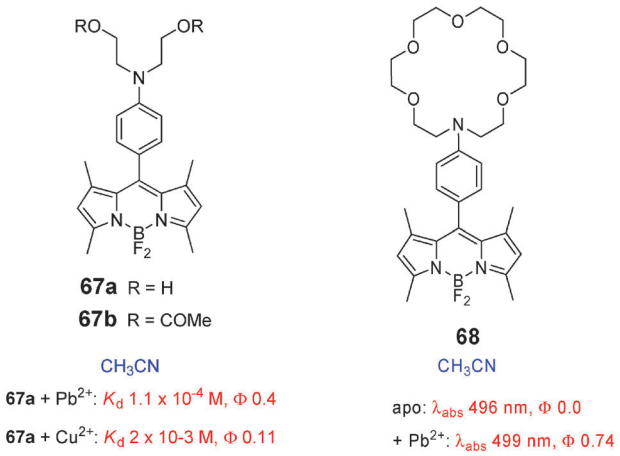

Fig. 20 Pb^{2+} probes.

Compound **68** having a 16-phenyl-1,4,7,10,13-pentaoxa-16-azacyclooctadecane chelator at the *meso*-position of BODIPY is a turn-on fluorescent indicator for Pb^{2+}.[110] Compared to the open-chain receptor in analogue **67**, sensor **68** has a macrocyclic chelating moiety. The apo form of probe **68** is essentially nonfluorescent ($\Phi \approx 0$), whereas the Pb^{2+}–**68** complex is highly fluorescent (Φ 0.74). Of the competing metal ions screened, only Sr^{2+}, Ba^{2+} and Hg^{2+} could illicit a spectral response from the sensor (Fig. 20).

A conformationally restricted and sterically hindered BODIPY core has been used to construct a selective Cu^{2+} detector based on 8-hydroxyquinoline (**69**).[111] 8-Hydroxyquinoline is an important ionophore used for sensing Hg^{2+} and Cu^{2+}.[112] Significant fluorescence quenching of **69** in the presence of Cu^{2+} and Hg^{2+} was observed, with markedly higher selectivity for Cu^{2+} than Hg^{2+}.

Derivative **70** containing a *meso* thiacalix[4](*N*-phenylaza-crown-5)ether with strong chelation-induced emission enhancement in the presence of Cu^{2+}, Fe^{3+} and Hg^{2+} was described by Bitter and coworkers.[113] Apo **70** is nearly nonfluorescent (Φ 0.0016), but upon addition of Cu^{2+}, Fe^{3+} and Hg^{2+} large fluorescence increases were observed. Ag^{+} reduces the sensitivity of Cu^{2+} sensing in a competitive process. The stability of the 1 : 1 metal ion complexes with **70** decreases in the order $Cu^{2+} \approx Hg^{2+} > Fe^{3+}$ (Fig. 21).

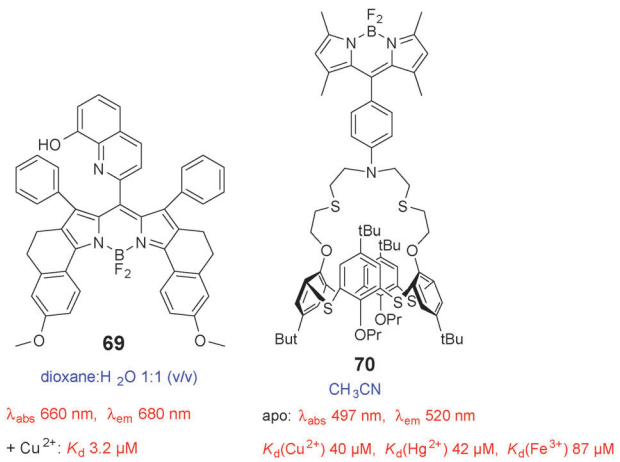

Fig. 21 BODIPY chemosensors for Cu^{2+}.

Compound **71** is a colorimetric and NIR fluorescent turn-on BODIPY-based probe with di(2-picolyl)amine as a chelator with high selectivity for Cu^{2+}.[114] Upon binding of Cu^{2+}, the main absorption band at 526 nm decreases in intensity and shifts to 536 nm, while a new band at 621 nm appears, resulting in a naked eye color change. Excitation at 620 nm in the presence of Cu^{2+} produces a strong fluorescence band with λ_{abs} at 651 nm.

Gold nanoparticles functionalized with **72** were developed for imaging Cu^{2+} in living cells.[115] Addition of increasing Cu^{2+} concentrations to the functionalized nanoparticles in 20 mM HEPES buffer (with 10% MeCN) at pH 7.4 gave a blue shift of the absorption band and quenching of the fluorescence without a spectral shift. The nanoparticles exhibited a high selectivity for Cu^{2+} over other competing metal ions. The dissociation constant K_d for the 1 : 1 complex of Cu^{2+} coordinated to **72** attached to the gold nanoparticles was found to be 1.6×10^{-5} M. The BODIPY-functionalized gold nanoparticles could respond to changes in intracellular [Cu^{2+}] within live cells. Apo **72** in MeCN has λ_{abs} and λ_{em} of 594 nm and 691 nm (Φ 0.3), respectively, comparable to the values found for **72** tethered to gold nanoparticles. Upon addition of Cu^{2+}, λ_{abs} of **72** shifted to 502 nm, while the emission at 691 nm was gradually quenched ($\Phi < 10^{-5}$) (Fig. 22).

For the detection and removal of Pb^{2+} in both water and human blood, fluorescent sensor **73** was covalently anchored onto the surface of nickel nanoparticles coated with silica shells (Fig. 23).[116] The magnetic nanoparticles functionalized with apo **73** are virtually nonfluorescent ($\Phi < 0.003$) presumably by reductive PET. Addition of Pb^{2+} to these nanoparticles results in formation of a 1 : 1 Pb^{2+}–**73** complex (K_d 9.5 μM) with associated fluorescence amplification (Φ 0.019). Similar observations were made for sensor **73** in MeCN solution, but the fluorescence quantum yields are much higher (Φ 0.067 for apo **73** and 0.189 for the Pb^{2+}-saturated form). The stability of the 1 : 1 Pb^{2+}-complex with **73** immobilized on the nanoparticle is *ca.* 12-fold higher than that for analogous **67a** (derived from the K_d values)[109] because of the preorganization of **73** on the surface of the nanoparticle and the C=O···Pb^{2+} coordination possibility. Compound **73** immobilized on nanoparticles (Fig. 23) in aqueous solution and sensor **73** in acetonitrile solution display large fluorescence increases only with Pb^{2+} among the metal ions tested. Compound **67a** also exhibits large fluorescence amplification with Pb^{2+} whereas small increases with Zn^{2+} and Cu^{2+} were found.[109] This difference suggests that the carbonyl groups in **73** play an important role in the selectivity for Pb^{2+} over other competing metal ions. The magnetic nanoparticles functionalized with the fluorescent indicator **73** were able to remove successfully Pb^{2+} from water and human blood.

Nanoparticles with a Fe_3O_4 core and silica shell were functionalized with BODIPY-based fluorescent sensor **74** as a selective turn-on fluoro-chromogenic probe for detecting Pb^{2+} in living cells (Fig. 24).[117] The nanoparticles are virtually nonfluorescent ($\Phi < 0.0005$) in their apo state. Addition of Pb^{2+} to these nanoparticles results in a large fluorescence enhancement (Φ 0.054). The blue-shifted and broad fluorescence emission spectra (full width at half height of the maximum of the

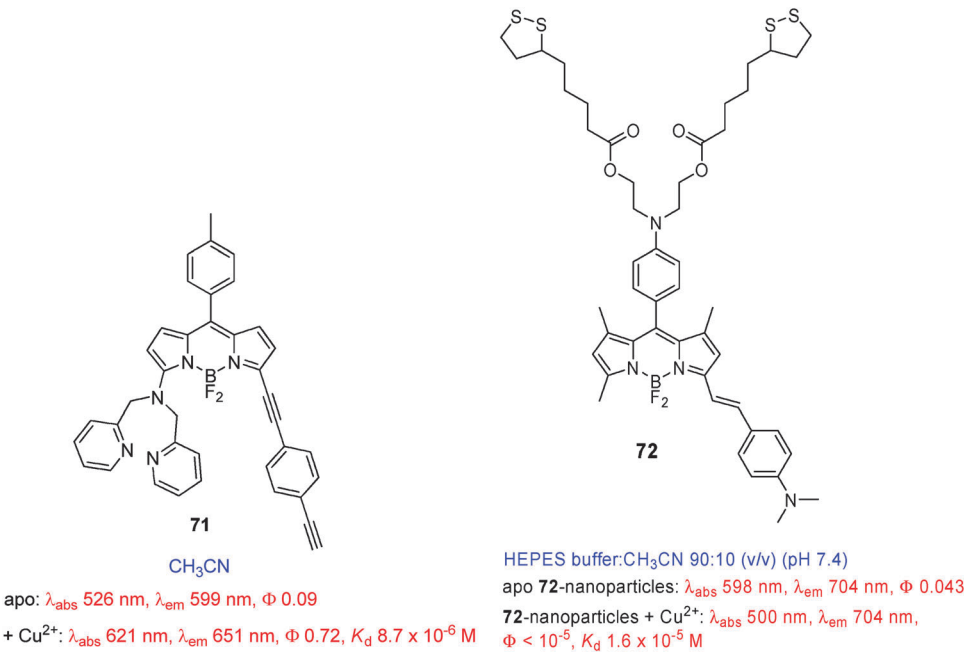

Fig. 22 Fluorescent probes for Cu^{2+}.

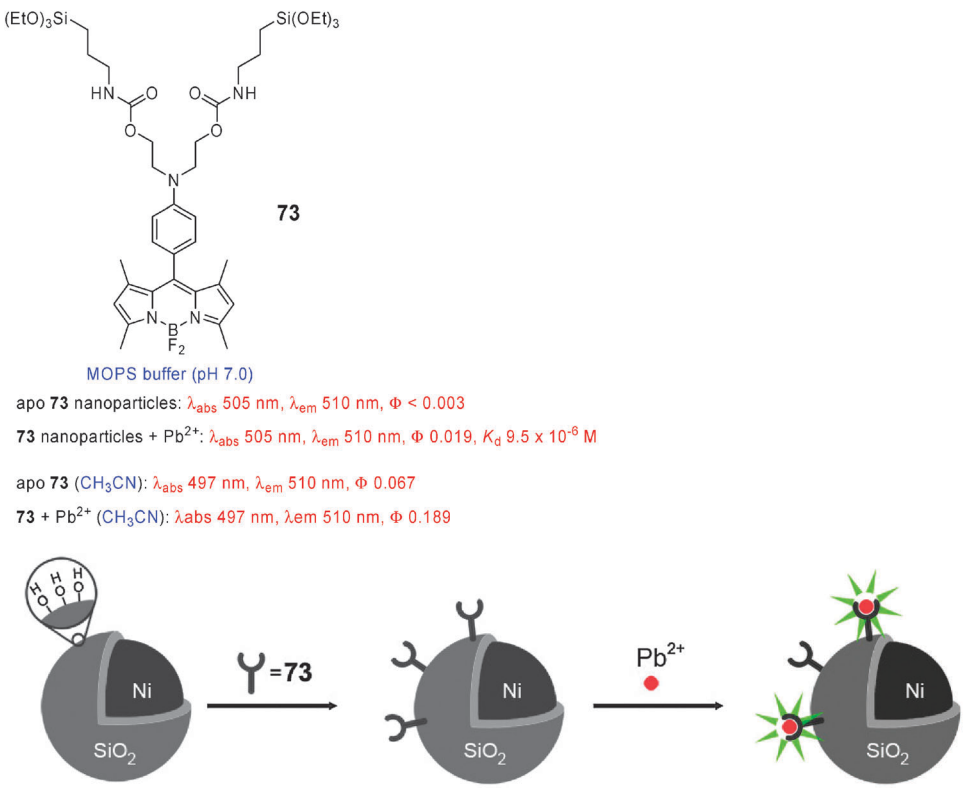

Fig. 23 BODIPY–**73**-functionalized, magnetic nanoparticles with a Ni core and silica shell for the detection and removal of Pb^{2+} from water and human blood.

emission band $> 5 \times 10^3$ cm^{-1}) of the BODIPY-functionalized nanoparticles in HEPES buffer as a function of [Pb^{2+}] and of dye **74** in acetonitrile with emission maxima at 460 nm and 456 nm, respectively, are not BODIPY-like. Indeed, fluorescent indicators **24**,[30] **34**,[73] **35**,[29] **51**,[97] **83**,[118] **84**,[119] **87**,[120] **92**,[121] and **109**,[122] with a *p*-*N*,*N*-dialkylaminostyryl group at the 3-position of the BODIPY core all have λ_{abs} and λ_{em} in the red to NIR spectral region. Detailed spectroscopic solvent-dependent studies of BODIPY dyes having styryl substituents at the 3-position confirm this.[37,123]

Dye **75** with an *o*-aminophenol chelator at the *meso*-position of BODIPY is sensitive to Hg^{2+} and Cu^{2+} (Fig. 25).[124]

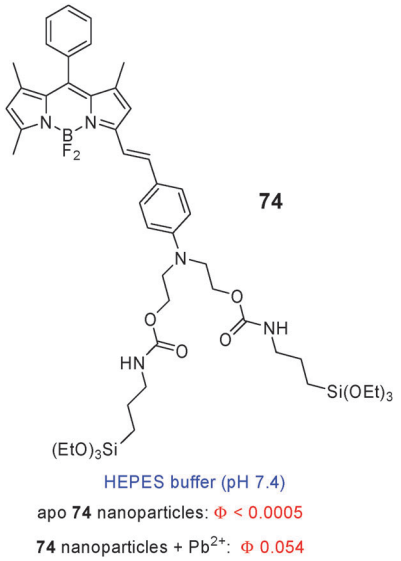

Fig. 24 Pb^{2+}-sensitive dye **74** was attached to Fe_3O_4 nanoparticles.

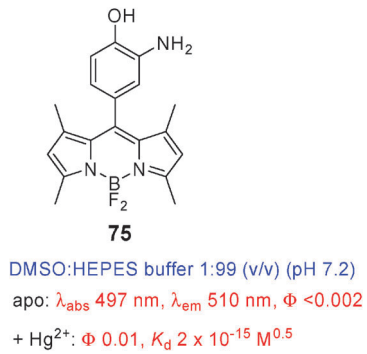

Fig. 25 *o*-Aminophenol substituted BODIPY for the detection of Hg^{2+} and Cu^{2+}.

Apo **75** has a low quantum yield ($\Phi < 0.002$) which increases in the presence of Hg^{2+} (Φ 0.01). A 1 : 2 complex was put forward in which two molecules of **75** bind a single Hg^{2+} ion (K_d 2×10^{-15} $M^{0.5}$). The bathochromically shifted absorption and fluorescence emission bands observed in the presence of Cu^{2+} were attributed to J-aggregate formation of Cu^{2+}–$\mathbf{75}_2$.

Four isomeric 3,4,4,8-tetrathienyl-substituted BODIPY derivatives **76** have been investigated as Cu^{2+} and Hg^{2+} sensors.[125] All the apo isomers **76** have λ_{abs} in the 531–563 nm range, while λ_{em} values are between 562 and 593 nm. The fluorescence quantum yields are extremely low for all unbound isomers. Derivatives **76a** and **76b** form stable 1 : 2 complexes with Cu^{2+} in which two indicator molecules coordinate to one Cu^{2+} ion, while 1 : 1 binding was found for **76c** and **76d**. Conversely, **76c** and **76d** give 1 : 2 (Hg^{2+} : indicator) complexes, whereas 1 : 1 (Hg^{2+} : indicator) complexes were formed with **76a** and **76b**.

meso-Thienyl substituted BODIPY isomers **77** have been shown to coordinate to Cu^{2+} and Hg^{2+}.[126] 1 : 1 complex formation with Cu^{2+} in acetonitrile solution resulted in smooth absorbance decreases, while for Hg^{2+} a 1 : 2 metal-to-indicator binding was found (Fig. 26).

Water-soluble, ratiometric, distyryl BODIPY sensor **78** for Zn^{2+} ions was described by Akkaya *et al.*[127] The Zn^{2+} chelator in **78** is the same and, moreover, at the same 3-position of BODIPY as in the Cd^{2+} selective sensor **83** reported by Peng and coworkers (Fig. 27).[118] The different solution composition used in the complexation studies might be responsible for the different selectivity. Based on the ICT mechanism, the NIR absorption and emission maxima of **78** undergo blue shifts upon Zn^{2+} complexation with a simultaneous increase of fluorescence emission intensity (no Φ data available). The largest emission intensity increases were found in the presence of Zn^{2+}, although Hg^{2+} and Cd^{2+} also showed some response. A K_d value of 20 μM was found for the 1 : 1 Zn^{2+}–**78** complex, much less than that of the Zn^{2+}–**80** complex (K_d 1 nM).[128]

Fluorescence enhancement upon Zn^{2+} chelation of **79** has been attributed to shutting down of reductive PET.[129] Φ for apo **79** amounts to 0.003 and increases to 0.058 upon Zn^{2+} binding. The maxima of the excitation and emission spectra are almost unchanged by Zn^{2+}. A Job's plot analysis revealed a 1 : 1 Zn^{2+}–**79** complex, but no K_d was reported.

Di(2-picolyl)amine was attached at the *meso*-position of BODIPY *via* a CH_2 linker to construct detector **80** for the selective visualization of Zn^{2+} in living cells (Fig. 28).[128] The suppression of reductive PET was assumed responsible for a *ca.* 11-fold increase of Φ in going from the apo to the zinc-bound form of **80**. Cd^{2+} also induces a large fluorescence enhancement and interferes with the selectivity. Cations such as Na^+, K^+, Ca^{2+} and Mg^{2+}, which exist at high concentrations under physiological conditions, have no influence on fluorescence enhancement. Formation of a Zn^{2+}–**80** complex with 1 : 1 stoichiometry and high affinity (K_d 1 nM) was obtained from direct fluorometric titration. Compound **80** is pH insensitive in a wide pH range (pH 4–10), is cell-permeable and can visualize intracellular Zn^{2+} changes.

Terpyridine-functionalized BODIPY **81** forms 1 : 1 and 1 : 2 (metal : indicator) complexes with various divalent metal cations M^{2+}. The most stable complexes are those with Zn^{2+} (K_d values for the 1 : 1 and 1 : 2 complexes are 6.3×10^{-9} M and 5×10^{-15} $M^{0.5}$, respectively).[130] The 1 : 1 and 1 : 2 complexes with Mg^{2+} and Ca^{2+} are two orders less stable than the corresponding Zn^{2+} complexes. Ion-free **81** has high fluorescence quantum yields (*e.g.*, Φ 0.87 in dichloromethane) and its absorption and emission maxima are virtually solvent independent ($\lambda_{abs} \approx 530$ nm, $\lambda_{em} \approx 550$ nm).

The intense green BODIPY fluorescence of **82** (Φ 0.39) is quenched by oxidative PET from the excited-state fluorophore to the bipyridyl moiety coordinated to metal cations (Fig. 29).[55] Zn^{2+} formed the most stable 1 : 1 complex with **82** (K_d 9×10^{-8} M) and was the most effective fluorescence quencher. The complexes with Cd^{2+} (K_d 5×10^{-5} M) and Hg^{2+} (K_d 6×10^{-4} M) are definitely less stable.

Compound **83** is the first ratiometric, fluorescent sensor for imaging Cd^{2+} in living cells based on the ICT mechanism.[118] Although Cd^{2+} and Zn^{2+} have very similar properties, BODIPY derivative **83** was described as the first fluorescent sensor which can distinguish Cd^{2+} from Zn^{2+}. Coordination of Cd^{2+} with **83** produces blue shifts in the absorption and fluorescence emission spectra with a simultaneous increase of Φ from 0.12 to 0.59. Direct and ratiometric fluorometric measurements are possible and yielded K_d values of 48 μM

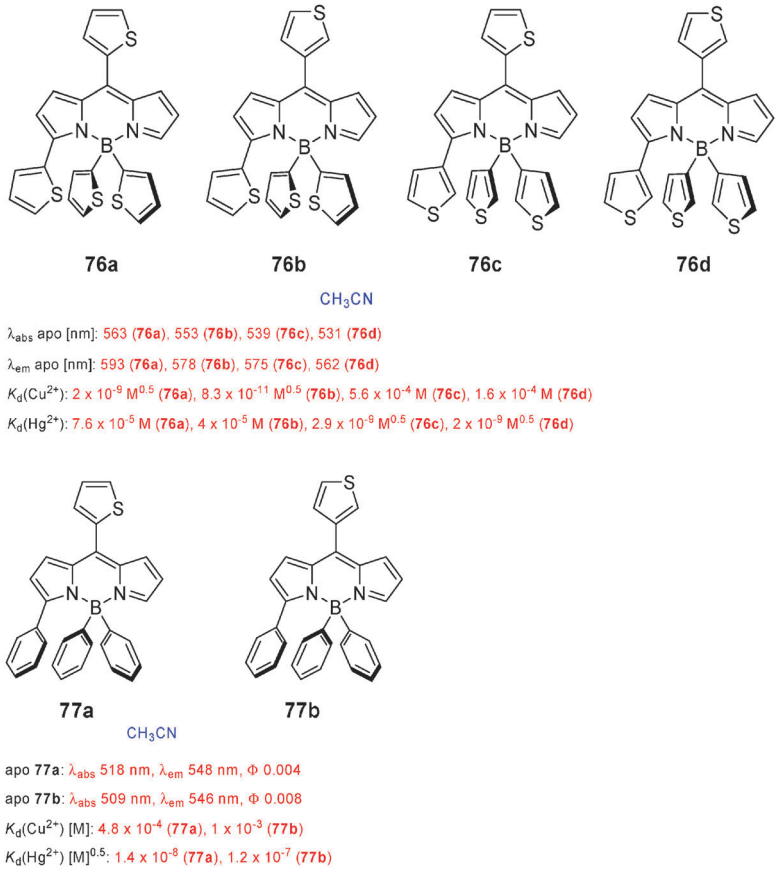

Fig. 26 Thiophene-containing dyes and their response to metal ions.

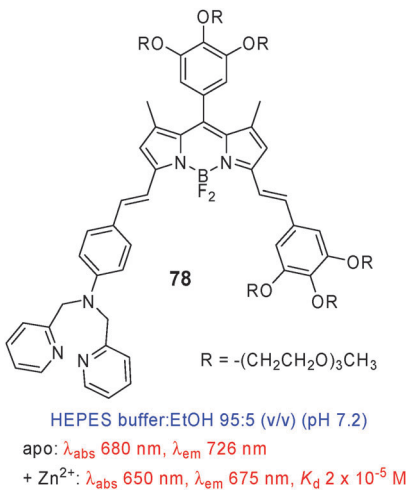

Fig. 27 Water-soluble dye with selective response to Zn^{2+}.

and 70 μM, respectively, for the 1 : 1 Cd^{2+}–**83** complex. Excellent selectivity for Cd^{2+} over other metal ions was observed, including Zn^{2+}. Sensor **83** can be used to image intracellular Cd^{2+} in living cells in direct and ratiometric mode.

Chemosensor **84** is a water-soluble, 'off–on' PET-based probe featuring the same tetraamide chelator as in Hg^{2+}-sensor **96c**.[119] However, in **84** the tetraamide chelator is connected to the 3-position of the BODIPY platform *via* a vinyl bridge. Apo **84** has an absorption peak at 578 nm and is weakly fluorescent (Φ 0.003). Upon Cd^{2+} addition, the absorption peak at 578 nm decreases and a new peak at 562 nm appears, while Φ increases *ca.* 100-fold without change in emission wavelength. A Job's plot indicated that two Cd^{2+} ions coordinate to one molecule **84**. K_d values for the 1 : 1 and 2 : 1 Cd^{2+}–**84** complexes were determined to be 1.4×10^{-4} M and 7.7×10^{-6} M^2, respectively. Almost no fluorescence intensity changes were observed with Zn^{2+}, so that sensor **84** can distinguish Cd^{2+} from Zn^{2+}. Living cell experiments showed the potential for Cd^{2+} imaging (Fig. 30).

BODIPY-based **85** with a 13-phenyl-1,4,7,10-tetrathia-13-azacyclopentadecane chelating subunit linked at the *meso*-position shows strong enhancement of Φ selectively with Hg^{2+} (5900-fold), Ag^{+} (2200-fold) and Cu^{2+} (2500-fold).[131] Excitation of apo **85** at the BODIPY absorption band leads to a LE state which undergoes a fast ICT process. The LE emission band is insensitive to solvent polarity, while the maximum of the ICT band shifts to lower energy with increasing solvent polarity. Binding of Hg^{2+}, Ag^{+} and Cu^{2+} inhibits the ICT process and is accompanied by a large increase in LE fluorescence. Sensor **85** forms 1 : 1 complexes with Hg^{2+} ($K_d < 1.8$ μM) and Ag^{+} (K_d 16 μM) in acetonitrile. Initial studies in mixed MeCN : H_2O 1 : 3 (v/v) indicate that **85** also gives fluorescence turn-on in water, although with lower increases of Φ (223-fold for Hg^{2+}, 92-fold for Ag^{+}, only 2-fold for Cu^{2+}).

8-Hydroxyquinoline was used as an ion signaling unit in the construction of the Hg^{2+}-selective chromo- and

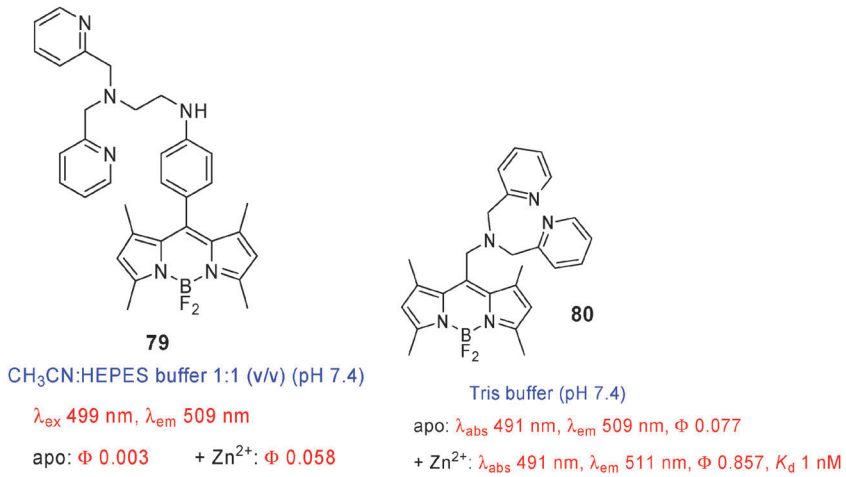

Fig. 28 Zn^{2+} probes with dipicolylamine chelator attached at the *meso*-position.

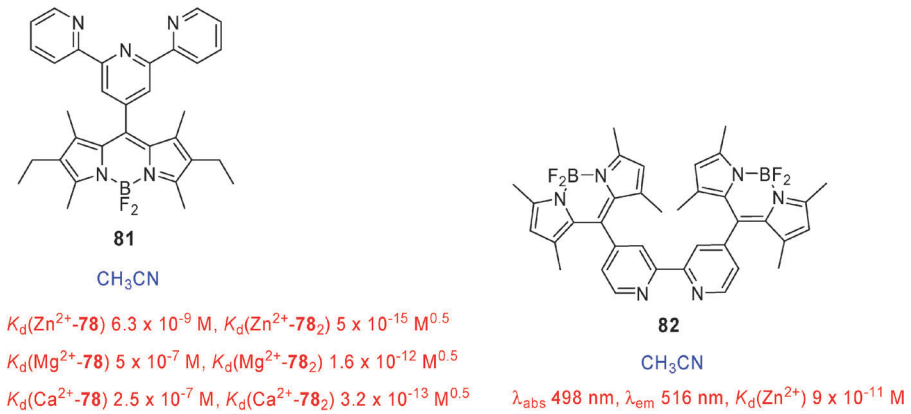

Fig. 29 Pyridine containing chelators for metal ions.

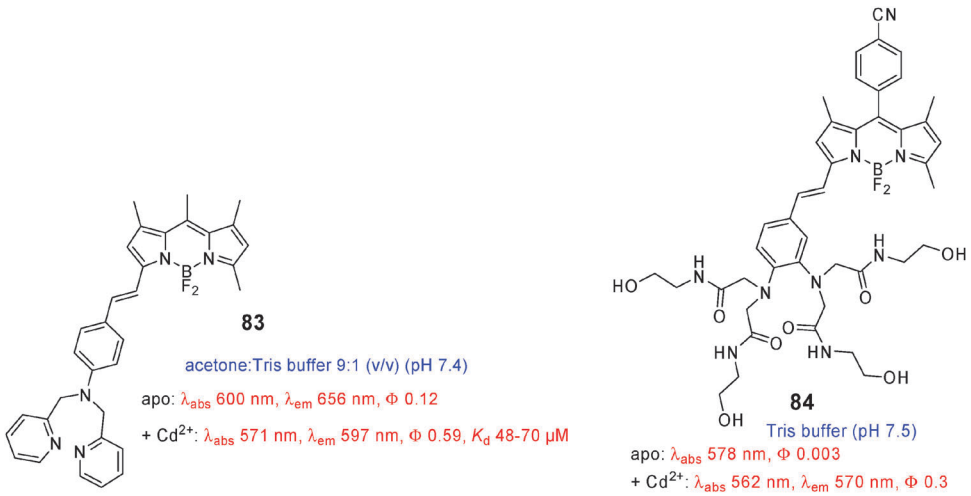

Fig. 30 Fluorescent probes with selectivity for Cd^{2+}.

fluoro-ionophore **86**.[112] The fluorescence emission of this compound is scarcely affected by the presence of HTM ions such as Co^{2+}, Ni^{2+}, Zn^{2+} and Cd^{2+}, but is quenched by more than 98% with 5 equiv. of Hg^{2+} ions, while the color of the solution changes from light amber to red. Cu^{2+} and Pb^{2+} ions also showed some quenching effects on **86**. A 1 : 1 complex with Hg^{2+} is formed (K_d 13 μM) in which the BODIPY core of **86** adopts a nearly orthogonal conformation with the 8-hydroxyquinoline moiety due to the presence of methyl groups at the 1,7-positions of the BODIPY core. This arrangement secures the binding site of 8-hydroxyquinoline for the accommodation of metal ions (Fig. 31).

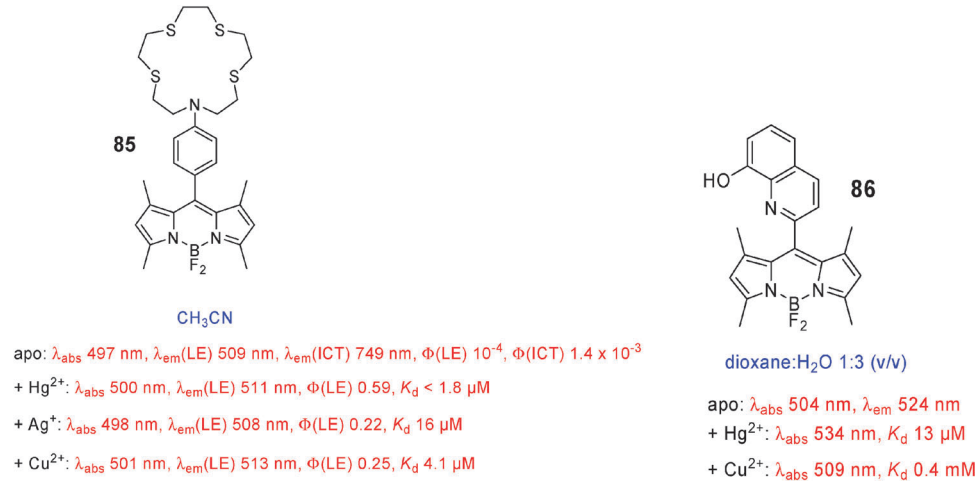

Fig. 31 Chemosensors responsive to multiple metal ions.

Emission-ratiometric sensor **87** contains a BODIPY dyad and a Hg^{2+}-sensitive azadioxadithia-15-crown-5 chelator.[120] Binding of Hg^{2+} causes a blue shift in the absorption spectrum of the longer wavelength dye (*i.e.*, red BODIPY moiety with a crown chelator, the energy acceptor) and hence increases the overlap between the emission spectrum of the energy donor (*i.e.*, blue BODIPY core with alkyl substituents) and the absorption spectrum of the energy acceptor. This results in more efficient Förster type RET[48,52,61] in the Hg^{2+}–**87** complex and higher fluorescence emission of the complex, hence increasing the signal ratio of apo and bound forms of **87**. K_d of the 1 : 1 Hg^{2+}–**87** complex was determined to be 4.5×10^{-7} M in THF.

Two chelating azadioxadithia (NO_2S_2) macrocycles were placed on the 3,8-positions of the BODIPY platform to construct indicator **88** for the colorimetric and fluorescent ratiometric detection of Hg^{2+}.[121] The ion-free form of **88** displays broad absorption (λ_{abs} 606 nm) and emission (λ_{em} 668 nm) bands and is virtually nonfluorescent (Φ 0.04). Addition of Hg^{2+} caused the disappearance of the band at 606 nm and the simultaneous appearance of a new, sharper, blue-shifted band at 564 nm. These concomitant absorption changes are clearly visible, turning the solution color from purple to red-pink. Addition of Mg^{2+}, Fe^{3+}, Co^{2+}, Ni^{2+}, Zn^{2+}, Cd^{2+}, Mn^{2+}, Pb^{2+}, Ag^{+} and Al^{3+} results in negligible absorbance or fluorescence changes. Upon addition of Hg^{2+}, the fluorescence intensity increases *ca.* 7-fold in conjunction with a hypsochromic shift in the emission spectra to 578 nm, allowing ratiometric fluorescent detection of Hg^{2+}. The dissociation constants K_d for the Hg^{2+} complexes with the two macrocycle chelators in **88** were determined using reference compounds. K_d values of 23 μM and 34 μM were determined for the 1 : 1 Hg^{2+} complexes with the binding site decoupled from the BODIPY chromophore (on 8-position) and the one conjugated to the BODIPY system (on 3-position), respectively. Both PET and ICT were invoked to rationalize the colorimetric and fluorescence responses of **88** to Hg^{2+}. Coordination of Hg^{2+} to the 8-appended macrocycle reduces the PET process and this is the main reason for the fluorescence emission enhancement. Coordination of Hg^{2+} to the 3-appended macrocycle suppresses the ICT process and this is assumed to be responsible for the blue shifts in the absorption and emission spectra.

NIR emitting dye **89**[132] resembles the ratiometric Hg^{2+}-selective sensor **88** described by Li and colleagues.[121] In **89**, the two chelating azadioxadithia (NO_2S_2) macrocycles are attached to the 3,5-positions of BODIPY *via* styryl linkers. Addition of Hg^{2+} to **89** causes the disappearance of the absorption band at 720 nm and the simultaneous appearance of a new hypsochromic band at 630 nm. In metal-ion-free **89**, the ICT process from the crown subunits to BODIPY leads to very weak fluorescence ($\lambda_{em} \approx 750$ nm). Upon binding of Hg^{2+}, a ~90 nm blue shift is observed in the emission spectra. Compound **89** can be used as a colorimetric and fluorometric Hg^{2+} sensor. A 2 : 1 stoichiometry for the Hg^{2+}–**89** complex was found with a K_d of 1.8×10^{-6} M^2, indicating that each azadioxadithia crown-15 macrocycle binds one Hg^{2+} ion.

In indicator **90**, two BODIPY fluorophores are combined with one macrocyclic azadioxadithia (NO_2S_2) chelator for selective Hg^{2+} sensing.[133] This molecular arrangement with an excitation energy donor (blue BODIPY in **90**, Fig. 32), energy acceptor (red BODIPY) and cation selective chelator exhibits red to NIR emission. For apo **90** in THF, two absorption bands are observed with λ_{abs} at 500 nm (blue BODIPY) and 690 nm (red distyryl BODIPY) and two associated emission bands with λ_{em} at 518 nm and 725 nm. In the presence of Hg^{2+}, the shorter wavelengths λ_{abs} and λ_{em} are not shifted. However, the longer wavelength absorption band shifts hypsochromically to 650 nm and concomitantly, the longer wavelength emission peak shifts to ~665 nm and increases its intensity. The decrease in the emission intensity of the shorter wavelength emitting BODIPY upon binding of Hg^{2+} is indicative of the increased RET efficiency because of the larger spectral overlap between the donor emission spectrum (blue fluorophore) and the acceptor absorption spectrum (red chromophore). The K_d value of the 1 : 1 Hg^{2+}–**90** complex was 3 μM.

Compound **91** with an azaBODIPY chromophore and 1,7-bis(2-pyridyl) substituents is a NIR fluorescent probe for Hg^{2+} (Fig. 33).[134] Coordination with Hg^{2+} induces bathochromic shifts in both the absorption and fluorescence emission maxima, allowing ratiometric measurements.

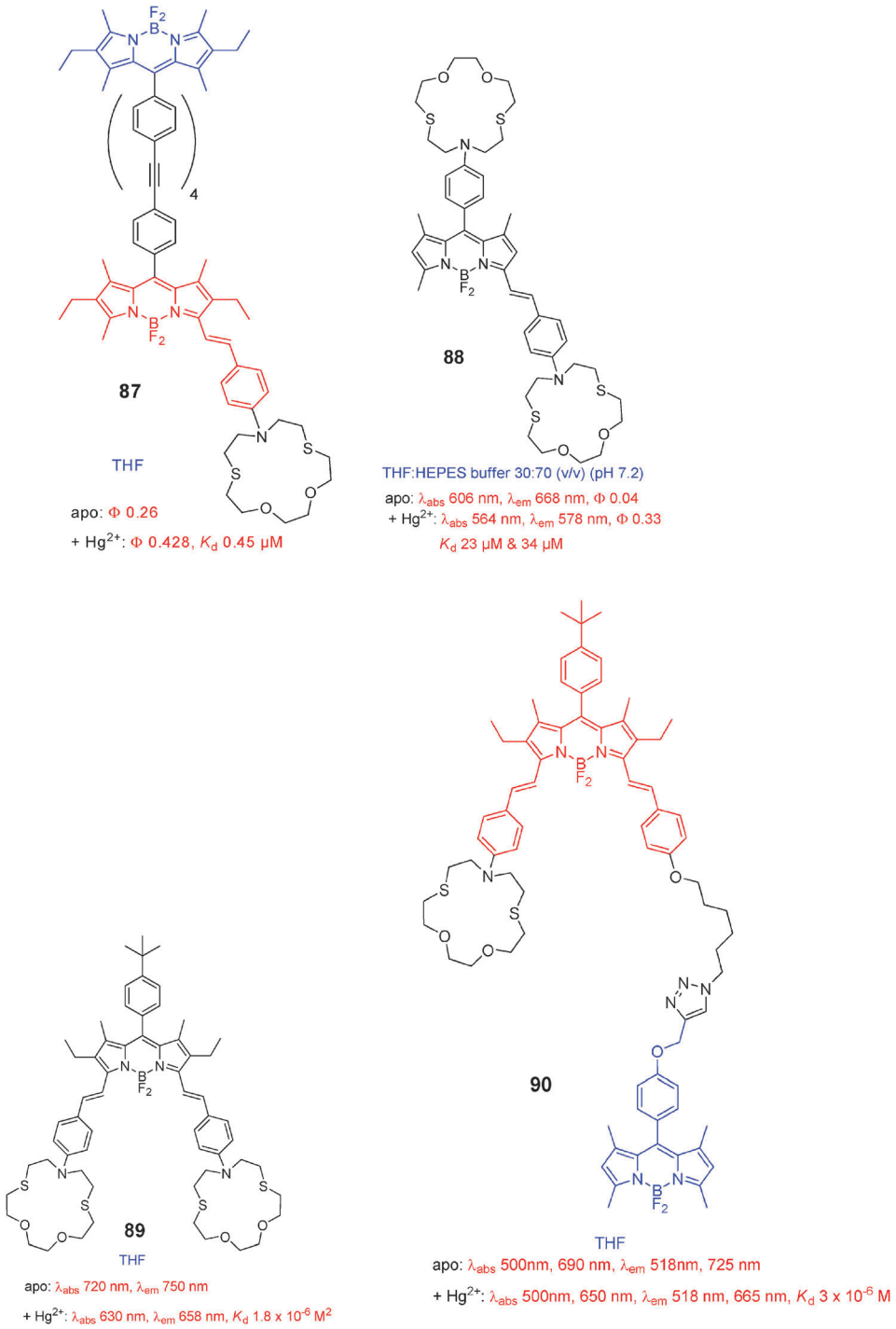

Fig. 32 Chemosensors with azadioxadithia-15-crown-5 as a chelator for Hg^{2+}.

The K_d value of the 1 : 1 Hg^{2+}–**91** complex was determined to be 5.4×10^{-6} M.

Sensor **92** with an open-chain azadioxadithia (NO_2S_2) chelator is a highly selective fluorescent sensor for Hg^{2+} in an aqueous environment.[135] Apo **92** has a low Φ (0.008), indicative of efficient reductive PET from the NO_2S_2 chelator to BODIPY. Addition of Hg^{2+} inhibits PET and simultaneously produces a large increase in fluorescence (Φ 0.58). Fluorometric titration revealed a 1 : 1 stoichiometry for the Hg^{2+}–**92** complex with a K_d of 4×10^{-5} M. The bright fluorescence of the Hg^{2+}–**92** complex is controlled by some anions (Cl^-, Br^-, CO_3^{2-}, SCN^- and $CH_3CO_2^-$). This has been attributed to the significant coordinating ability of these anions to Hg^{2+}. The presence of the aniline function also creates a pH indicator with a low pK_a of 1.97.

Probe **93** exhibits a large, selective fluorescence enhancement towards Hg^{2+} over other metal ions, except Ag^+, Pb^{2+} and Cu^{2+}.[136] In contrast to analogous **92**, reported by the same research group, the fluorescence response of **93** was unaffected by the presence of anions existing in the

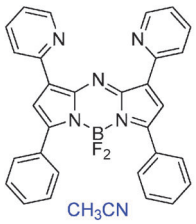

Fig. 33 An azaBODIPY-based indicator for Hg^{2+}.

environment (NO_3^-, AcO^-, Cl^-, ClO_4^-, SO_4^{2-} and $H_2PO_4^-$). Probe **93** formed a 1 : 1 complex with Hg^{2+} with a K_d of 5 μM (Fig. 34).

Derivative **94** containing a tridentate diazaoxa (N_2O) chelator was synthesized as a fluorescent turn-on sensor with high selectivity for Hg^{2+} over other cations in an aqueous environment.[137] The very weak fluorescence of apo **94** was attributed to reductive PET. Upon Hg^{2+} chelation, the fluorescence increases *ca.* 27-fold with a virtually unchanged λ_{em} position (~509 nm). A global K_d value of 6.3×10^{-19} M^2 was determined for the 2 : 1 Hg^{2+}–**94** complex. Derivative **94** can be used for intracellular monitoring/imaging of Hg^{2+}.

A highly selective fluorescence turn-on response in the presence of Hg^{2+} over other metal ions (Li^+, Na^+, K^+, Ca^{2+}, Mg^{2+}, Pb^{2+}, Fe^{2+}, Co^{2+}, Ni^{2+}, Cu^{2+}, Zn^{2+}, Cd^{2+}, Ag^+, Mn^{2+}) was found for probe **95** (Fig. 35).[138] Theoretical calculations of the energy levels indicated that reductive PET from the aniline subunit to excited-state BODIPY is responsible for the low Φ (0.003) of apo **95**. In metal complexes, the frontier MO energy levels change to a great extent. For the Hg^{2+}–**95** complex, both reductive and oxidative PETs are prohibited, and therefore, strong fluorescence BODIPY emission (Φ 0.13) was observed without pronounced spectral shifts.

Three fluorescent PET sensors **96** were designed by Wang and Qian to provide an insight into what constitutes a chelator for Hg^{2+}. Molecules **96a**, **96b** and **96c** were synthesized by incorporating two, three and four amide arms into the aniline, *o*-hydroxyaniline and *o*-phenylenediamine subunits, respectively, attached at the *meso*-position of the BODIPY platform (Fig. 36).[139] Compounds **96** have similar absorption spectra in the absence or presence of Hg^{2+} (λ_{abs} 523 nm). Before addition of Hg^{2+}, they are weakly fluorescent due to reductive PET. Addition of Hg^{2+} to **96b** and **96c** efficiently blocks the PET quenching pathway. The fluorescence quantum yield increases without noticeable shifts of λ_{em}. A Job's plot indicated that sensor **96b** chelates Hg^{2+} with a 1 : 1 stoichiometry (K_d 20 μM). Sensor **96c** can accommodate two Hg^{2+} ions to form a 2 : 1 Hg^{2+}–**96c** complex with a bridging H_2O molecule where each Hg^{2+} ion is coordinated by three nitrogen atoms of one diamide arm. K_d values for the 1 : 1 and 2 : 1 Hg^{2+}–**96c** complexes were determined to be

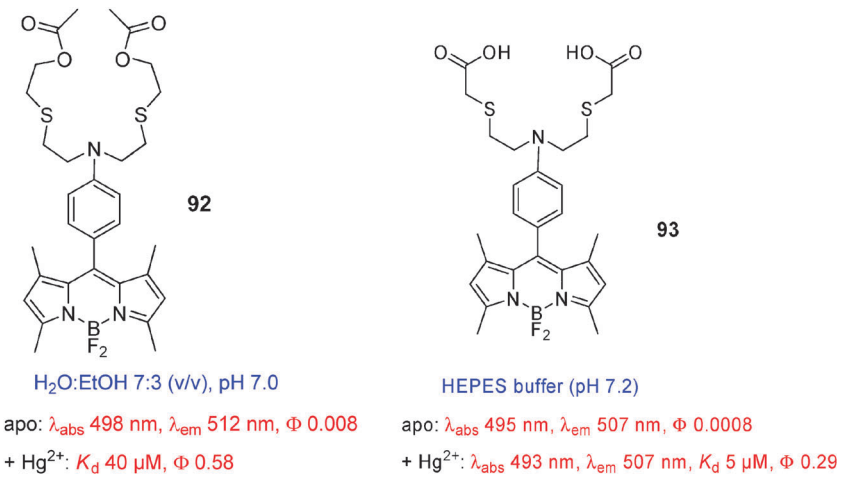

Fig. 34 Open-chain chelators for the sensing of Hg^{2+}.

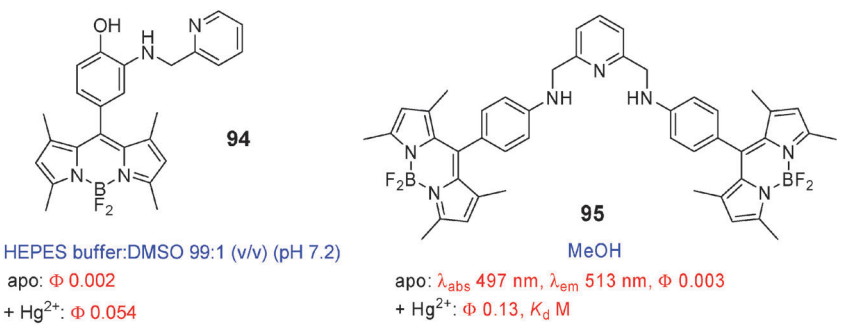

Fig. 35 Turn-on sensors for Hg^{2+}.

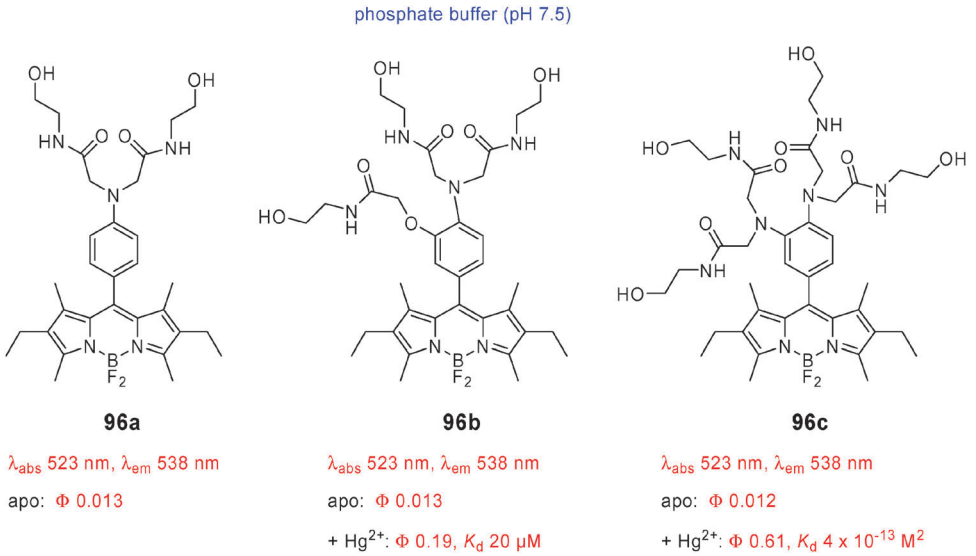

Fig. 36 Comparison of amide-containing BODIPY dyes for Hg^{2+} sensing.

9.1×10^{-7} M and 4.2×10^{-7} M^2, respectively. In sharp contrast, compound **96a** does not exhibit any measurable fluorescence intensity change in the presence of Hg^{2+}; obviously **96a** does not form a complex with Hg^{2+}.

A fluorescent, ratiometric probe based on a BODIPY–rhodamine RET system was used for detecting Hg^{2+} in ethanol:water solution and in live cells.[140] Leuco-rhodamine derivative **97a** was chosen as a Hg^{2+} detector. A Hg^{2+} induced ring-opening reaction generates the long-wavelength rhodamine (in **97b**) which can act as an energy acceptor (Scheme 9). BODIPY was chosen as the energy donor because its fluorescence emission spectrum overlaps well with the absorption spectrum of the energy acceptor rhodamine. The UV-vis spectrum of **97a** showed only the absorption profile of the donor BODIPY and excitation of **97a** at 488 nm resulted in the emission profile of BODIPY (λ_{em} 514 nm, Φ 0.35). Addition of Hg^{2+} promotes the formation of ring-opened compound **97b** and a highly efficient RET process is turned on. Excitation of BODIPY at 488 nm now results in the emission of rhodamine with a λ_{em} of 589 nm (Φ 0.20). Measurement of the fluorescence intensity ratio (F_{589nm}/F_{514nm}) allows the detection of Hg^{2+}.

Dithia-18-benzocrown-6 appended BODIPY **98** displays Hg^{2+} and Ag^{+} selective fluorescence enhancement.[141] The 1 : 1 complex with Hg^{2+} has a K_d of 6.3 μM.

The size-restricted 7-aza-1-oxa-4,10-dithiacyclododecane macrocycle was attached to the *meso*-position of BODIPY *via* a phenyl linker to produce probe **99** for the selective detection of Fe^{3+} in various media.[142] In the polar organic solvents acetonitrile and methanol, **99** exhibits amplified fluorescence (>500 fold) upon Fe^{3+} binding without pronounced spectral shifts (Fig. 37). K_d values of the 1 : 1 Fe^{3+}–**99** complexes in MeCN and MeOH were determined to be $<3.2 \times 10^{-6}$ M and 1.6×10^{-5} M, respectively. In neat as well as buffered aqueous solution, Fe^{3+} binding leads to an increase of the typical BODIPY LE fluorescence (around 510 nm)

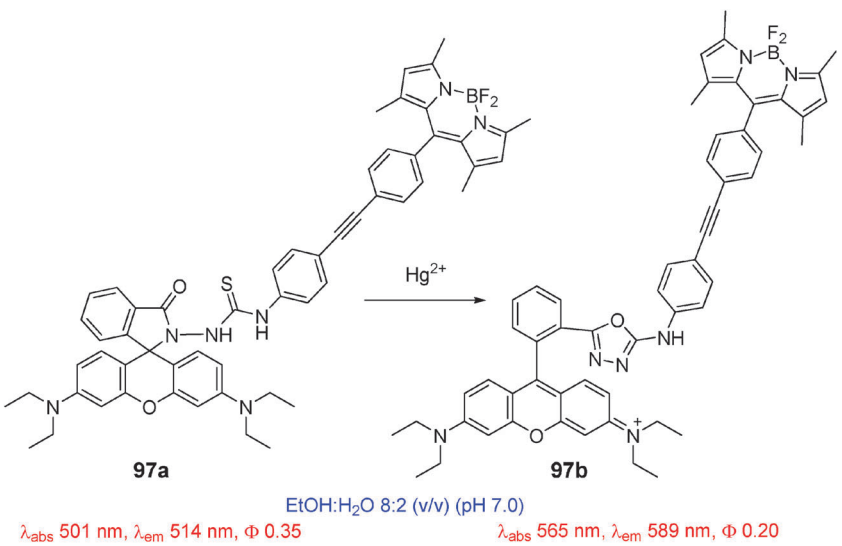

Scheme 9 Hg^{2+} ions induce heterocycle formation and concomitant RET process allows sensing.

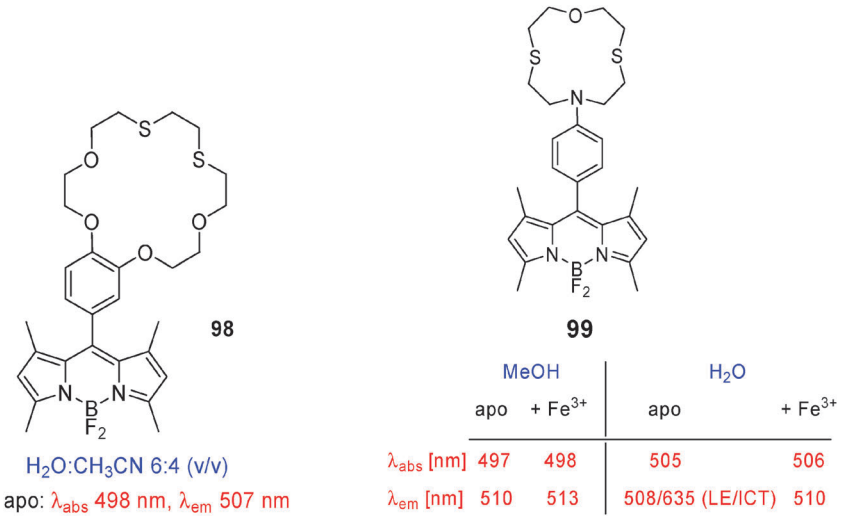

Fig. 37 Sensing of metal ions with sulfur-containing crown ether BODIPY-based dyes.

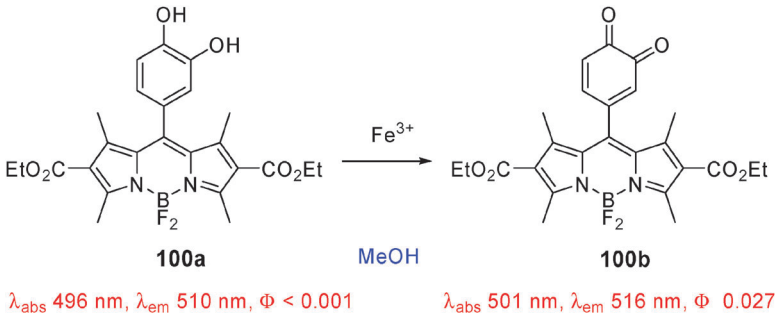

Fig. 38 Fe^{3+} mediated *o*-quinone formation in a catechol-substituted BODIPY.

and a concomitant decrease of the ICT fluorescence (around 630 nm). The formed 1 : 1 Fe^{3+}–**99** complexes in aqueous solution are less stable than those in MeCN and MeOH. K_d values of 6.3×10^{-5} M, 10^{-4} M, and 7.9×10^{-5} M in H_2O, 0.01 M MOPS, and 0.01 M Tris buffer, respectively, were measured.

The *meso*-catechol subunit in **100a** is oxidized to the corresponding *o*-quinone in **100b** by excess $FeCl_3$, $CuCl_2$, $[Co(NH_3)_5Cl]Cl_2$, DDQ, or ceric ammonium nitrate [CAN: $Ce(NH_4)_2(NO_3)_6$] in methanol (Fig. 38).[143] Compound **100a** is virtually nonfluorescent in methanol due to reductive PET from catechol to BODIPY. Upon oxidation to **100b**, significant fluorescence enhancement is observed because PET from the *o*-quinone group to BODIPY becomes energetically unfavorable. ROS such as H_2O_2, $^{\bullet}OH$, $^1O_2$, $O_2^{\bullet-}$, ^-OCl did not drastically change the fluorescence properties of **100a**.

Distyryl BODIPY derivative **101** was reported as a fluorescent probe for the detection of Cr^{3+} (Fig. 39).[144] Ion-free **101** is practically nonfluorescent (Φ 0.003). Binding of Cr^{3+} produces a color change from green to blue and an impressive fluorescence increase (Φ 0.69) without shift of Φ_{em}. 1 : 2 (metal : indicator) and 2 : 2 complexes between Cr^{3+} and **101** were postulated *via* sequential coordination. Job's plot analysis could not provide a clear stoichiometry, however.

6.2. Indicators for anions

6.2.1. Fluoride (F^-). Although anions play decisive roles in a multitude of essential biological processes, the design of selective fluorescent indicators for anions has received much less attention than that for fluoroionophores for cations.

The most popular, reported BODIPY-derived anion sensors/dosimeters are those for fluoride. An unidentified, irreversible reaction of compound **24**[30] with tetrabutylammonium fluoride (TBAF) in acetone solution led to disappearance of the main $S_1 \leftarrow S_0$ absorption band at

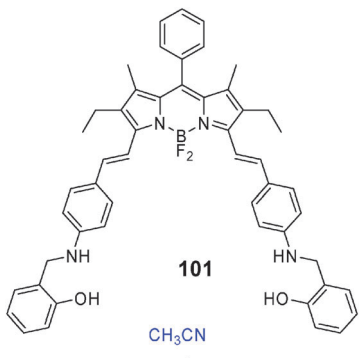

Fig. 39 Sensor with turn-on response to Cr^{3+}.

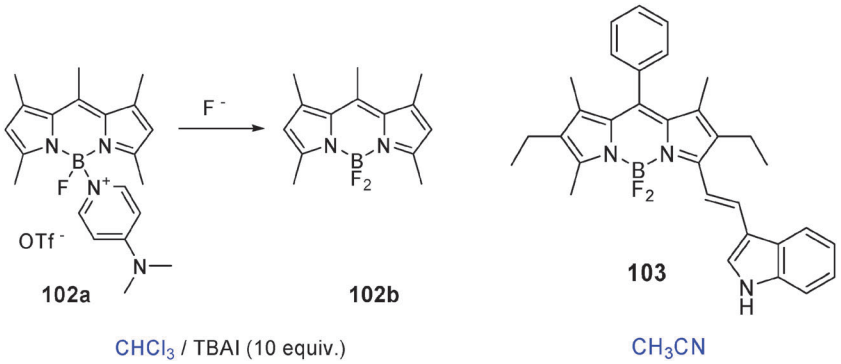

Fig. 40 Fluorescent indicators responsive to fluoride.

599 nm and the emission peak at 686 nm, while the peak intensities at 452 and 482 nm increased.[145]

The cationic adduct of 4-dimethylaminopyridine with BODIPY **102a** reacts with TBAF to yield the strongly fluorescent, neutral BODIPY derivative **102b**.[146] To boost the fluorescence increase upon F^- addition, the reaction was done in the presence of iodide ions. The addition of tetrabutylammonium iodide (TBAI) to **102a** in $CHCl_3$ results in a drastic fluorescence quenching, supposedly by the high sensitivity of the cationic adduct to the external heavy atom effect imparted by I^-. When subsequently TBAF was added, the fluorescence increased spectacularly, due to formation of **102b** and the lower sensitivity of this neutral compound to the external spin–orbit coupling effect of I^-.

Compound **103** has been proposed as a colorimetric and fluorometric probe for selective fluoride detection (Fig. 40).[147] Apo **103** was found to be moderately fluorescent in acetonitrile solution (Φ 0.353). In the presence of fluoride ions, the main absorption band of **103** with λ_{abs} at 599 nm disappeared and a new red-shifted band appeared at 718 nm. At high F^- concentrations, the fluorescence of **103** was completely quenched. These changes have been explained by the authors as driven by a 1 : 1 hydrogen bonding interaction between the indolic NH proton and F^-. However, one cannot exclude complete deprotonation of the indolic NH proton by the rather basic fluoride at high F^- concentrations. A very efficient ICT in the excited state from the indole anion to BODIPY will then completely turn-off the fluorescence. The anions Cl^-, Br^-, I^-, ClO_4^-, HSO_4^-, NO_3^-, ... are not basic enough to deprotonate the indolic NH.

Analogues **104a** and **105a** with trimethylsilylethynyl substituents at the 3,5- (for **104a**) and 8-positions (for **105a**) were deprotected with TBAF in dichloromethane solution.[148] In these irreversible reactions, the electron-rich trimethylsilylethynyl group was converted into the electron-deficient ethynyl function. The absorption and emission maxima of deprotected compound **104b** shifted 20 nm hypsochromically with respect to those of **104a**. As expected, no changes of λ_{abs} and λ_{em} were detected between the *meso*-substituted compounds **105a** and **105b**. Although the authors described compound **104a** as a specific dosimeter for fluoride ions, other anions are capable of inducing cleavage of the $SiMe_3$ group.[149] Conversely, anions such as Cl^-, Br^-, I^-, ClO_4^- and HPO_4^{2-} are known not to cleave the $SiMe_3$ protective group from ethynes. However, a similar response might be observed in the presence of hydroxide and alkoxide anions. Moreover, some transition metal salts, such as Ag(I) and Cu(I), have been shown to deprotect terminal alkynes, and spectroscopic effects may thus be observed in the presence of these metal ions.[150]

A similar desilylation reaction of two silyl ethers **106a–b** was reported by Akkaya *et al.* (Fig. 41).[151] The location of the emerging phenolate group on BODIPY is critical. Removal of the triisopropylsilyl protective group from **106b** by fluoride ions triggers reductive PET and leads to a drastic decrease of fluorescence intensity and a small blue shift (10 nm) of λ_{abs}. In contrast, upon exposure to fluoride ions, the absorption peak of **106a** at 560 nm gradually decreases and a new peak at 682 nm emerges. Deprotection of **106a** generates strong ICT and leads to the formation of the nonemissive phenolate. Although these deprotection reactions were claimed to be highly selective for fluoride, other anions can also cleave silyl ethers. Conversely, Cl^-, Br^-, I^-, AcO^-, CN^-, $H_2PO_4^-$, HSO_4^- and NO_3^- are not known to deprotect silyl ethers under mild conditions. Again, alkylsilyl based protecting groups can be removed under a range of conditions,[149] and because triisopropylsilyl ethers are efficiently cleaved by mild acid, some caution is advised regarding the pH sensitivity of such probes.

6.2.2. Cyanide (CN^-). Reaction of compound **107** with tetrabutylammonium cyanide resulted in a color change from pink to blue (33 nm bathochromic shift of λ_{abs}) and a fluorescence turn-off (Φ 0.01) was attributed to cyanohydrin formation.[152] The reaction is reversible and compound **107** can be restored on the addition of trifluoroacetic acid.

Di(2-picolyl)amine containing dye **108** forms a virtually nonfluorescent complex with Cu^{2+}. Decomplexation of Cu^{2+} ions from this Cu^{2+}–**108** complex (in THF) by CN^- ions (in H_2O) gave tetracyanocuprate ions and restored apo **108** and its concomitant fluorescence (Fig. 42).[153]

6.2.3. Hydrogenphosphate (HPO_4^{2-}) and other anions (F^-, OAc^-, ...). The fluorescence emission intensity of the 1 : 1 Zn^{2+}–**82** complex[55] was found to be highly sensitive to anion (HPO_4^{2-}, F^-, Cl^-, Br^-, and OAc^-) coordination to zinc.[154] In the 1 : 1 Zn^{2+}–**82** complex, oxidative PET from the excited-state BODIPY moiety to the Zn^{2+} chelated bipyridyl group was assumed to be responsible for fluorescence quenching.

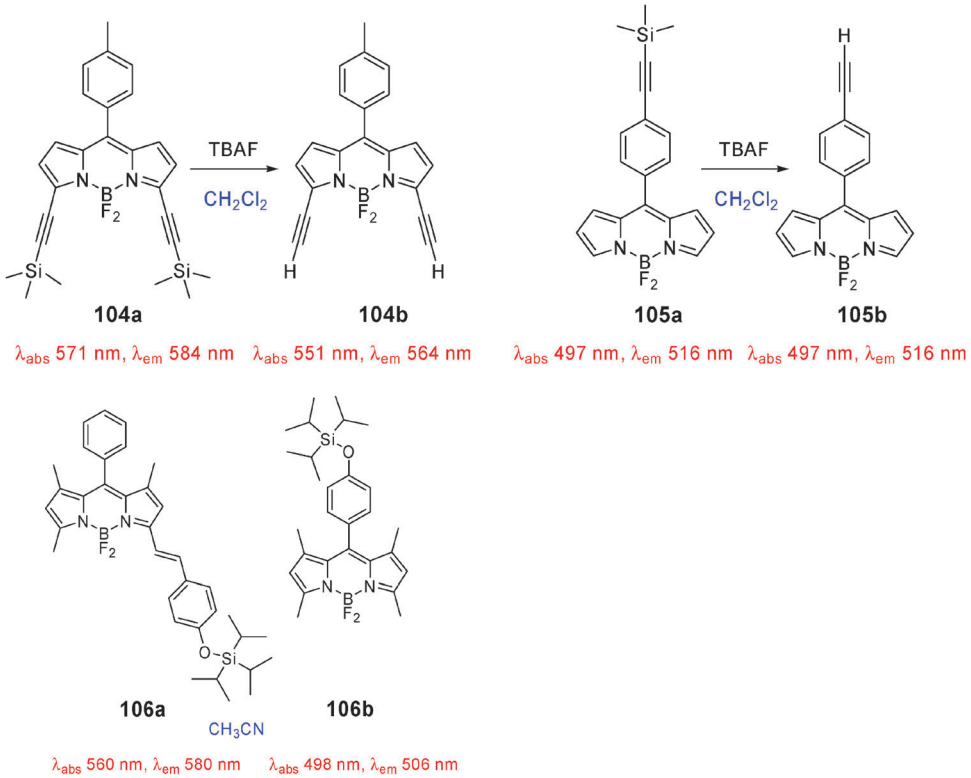

Fig. 41 Fluorescent dosimeters for fluoride based on desilylation reactions.

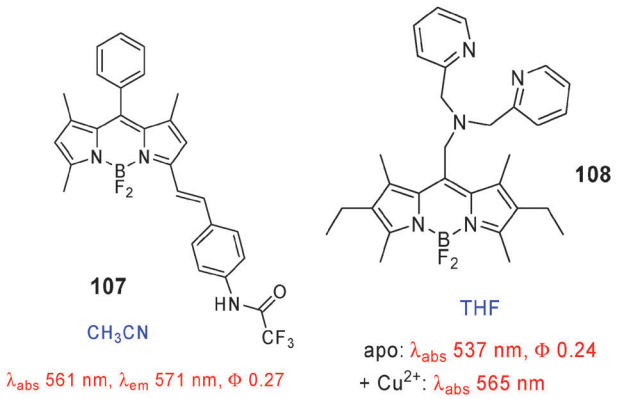

Fig. 42 Cyanide indicators.

Chelation of the anions to the metal center partially neutralizes the charge on the metal center and this turns off the oxidative PET process and restores the full emission intensity of the BODIPY fluorophore. K_d values of the anion complexes with the 1 : 1 Zn^{2+}–**82** complex were similar and ranged from 2.1×10^{-4} M (for OAc^-) to 4.0×10^{-4} M (for Br^-).

BODIPY derivative **109** with a dipicolylaminylethylamine group was reported forming a 1 : 1 complex with Zn^{2+} (Fig. 43).[122] Addition of anions (F^-, HPO_4^{2-}, OAc^-) to this 1 : 1 Zn^{2+}–**109** complex produces large changes in the absorption and emission spectra. Analysis of the electrostatic binding of these anions to the metal center yielded comparable K_d values [(2.2–2.4) $\times 10^{-5}$ M].

6.3. Indicators for biomolecules

6.3.1. Saxitoxin. Compound **110**—with the aza-18-crown-6 ether chelator and the azaBODIPY chromophore—has been used as a visible sensor for the marine toxin saxitoxin, the most toxic component of paralytic shellfish poisons.[155] This sensor is based on the concept of reductive PET. In the absence of saxitoxin, PET from the azacrown ether to the azaBODIPY quenches the fluorescence. Upon complexation of saxitoxin, PET is switched off and fluorescence is turned on. At ~1 : 1

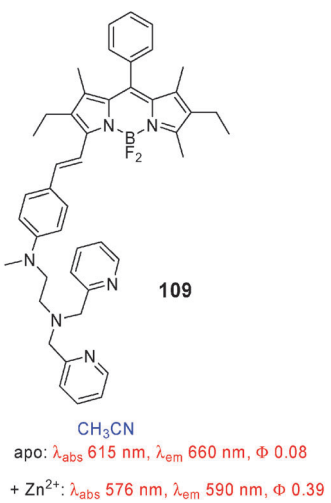

Fig. 43 The 1 : 1 Zn^{2+} complex with **109** is sensitive to several anions.

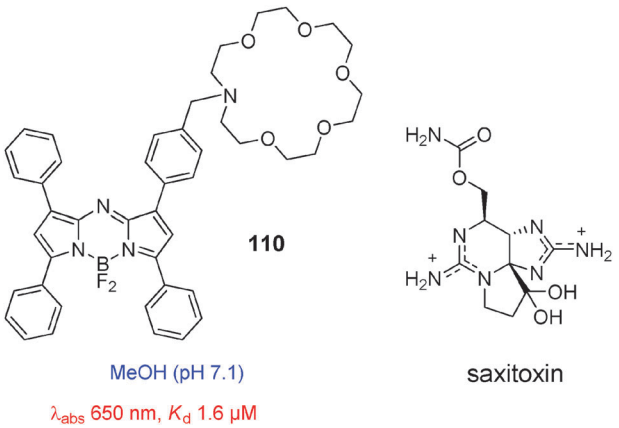

Fig. 44 Fluorescent probe for saxitoxin.

saxitoxin–**110** stoichiometry, the fluorescence enhancement was over 100%. K_d of the 1 : 1 saxitoxin–**110** complex was determined to be 1.6 μM, while an analogous compound with a larger crown ether (aza-27-crown-9 instead of aza-18-crown-6 in **110**) bound the toxin less strongly (K_d 71 μM) and gave insignificant fluorescence enhancement (Fig. 44).

6.3.2. Peptides and proteins. Three BODIPY-based probes with stilbene or diphenylacetylene moieties connected *via* a polyethylene glycol linker of different lengths to the phenylethynyl group at the *meso*-position were synthesized for targeting β-amyloid plaques.[156] However, no experimental evidence was presented that these fluorescent probes bind to β-amyloid plaques.

Triazole containing BODIPY dyes **111** can distinguish between secondary structure conformations of soluble oligomers of amyloid Aβ(1–42) peptide.[157] The fluorescence emission spectra of **111** showed different intensity enhancements in the presence of unordered and ordered, β-sheet-rich Aβ(1–42) soluble oligomers.

BODIPY-derived **112** has been developed as a dual nuclear and fluorescent imaging probe targeting β-amyloid (Aβ) aggregates in the brain.[158] *In vitro* experiments showed that this fluorescent dye has a high affinity for synthetic Aβ(1–42) aggregates and could serve as a probe for detecting Aβ plaques in mouse brain sections. However, additional structural changes are needed to improve its ability to cross the blood–brain barrier.

Fluorescent probe **113** incorporates BODIPY and two Zn^{2+}–di(2-picolyl)amine complexes for the selective detection and visualization of neurofibrillary tangles (NFTs) of hyperphosphorylated tau proteins, materials representative of many neurodegenerative disorders, including Alzheimer's disease.[159] Compound **113** forms 1 : 1 complexes with several tau peptide fragments containing phosphorylated amino acid residues at (i, i + 4) positions, with K_d values in the μM range. The selective detection of NFTs is based on the coordination of **113** with the multiple phosphate groups of the hyperphosphorylated tau proteins. Probe **113** clearly discriminates between NFTs and the plaques assembled from β-amyloid peptide.

Granisetron appended BODIPY derivative **114** was found to bind with high affinity to human serotonin receptors.[160] The BODIPY fluorophore was attached at the N1-position of indazole because it was the most tolerant regarding substitution.

By means of a fluorescence image-based screening against three cell lines, probe **115** was found to selectively stain AlphaTC1 cells, which secrete glucagon.[161] The selectivity of **115** toward glucagon was further confirmed *in vitro*. Apo **115** is weakly fluorescent (Φ 0.012) but becomes markedly more fluorescent in the presence of 200 μM glucagon (Φ 0.151). λ_{abs} and λ_{em} of **115** are hardly influenced by the presence of glucagon (Fig. 45).

6.3.3. Monosaccharides. Boronic acid is an important functional group in the design of receptors and sensors for carbohydrates.[162] The boronic acid-based carbohydrate sensing field is very extensive with a large number of active laboratories. BODIPY functionalized with a phenylboronic acid **116** displayed spectral changes in the absorption and emission spectra in the presence of sugars (D-fructose, D-glucose, D-galactose).[163] The affinity of **116** for the sugars decreased in the order D-fructose > D-galactose > D-glucose (Fig. 46).

6.3.4. Thiol (Cys). Compound **117a** is a fluorescent turn-on dosimeter for the optical sensing and imaging of thiols.[58] The fluorescence of dye **117a** is quenched by oxidative PET from the excited BODIPY fluorophore to the electron-poor 2,4-dinitrobenzenesulfonate moiety. Highly fluorescent phenolic compound **117b** is formed by the thiol-specific S_NAr reaction. The potential of the probe was demonstrated by imaging of thiols in live cells. Based on the same S_NAr reaction with thiols, very comparable fluorescent turn-on dosimeters have been reported by Lu and coworkers[59] (compound **118a**) and Shao *et al.*[60] (compound **119a**). Fluorescence of **118a** and **119a** is also quenched by oxidative PET from the excited BODIPY subunit to the electron-poor 2,4-dinitrobenzenesulfonate moiety. After S_NAr reaction with thiol, derivatives **118b** and **119b** are formed, producing a large fluorescence enhancement. The applicability of probe **118** was demonstrated by the determination of μM levels of non-protein cysteine in human serum. Sensor **119** was used for fluorescent imaging of cellular thiols (Scheme 10).

6.4. Indicators for reactive oxygen species (ROS) and reactive nitrogen species (RNS)

The type of ROS and RNS is diverse including species like superoxide radical anion ($O_2^{\bullet-}$), peroxynitrite ($ONOO^-$), nitrite (NO_2^-), nitric oxide (NO), peroxyl radical ($ROO^\bullet$), hydroperoxyl radical ($HOO^\bullet$), hydroxyl radical ($HO^\bullet$), and alkoxyl radical ($RO^\bullet$). Also included in the definition are molecules such as hypochlorous acid (HOCl), hydrogen peroxide (H_2O_2), nitroxyl (HNO), and electronically excited species like singlet oxygen ($^1O_2$).

Since most of the BODIPY-derived probes for ROS/RNS react irreversibly with the ROS/RNS, their structure is destroyed in the reaction. Hence, these indicators should be labeled as dosimeters.

6.4.1. $ONOO^-$ (peroxynitrite). Peroxynitrite ($ONOO^-$) is a reactive oxygen species (ROS) and reactive nitrogen species

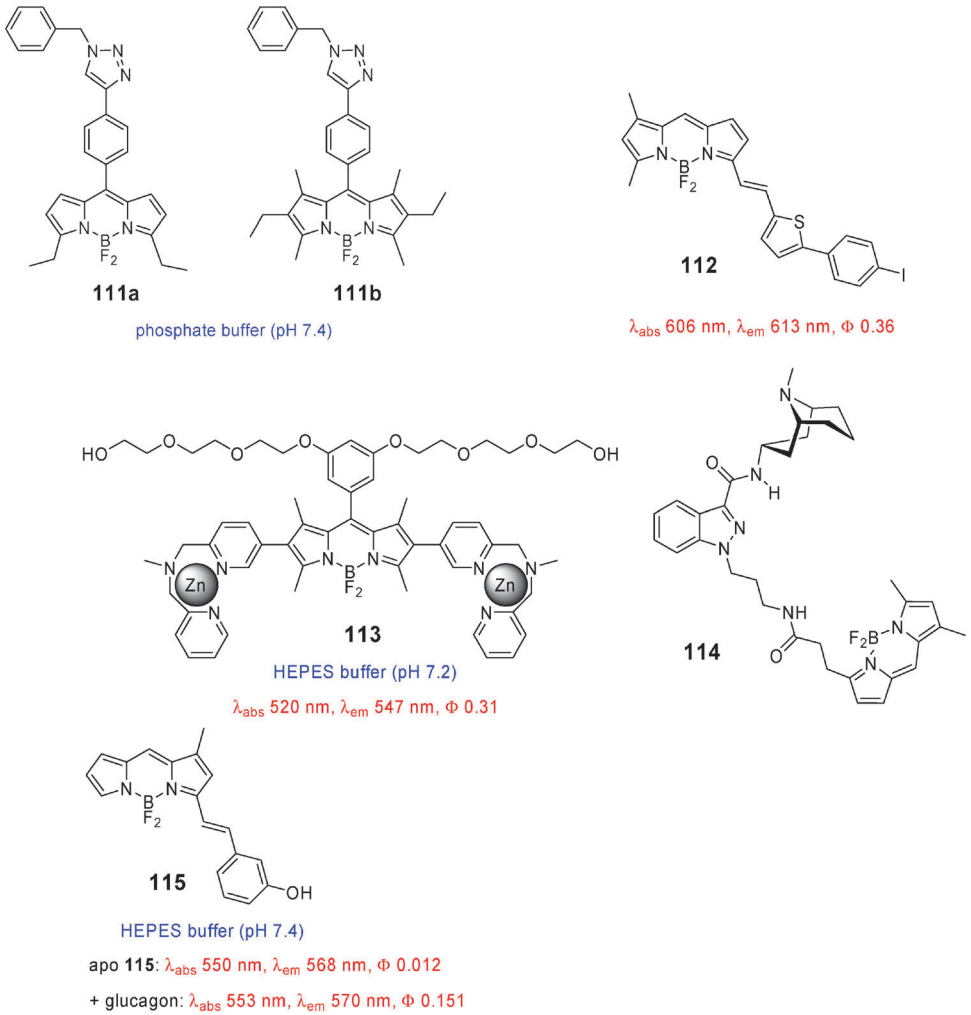

Fig. 45 Protein-sensitive BODIPY-based probes.

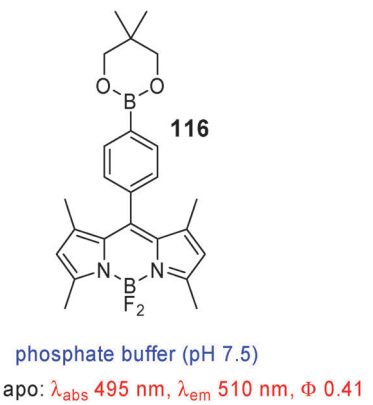

Fig. 46 Indicator for D-fructose, D-glucose and D-galactose.

(RNS). Reaction between nonfluorescent **120a** with peroxynitrite produces fluorescent dye **120b**.[164] Compound **120a** is nonfluorescent due to reductive PET from the phenol subunit to BODIPY. The HOMO of the quinoid structure in **120b** is lower in energy than the HOMO of BODIPY so that the PET process is switched off and fluorescence is turned on. Compound **120a** is highly selective for peroxynitrite: of the other ROS and RNS, only $^{\bullet}OH$ could generate a (weaker) fluorescence response. Probe **120a** was also used for visualizing peroxynitrite in murine macrophage cells treated with various stimulants.

The fluorescence intensity of **121** was dramatically enhanced upon addition of peroxynitrite ($ONOO^-$), a potent nitrating agent. Other ROS ($^{\bullet}OH$, ^-OCl, $^1O_2$, NO, $O_2^{\bullet-}$, H_2O_2) gave little fluorescence augmentation (Fig. 47).[165] Formation of a nitrated product and resultant suppression of the PET process are responsible for the fluorescence intensity increase (see also Section 6.5.2). Compound **121** is applicable for fluorescence imaging of $ONOO^-$ in living cells.

6.4.2. $O_2^{\bullet-}$ (superoxide radical anion). The luminescence of imidazo[1,2-*a*]pyrazin-3(7*H*)-one compounds **122a** has been reviewed recently.[166] In chemiluminescent probes based on **122a**, a fluorophore is one of the R substituents. Reaction of **122a** with ROS generates **122b** in the excited state (indicated by *), which returns to the ground state *via* nonradiative pathways and emission of light.

In compound **123**, the imidazopyrazinone moiety is connected through a direct bond at the 2-position of the fluorophore BODIPY.[167] Dye **123** emits yellow-green luminescence

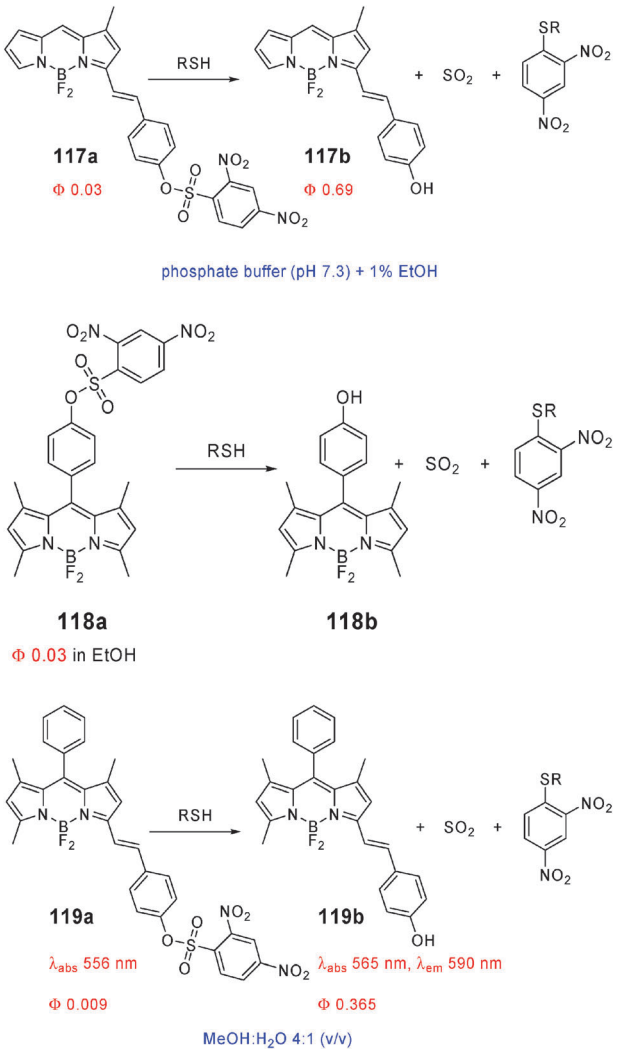

Scheme 10 Fluorescent dosimeters for thiols.

under neutral pH conditions after oxidation by $O_2^{\bullet-}$. λ_{em} of **123** in the presence of ROS was located at longer wavelengths (λ_{em} 545 nm) than the fluorescence emission of BODIPY, suggesting that the emitting species is the fully conjugated **123** with its oxidized imidazopyrazine subunit (see structure **122b**), rather than the BODIPY moiety alone. This is an indication against RET from the excited-state, oxidized imidazopyrazine to BODIPY. Compound **123** provided the highest luminescence response towards $O_2^{\bullet-}$ among the various ROS tested. BODIPY derivative **123** was also used for the detection of ROS generated from stimulated cells.

In lipophilic indicator **124**, the imidazopyrazinone subunit is connected to the *meso*-position of BODIPY *via* a *p*-phenylene linker.[168] The $O_2^{\bullet-}$-induced chemiluminescence of **124** has λ_{em} at 542 nm (Fig. 48).

6.4.3. HOCl (hypochlorous acid). Fluorescent probe **125a** has been developed for the selective detection of HOCl on the basis of a specific reaction with *p*-methoxyphenol yielding *p*-benzoquinone-substituted **125b**.[169] Compound **125a** is almost nonfluorescent ($\Phi < 0.01$) due to reductive PET (the HOMO energy of the *p*-methoxyphenol moiety is higher than that of the BODIPY subunit). After oxidation of the *p*-methoxyphenol subunit of **125a**, the HOMO energy of the *p*-benzoquinone moiety in **125b** is lower that that of the BODIPY core and therefore the PET process is prohibited, so that **125b** is fluorescent. Formation of HOCl has been successfully detected in an abiotic as well as in an enzymatic system and in live macrophage cells upon stimulation (Fig. 49).

6.4.4. ROO$^{\bullet}$ (peroxyl radical). BODIPY–α-tocopherol adduct **126** is a lipophilic fluorescent probe for the detection of peroxyl radicals in model membrane systems and their imaging in the lipid membranes of live cells (Fig. 50).[170,171] Reductive PET from the chromanol moiety to the singlet-excited BODIPY renders **126** nonemissive. Upon peroxyl radical scavenging, oxidation of the chromanol moiety switches off PET, leading to a significant fluorescence enhancement, which is independent of the solution pH and membrane composition.

6.4.5. HNO (nitroxyl). BODIPY derivative **127** forms a 1 : 1 Cu^{2+} complex (K_d 3 × 10^{-6} M) involving the di(2-picolyl)amine chelator and the triazole bridge. This Cu^{2+} complex can be used for the direct detection of HNO in aqueous solution.[56] The fluorescence of **127** (Φ 0.12) is strongly quenched upon formation of the Cu^{2+}–**127** complex (Φ 0.01), supposedly by oxidative PET from excited BODIPY to the bound Cu^{2+} ion. In the presence of HNO, reduction of the Cu^{2+}–**127** complex generates NO(g) and Cu^{+}–**127**, with concomitant restoration of BODIPY fluorescence. Other RNS and ROS (NO, NO_2^-, NO_3^-, $ONOO^-$, H_2O_2, and OCl^-) failed to induce significant fluorescence amplification of the Cu^{2+}–**127** complex, making this system potentially valuable for studying the individual roles of NO and HNO in biology (Fig. 51).

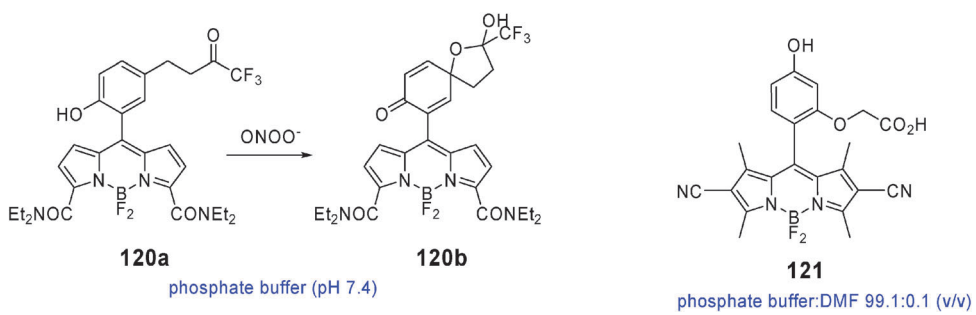

Fig. 47 Fluorescent dosimeters for peroxynitrite.

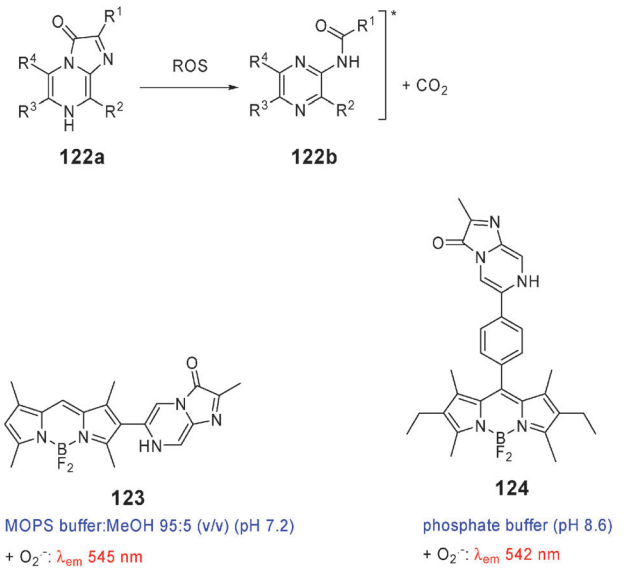

Fig. 48 Fluorescent dosimeters for $O_2^{\bullet -}$.

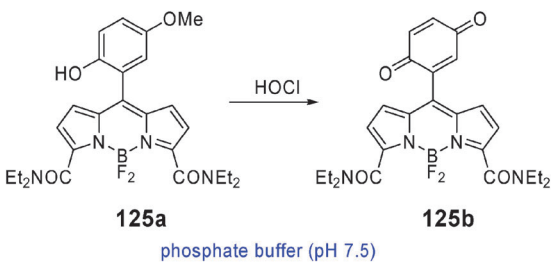

Fig. 49 Fluorescent dosimeter for HOCl.

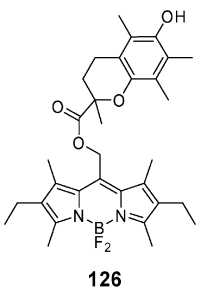

Fig. 50 Fluorescent dosimeter for ROO$^{\bullet}$.

6.4.6. NO_2^- (nitrite). Probe **128** is a BODIPY dye with a *meso p*-aminophenyl substituent for the determination of nitrite.[172] Reaction of nitrite with **128** in acidic solution yields a diazonium salt, which is converted in basic solution to a diazoate, a stable and highly fluorescent compound. Compound **128** has been used to monitor trace nitrite in drinking water and in fresh vegetable without extraction (Fig. 52).

6.4.7. NO (nitric oxide). Free radical nitric oxide (NO) is an essential molecule for cellular signal transduction. NO plays a crucial role in signal transduction pathways in the cardiovascular[173] and nervous systems[174] and is a vital component of the cytostatic/cytotoxic function of the immune

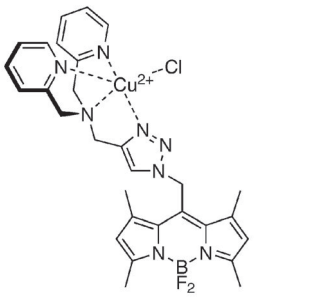

Fig. 51 Fluorescent dosimeter for nitroxyl.

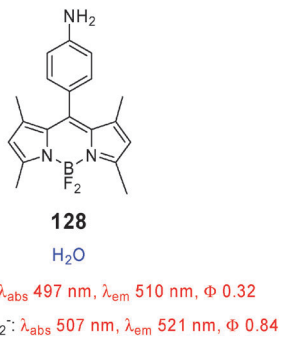

Fig. 52 Fluorescent dosimeter for NO_2^-.

system.[175–177] The literature on fluorescent indicators for NO has been reviewed recently.[178] Nearly all the probes for detection of NO are aromatic vicinal diamines. The changes in fluorescence of these organic molecules require reactions with intermediate RNS and not with NO itself. Therefore, their fluorescence response does not necessarily reflect real-time NO production. A 1 : 1 Cu^{2+} complex of a fluorescein derivative (Φ 0.077) allows for the direct detection of NO by the irreversible reduction of the complex to Cu^{+} with release of the bright nitrosylated fluorophore (Φ 0.58). This derivative showed selectivity for NO over other ROS and RNS.[179]

All reported BODIPY-derived probes for the detection of NO employ the *o*-phenylenediamine scaffold on the *meso*-position which is converted to the corresponding benzotriazole group upon reaction with NO in the presence of O_2 or with $NaNO_2$ and HCl.

Compound **129a** is the first example of a BODIPY-based probe for NO.[180,181] The benzotriazole-forming reactions of **129a** and **131** with $NaNO_2$ + HCl have been used also for the detection of nitrite.[182,183] Additional probes for NO have been reported by Nagano and coworkers (**129b–e**, **132**)[181,184] and H.-S. Zhang *et al.* (**133**, **134**).[20,185] The spectral properties and fluorescence quantum yields of **129a** and **130a** reported by Nagano *et al.*[181] are completely divergent from those of Zhang and coworkers.[180] Conversion of the diamino dyes **129** to the corresponding benzotriazole derivatives **130** caused little change of λ_{abs} and λ_{em} but greatly increased Φ, a typical feature of probes based on the reductive PET mechanism

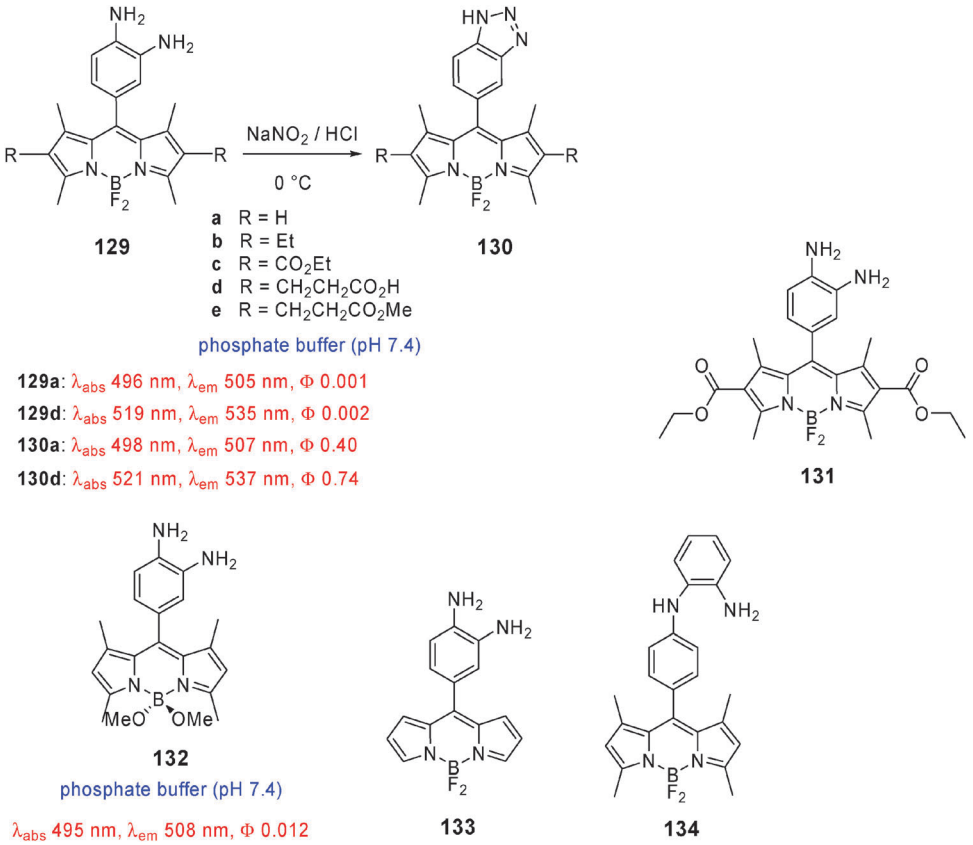

Fig. 53 Fluorescent dosimeters for NO.

(Fig. 53).[181] A similar increase in Φ values was found when **132** (Φ 0.012) was converted to its corresponding benzotriazole derivative (Φ 0.496). The high selectivity of these *o*-phenylenediamine-derived probes for NO under aerated conditions has contributed to their success, because the fluorescent benzotriazole product is not formed by reaction with the ROS superoxide ($O_2^{\bullet-}$), hydrogen peroxide (H_2O_2) or peroxynitrite ($ONOO^-$).

6.4.8. H_2O_2 (hydrogen peroxide). In an endeavor to develop reusable redox-responsive fluorescent indicators, the reversible quinone–hydroquinone couple was used. Compound **135a** contains the hydroquinone group which can be oxidized to the quinone moiety in **135b** (Fig. 54).[186] The process to convert the quinone back to the hydroquinone is fully reversible. The quinone group is an excellent electron acceptor. Hence, fluorescence of **135b** (quinone) is efficiently quenched by oxidative PET from the BODIPY fluorophore to the quinone group ('off' state), but not in **135a** (hydroquinone; 'on' state). This is the opposite effect of how probes **125** and **136** operate. Fluorescence from **135a** in water containing 5% (v/v) Triton-X fades as hydrogen peroxide converts the hydroquinone to quinone (**135b**). Unlike the irreversible ROS detectors (*i.e.*, dosimeters) the system can be re-set, because addition of sodium ascorbate reduces the quinone back to the hydroquinone form. Cycling of the reversible system between 'on' and 'off' can be repeated many times with no obvious drop in performance. The indicator system **135** can be catalogued also as a redox-responsive system (6.5.1).

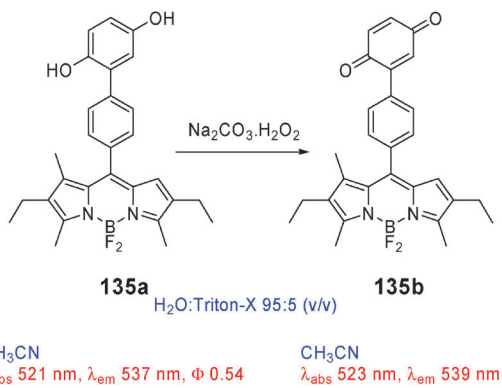

Fig. 54 Fluorescent indicator for H_2O_2.

6.5. Indicators for other phenomena

All the fluorescent indicators discussed in Sections 6.1–6.4 transform *chemical* information (*e.g.*, the presence of an analyte) into a spectroscopically useful signal. These indicators are adequately described by the usual definition given in the Introduction. However, the probes in Section 6.5 warrant a more general definition, because they are responsive to sometimes purely *physical* phenomena. A fluorescent probe can then be defined generally as a compound capable of converting any chemical and/or physical information of the probe's environment into a functional fluorescence output signal.

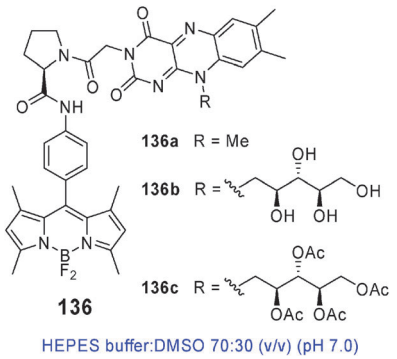

Fig. 55 Fluorescent sensor for redox potential.

6.5.1. Redox potential. In fluorescent redox potential sensors **136**, flavin was connected to BODIPY *via* an L-proline linker.[187] The fluorescence of **136a** was considerably quenched when the flavin subunit was in the reduced form (Φ 0.05, 'off' state) compared to the oxidized form (Φ 0.31) ('on' state, as shown in Fig. 55), presumably by reductive PET from reduced flavin to BODIPY. This is precisely the opposite effect of how indicator **135** operates. Compounds **136** were shown to reversibly respond to the thiol–disulfide equilibria associated with intracellular thiols such as glutathione and thioredoxin, which play a critical role in regulating structures and functions of proteins. Hela cells stained with **136a** could be cycled through a readily observable fluorescence change by the successive additions of $Na_2S_2O_4$ (leading to 'off' state) and H_2O_2 (producing 'on' state).

6.5.2. Nitration. Nitration of the aromatic *meso*-substituent in **137a** lowers the HOMO energy level significantly, so that reductive PET to BODIPY is switched off and compound **137b** becomes highly fluorescent (Fig. 56).[188] Conversely, the nitrile functional groups on BODIPY lower the LUMO energy level of BODIPY due to their electron-withdrawing effect, so that oxidative PET from excited BODIPY to the *meso*-nitroaromatic group in **137b** is suppressed. As a result, the nitro group induces fluorescence, whereas the common idea is that this group is a fluorescence quencher. The transformation of **137a** into **137b** and the ensuing fluorescence enhancement demonstrate that by judiciously controlling the MO energy levels of BODIPY and *meso*-substituent *vis-à-vis* each other the reductive and oxidative PET processes can be switched 'on' or 'off'.

6.5.3. Hydrolysis of esters. Hydrolysis of the esters at the 2,6-positions of **138a** to the corresponding carboxylates **138b** leads to 15–20 nm bathochromic shifts of the excitation and

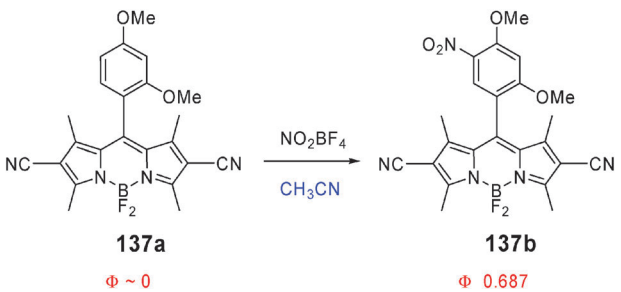

Fig. 56 Fluorescent dye responsive to nitration.

emission maxima in **138b** attributed to a mitigation of the electron-withdrawing capacity of esters (in **138a**) compared to carboxylates (in **138b**) (Fig. 57).[189] The spectral changes can be used to detect esterase activity in living cells.

6.5.4. Biocatalytic Diels–Alder reactions. Dyads **139a–b** are water-soluble fluorescent sensors for investigating RNA-catalyzed Diels–Alder reactions.[190] These probes consist of anthracene and sulfonated BODIPY fluorophores linked at the *meso*-position by conjugated phenylethynyl bridges. Anthracene in **139a–b** efficiently quenches BODIPY fluorescence, supposedly by reductive PET. The differences in Φ of **139a** (0.006) and **139b** (0.014) correlate well with the degree of conjugation between anthracene and the phenylethynyl bridge. Upon destruction of the anthracene group of **139b** by the Diels–Alder reaction, the fluorescence emission intensity of **139c** increases 20-fold (Φ 0.30) (Fig. 58). Binding in the hydrophobic catalytic pocket of a Diels–Alderase RNA increases significantly the fluorescence anisotropy of **139a–c** compared to aqueous Diels–Alderase (DAse) buffer or aqueous solution. Using fluorescent probes **139a–b**, RNA-catalyzed Diels–Alder reactions were monitored under single- and multiple-turnover conditions, down to the single-molecule level.

6.5.5. Viscosity. Viscosity is one of the important, physical parameters determining the diffusion rate of species in condensed media, including biological systems. While methods for measuring the macroscopic viscosity are well developed, methodologies based on fluorescence for investigating the "local" viscosity on the microscopic level (*e.g.*, within a cell membrane or within the cytosol of a cell) are rather new. The inherent drawbacks of conventional methods for measuring viscosity hamper real-time viscosity measurements. Conversely, fluorescence-based techniques such as fluorescence anisotropy[191] and fluorescence recovery after photobleaching[192,193] provide viscosity data with high spatial and temporal resolution. Very recent and promising developments employ fluorescent molecular rotors based on BODIPY (Fig. 59) that operate on the principle of hindered intramolecular rotation. Lindsey, Holten and coworkers[194] showed that the fluorescence quantum yield Φ and fluorescence lifetime τ of the S_1 excited state for 8-phenylBODIPY or 8-(4-*tert*-butylphenyl)BODIPY were significantly smaller than those for the sterically hindered analogues having an *o*-tolyl or mesityl group at the 8-position. It was proposed that free rotation of the 8-aryl group enhances nonradiative deactivation of the S_1 excited state. As a result, restriction of rotation of the 8-aryl substituent would reduce the nonradiative decay of S_1 and lead to higher Φ and τ values.

BODIPY derivative **140**[195] having a *p*-substituted phenyl group at the *meso*-position was used to image local microviscosity in live cells *via* fluorescence lifetime imaging microscopy (FLIM).[196,197] The increase of the fluorometric parameters Φ and τ and the rotational relaxation time θ of **140** with increasing solvent viscosity in methanol–glycerol mixtures is consistent with the hindered rotation of the *meso*-phenyl group in the medium of high viscosity. Confocal time-resolved fluorescence images of incubated cells containing **140** indicated a narrow distribution of τ (1.4–1.8 ns),

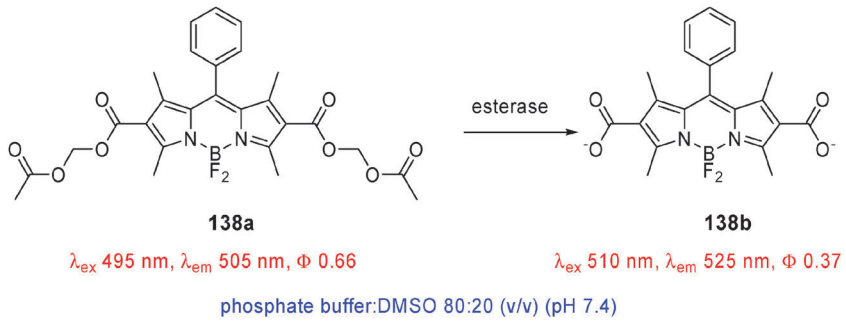

Fig. 57 Fluorescent dye sensitive to hydrolysis of its ester functions.

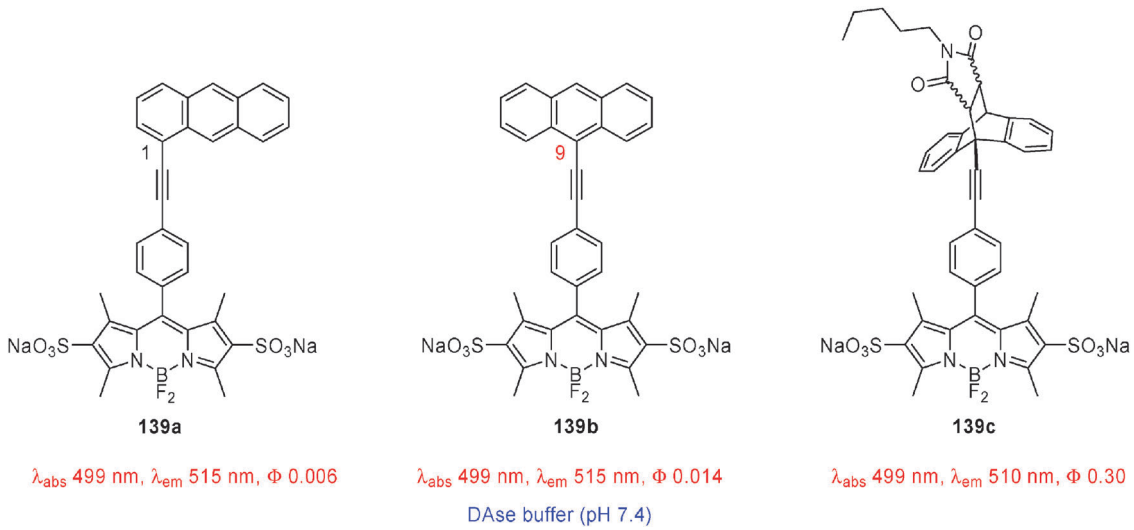

Fig. 58 Anthracene–BODIPY dyads **139a–b** as sensors for biocatalytic Diels–Alder reactions and the product **139c** of the Diels–Alder reaction between **139b** and *N*-pentylmaleimide as dienophile.

corresponding to an intracellular viscosity of *ca.* 140 cP. The average value of θ in cells was 1.1 ns, corresponding to a microviscosity of *ca.* 80 cP, in fair agreement with that obtained from FLIM.

A molecular rotor having two BODIPY fluorophores linked *via* a flexible chain (compound **141**) was proposed by Benniston, Harriman *et al.*[198] to measure the viscosity of the surrounding medium. It was shown that Φ and τ of **141** increase with increasing solvent viscosity in a homologous series of unbranched alkanols. The rate constant of nonradiative deactivation of S_1 decreases with increasing viscosity, while the rate constant of fluorescence remains reasonably constant. A key point in the mechanism by which the probe responds to changes in local viscosity is the structural distortion of the dipyrromethene framework that accompanies rotation of the *meso*-phenyl ring.

Ferrocene–BODIPY dyad **142** is a molecular rotor displaying significant enhancement of Φ as the solvent viscosity increases.[199] The viscosity-dependent properties of **142** were investigated in THF–ethylene glycol mixtures of varying viscosity.

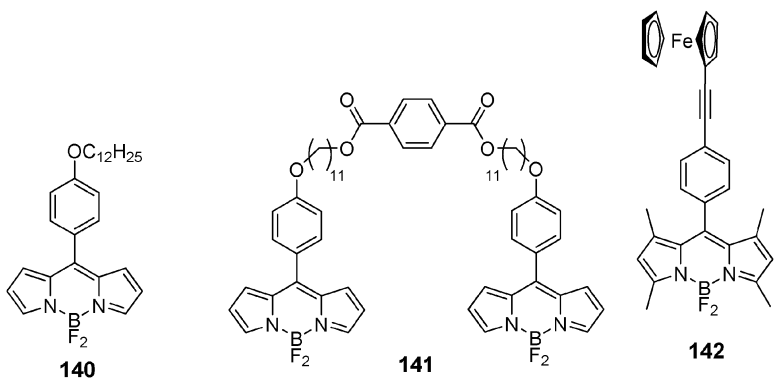

Fig. 59 Fluorescent molecular rotors for measurement of local viscosity.

Φ increased dramatically as the fraction of ethylene glycol increased. In low viscosity H_2O–THF mixtures, the fluorescence intensity of **142** varied linearly with the water fraction up to 60% H_2O. Since rotation of the *meso*-phenyl ring in **142** is restricted by the 1,7-dimethyl substituents of BODIPY, the critical factor for the nonradiative decay of **142** should be the rotation of the ferrocene subunit around the axis of the ethynyl group.

7. Conclusion and perspectives

In this critical review, we have given an overview of the developments for the period 1997–2010 in the area of fluorescent indicators built on the BODIPY scaffold. Although many such fluorescent probes have been described in the literature, only a relatively small number of them have found applications in environmental and biological milieus. We hope this review has emphasized the importance of rational design for developing 'ideal' probes for the many analytes that need to be detected, monitored and/or visualized. Since BODIPY already offers an outstanding fluorophore platform, the design work should focus primarily on constructing suitable chelators for specific analytes.

The versatility of the BODIPY scaffold is due to its synthetic adaptability. Recent progress in BODIPY chemistry makes it possible to build dyes by postfunctionalization of the BODIPY core rather than by starting from appropriately substituted pyrroles. By connecting suitable binding sites to the BODIPY nucleus at any position of the fluorophore, a wide range of fluorescent detectors can be realized. The photophysical mechanism of operation of the sensor can be switched depending on the position of the coordination site. In other words, each location of attachment can elicit different properties for the same receptor. The near-orthogonal geometries of BODIPY core and aromatic residues attached to the *meso*-position can minimize electronic communication between these subunits. Conversely, substituents at the pyrrole positions allow coplanar geometries that maximize electronic coupling. Organic moieties at the boron center have minimal effect on their spectroscopic properties, but they expand the variety of derivatives that can be made. For instance, efficient RET from a high-energy absorbing chromophore (*e.g.*, pyrene) at boron to the low-energy boradiazaindacene emitter can provide large virtual Stokes shift[200,201] and can be applied in suitably engineered sensors. Functional groups suitable for increasing the solubility in aqueous medium or for labeling biomolecules can be introduced at the boron center with minimal disturbance of the excellent spectroscopic properties of the BODIPY core. Attractive asymmetric dyes can be designed combining a chelator at one pyrrole site and a chromophore that moves the spectra to the red or NIR region at another pyrrole position.

There is still much scope to improve the chelators to satisfy the design criteria described in Section 3.1, such as high selectivity, fast reversible chelation, water solubility, fluorescence bio-imaging capacity, a feasible synthetic route, *etc.* Hence, improving the design of the coordination site is the key issue in order to create truly functional probes for environmental and biological applications.[202] Although very selective receptor groups are known for some analytes—*e.g.* BAPTA with high affinity for Ca^{2+}, APTRA as a chelator for Mg^{2+}, with low affinity for Ca^{2+}, . . .—considerable advances, such as reported in K^+ biosensing,[203] have to be made. Multidisciplinary collaboration between organic synthetic chemists, spectroscopists, physiologists, biochemists, materials scientists, . . . might facilitate this process. These novel probes will significantly expand the knowledge of the role of many analytes in environmental and biological systems.

There is a huge unfulfilled need for sensitive and selective sensors for detection and visualization of physiologically important *anions* in an aqueous environment. The number of indicators for anions is limited when compared to the abundance of probes for (metal) cations. Perhaps the most urgently needed receptors are those for chloride, because of their role in chloride channels and carriers. Most of the commercially available chloride probes are 6-methoxyquinolinium or acridinium derivatives that work on the principle of fluorescence quenching.[3] The loading of these indicators is done *via* long-term incubation requiring large dye excess or by hypotonic permeabilization. The limited selectivity, rapid leakage and low brightness of these indicators together with the need for UV-excitation for the 6-methoxyquinolinium analogues are unfavorable characteristics. In addition, the design and synthesis of sensitive, selective and user-friendly indicators for other physiologically relevant anions, such as phosphate and hydrogen carbonate (HCO_3^-) ions, also present a great challenge. The field of anion recognition requires further progress to achieve Nature's efficiency in strong and selective anion binding.

Biological applications require water-soluble and membrane-permeable probes which are well retained within the cytosol. These seemingly conflicting conditions have been fulfilled elegantly by R. Y. Tsien and coworkers,[50] who proposed membrane permeable dyes with attached esters which diffuse into cells where they are hydrolyzed by esterases to afford the charged form of these compounds. Good retention inside cells demands the creation of several negative charges and this implies several ester functionalities on the BODIPY core. The effect of the attachment of esters on the properties of BODIPY will have to be investigated. Finally, it is evident that NIR probes are favored for biological measurements. The design strategy for constructing NIR BODIPY derivatives with high brightness mainly aims at extending the conjugation length and introducing conformationally constrained (*i.e.*, rigid and fused) rings.[28,200,204–206]

8. Glossary of abbreviations

APTRA	*o*-aminophenol-*N*,*N*,*O*-triacetic acid
BAPTA	1,2-bis(*o*-aminophenoxy)ethane-*N*,*N*,*N*′,*N*′-tetraacetic acid
BODIPY	difluoro*bo*ron *dipy*rromethene or 4,4-difluoro-4-bora-3*a*,4*a*-diaza-*s*-indacene
DAse buffer	aqueous Diels–Alderase buffer (300 mM NaCl, 30 mM Tris·HCl, pH 7.4, 80 mM $MgCl_2$, 10% EtOH)
DDQ	2,3-dichloro-5,6-dicyano-*p*-benzoquinone
DMSO	dimethyl sulfoxide

EtOH	ethanol
FLIM	fluorescence lifetime imaging microscopy
HEPES	4-(2-hydroxyethyl)piperazine-1-ethanesulfonic acid
HOMO	highest occupied molecular orbital
HTM	heavy and transition metal
ICT	intramolecular charge transfer
K_d	ground-state dissociation constant
K_s	ground-state stability constant ($K_s = 1/K_d$)
LE state	locally excited state, Franck–Condon state
LUMO	lowest unoccupied molecular orbital
M	mole per dm^3
MeCN	acetonitrile
MeOH	methanol
MO	molecular orbital
MOPS	3-(*N*-morpholino)propanesulfonic acid
NIR	near-infrared
NO	nitric oxide
PET	photoinduced electron transfer
PIPES	piperazine-*N*,*N*′-bis(2-ethanesulfonic acid)
RET	resonance energy transfer
RNA	ribonucleic acid
RNS	reactive nitrogen species
ROS	reactive oxygen species
S_NAr	nucleophilic aromatic substitution
TBAF	tetrabutylammonium fluoride (Bu_4NF)
TBAI	tetrabutylammonium iodide (Bu_4NI)
THF	tetrahydrofuran
Tris	tris(hydroxymethyl)aminomethane
$\varepsilon(\lambda)$	molar absorption coefficient at excitation wavelength λ
Φ	fluorescence quantum yield
λ_{abs}	wavelength of maximal absorbance
λ_{em}	wavelength of maximal fluorescence emission spectral radiant power
λ_{ex}	wavelength of maximal fluorescence excitation spectral radiant power
τ	fluorescence lifetime (decay time)

Acknowledgements

The 'Instituut voor de aanmoediging van innovatie door Wetenschap en Technologie in Vlaanderen' (IWT) is acknowledged for a fellowship to VL.

References

1 A. Loudet and K. Burgess, *Chem. Rev.*, 2007, **107**, 4891–4932.
2 G. Ulrich, R. Ziessel and A. Harriman, *Angew. Chem., Int. Ed.*, 2008, **47**, 1184–1201.
3 R. P. Haugland, *The Handbook. A Guide to Fluorescent Probes and Labeling Technologies*, *Molecular Probes*, Invitrogen, Carlsbad, CA, 10th edn, 2005.
4 A. Treibs and F.-H. Kreuzer, *Justus Liebigs Ann. Chem.*, 1968, **718**, 208–223.
5 A. C. Benniston and G. Copley, *Phys. Chem. Chem. Phys.*, 2009, **11**, 4124–4131.
6 Life Technologies (formerly Invitrogen). Web site: http://probes.invitrogen.com.
7 T. E. Wood and A. Thompson, *Chem. Rev.*, 2007, **107**, 1831–1861.
8 T. Rohand, E. Dolusic, T. H. Ngo, W. Maes and W. Dehaen, *ARKIVOC*, 2007, **10**, 307–324, and references cited therein.
9 M. Shah, K. Thangaraj, M.-L. Soong, L. T. Wolford, J. H. Boyer, I. R. Politzer and T. G. Pavlopoulos, *Heteroat. Chem.*, 1990, **1**, 389–399.
10 J. H. Boyer, A. M. Haag, G. Sathyamoorthi, M.-L. Soong, K. Thangaraj and T. G. Pavlopoulos, *Heteroat. Chem.*, 1993, **4**, 39–49.
11 Z. Li, E. Mintzer and R. Bittman, *J. Org. Chem.*, 2006, **71**, 1718–1721.
12 V. P. Yakubovskyi, M. P. Shandura and Y. P. Kovtun, *Eur. J. Org. Chem.*, 2009, 3237–3243.
13 L. Wu and K. Burgess, *Chem. Commun.*, 2008, 4933–4935.
14 M. Rogers, *J. Chem. Soc.*, 1943, 590–596.
15 W. Davies and M. Rogers, *J. Chem. Soc.*, 1944, 126–131.
16 E. Knott, *J. Chem. Soc.*, 1947, 1196–1201.
17 T. H. Allik, R. E. Hermes, G. Sathyamoorthi and J. H. Boyer, *Proc. SPIE-Int. Soc. Opt. Eng.*, 1994, **2115**, 240–248.
18 J. Killoran, L. Allen, J. F. Gallagher, W. M. Gallagher and D. F. O'Shea, *Chem. Commun.*, 2002, 1862–1863.
19 A. Gorman, J. Killoran, C. O'Shea, T. Kenna, W. M. Gallagher and D. F. O'Shea, *J. Am. Chem. Soc.*, 2004, **126**, 10619–10631.
20 X. Zhang and H.-S. Zhang, *Spectrochim. Acta, Part A*, 2005, **61**, 1045–1049.
21 W. Zhao and E. M. Carreira, *Chem.–Eur. J.*, 2006, **12**, 7254–7263.
22 M. Liras, J. Bañuelos Prieto, M. Pintado-Sierra, F. López Arbeloa, I. García-Moreno, Á. Costela, L. Infantes, R. Sastre and F. Amat-Guerri, *Org. Lett.*, 2007, **9**, 4183–4186.
23 Y.-W. Wang, A. B. Descalzo, Z. Shen, X.-Z. You and K. Rurack, *Chem.–Eur. J.*, 2010, **16**, 2887–2903.
24 S. Shimizu, N. Watanabe, T. Kataoka, T. Shoji, N. Abe, S. Morishita and H. Ichimura, *Pyridine and Pyridine Derivatives*, *Ullmann's Encyclopedia of Industrial Chemistry*, Wiley-VCH, 2000.
25 K. Rurack, M. Kollmannsberger and J. Daub, *New J. Chem.*, 2001, **25**, 289–292.
26 E. Deniz, G. C. Isbasar, Ö. A. Bozdemir, L. T. Yildirim, A. Siemiarczuk and E. U. Akkaya, *Org. Lett.*, 2008, **10**, 3401–3403.
27 Z. Dost, S. Atilgan and E. U. Akkaya, *Tetrahedron*, 2006, **62**, 8484–8488.
28 Y.-H. Yu, A. B. Descalzo, Z. Shen, H. Röhr, Q. Liu, Y.-W. Wang, M. Spieles, Y.-Z. Li, K. Rurack and X.-Z. You, *Chem.–Asian J.*, 2006, **1**, 176–187.
29 M. Baruah, W. Qin, C. Flors, J. Hofkens, R. A. L. Vallée, D. Beljonne, M. Van der Auweraer, W. M. De Borggraeve and N. Boens, *J. Phys. Chem. A*, 2006, **110**, 5998–6009.
30 K. Rurack, M. Kollmannsberger and J. Daub, *Angew. Chem., Int. Ed.*, 2001, **40**, 385–387.
31 M. Baruah, W. Qin, N. Basarić, W. M. De Borggraeve and N. Boens, *J. Org. Chem.*, 2005, **70**, 4152–4157.
32 M. Baruah, W. Qin, R. A. L. Vallée, D. Beljonne, T. Rohand, W. Dehaen and N. Boens, *Org. Lett.*, 2005, **7**, 4377–4380.
33 T. Rohand, M. Baruah, W. Qin, N. Boens and W. Dehaen, *Chem. Commun.*, 2006, 266–268.
34 E. Fron, E. Coutiño-Gonzalez, L. Pandey, M. Sliwa, M. Van der Auweraer, F. C. De Schryver, J. Thomas, Z. Dong, V. Leen, M. Smet, W. Dehaen and T. Vosch, *New J. Chem.*, 2009, **33**, 1490–1496.
35 W. Qin, T. Rohand, M. Baruah, A. Stefan, M. Van der Auweraer, W. Dehaen and N. Boens, *Chem. Phys. Lett.*, 2006, **420**, 562–568.
36 T. Rohand, J. Lycoops, S. Smout, E. Braeken, M. Sliwa, M. Van der Auweraer, W. Dehaen, W. M. De Borggraeve and N. Boens, *Photochem. Photobiol. Sci.*, 2007, **6**, 1061–1066.
37 W. Qin, T. Rohand, W. Dehaen, J. N. Clifford, K. Driessen, D. Beljonne, B. Van Averbeke, M. Van der Auweraer and N. Boens, *J. Phys. Chem. A*, 2007, **111**, 8588–8597.
38 W. Qin, V. Leen, W. Dehaen, J. Cui, C. Xu, X. Tang, W. Liu, T. Rohand, D. Beljonne, B. Van Averbeke, J. Clifford, K. Driesen, K. Binnemans, M. Van der Auweraer and N. Boens, *J. Phys. Chem. C*, 2009, **113**, 11731–11740.
39 L. Li, B. Nguyen and K. Burgess, *Bioorg. Med. Chem. Lett.*, 2008, **18**, 3112–3116.
40 V. Leen, E. Braeken, K. Luckermans, C. Jackers, M. Van der Auweraer, N. Boens and W. Dehaen, *Chem. Commun.*, 2009, 4515–4517.

41 V. Leen, V. Zaragozí Gonzalvo, W. M. De Borggraeve, N. Boens and W. Dehaen, *Chem. Commun.*, 2010, **46**, 4908–4910.
42 T. Rohand, W. Qin, N. Boens and W. Dehaen, *Eur. J. Org. Chem.*, 2006, 4658–4663.
43 V. Leen, T. Leemans, N. Boens and W. Dehaen, *Eur. J. Org. Chem.*, 2011, DOI: 10.1002/ejoc.201100324, in press.
44 J. C. Forgie, P. J. Skabara, I. Stibor, F. Vilela and Z. Vobecka, *Chem. Mater.*, 2009, **21**, 1784–1786.
45 S. Yin, V. Leen, C. Jackers, M. Van der Auweraer, M. Smet, N. Boens and W. Dehaen, *Dyes Pigm.*, 2011, **88**, 372–377.
46 *Chemosensors of Ion and Molecule Recognition*, ed. J.-P. Desvergne and A. W. Czarnik, Kluwer, Dordrecht, The Netherlands, 1997.
47 A. P. de Silva, H. Q. N. Gunaratne, T. Gunnlaugsson, A. J. M. Huxley, C. P. McCoy, J. T. Rademacher and T. E. Rice, *Chem. Rev.*, 1997, **97**, 1515–1566.
48 B. Valeur, *Molecular Fluorescence. Principles and Applications*, Wiley-VCH, Weinheim, Germany, 2002.
49 S. E. Braslavsky, *Pure Appl. Chem.*, 2007, **79**, 293–465.
50 G. Grynkiewicz, M. Poenie and R. Y. Tsien, *J. Biol. Chem.*, 1985, **260**, 3440–3450.
51 Y. Urano, D. Asanuma, Y. Hama, Y. Koyama, T. Barrett, M. Kamiya, T. Nagano, T. Watanabe, A. Hasegawa, P. L. Choyke and H. Kobayashi, *Nat. Med. (N. Y.)*, 2009, **15**, 104–409.
52 J. R. Lakowicz, *Principles of Fluorescence Spectroscopy*, Springer, New York, 3rd edn, 2006.
53 R. A. Marcus, *Angew. Chem., Int. Ed. Engl.*, 1993, **32**, 1111–1121.
54 H. J. Kim and J. S. Kim, *Tetrahedron Lett.*, 2006, **47**, 7051–7055.
55 B. Tufan and E. U. Akkaya, *Org. Lett.*, 2002, **4**, 2857–2859.
56 J. Rosenthal and S. J. Lippard, *J. Am. Chem. Soc.*, 2010, **132**, 5536–5537.
57 T. Matsumoto, Y. Urano, T. Shoda, H. Kojima and T. Nagano, *Org. Lett.*, 2007, **9**, 3375–3377.
58 X. Li, S. Qian, Q. He, B. Yang, J. Li and Y. Hu, *Org. Biomol. Chem.*, 2010, **8**, 3627–3620.
59 J. Lu, C. Sun, W. Chen, H. Ma, W. Shi and X. Li, *Talanta*, 2011, **83**, 1050–1056.
60 J. Shao, H. Guo, S. Ji and J. Zhao, *Biosens. Bioelectron.*, 2011, **26**, 3012–3017.
61 T. Förster, *Ann. Phys. (Leipzig)*, 1948, **437**, 55–75.
62 A. Kowalczyk, N. Boens, V. Van den Bergh and F. C. De Schryver, *J. Phys. Chem.*, 1994, **98**, 8585–8590.
63 E. Cielen, A. Tahri, K. Ver Heyen, G. J. Hoornaert, F. C. De Schryver and N. Boens, *J. Chem. Soc., Perkin Trans. 2*, 1998, 1573–1580.
64 P. Job, *Ann. Chim.*, 1928, **9**, 113–134.
65 A. Kowalczyk, N. Boens, K. Meuwis and M. Ameloot, *Anal. Biochem.*, 1997, **245**, 28–37.
66 K. A. Connors, *Binding Constants. The Measurement of Molecular Complex Stability*, J. Wiley & Sons, New York, 1987.
67 H. A. Benesi and J. H. Hildebrand, *J. Am. Chem. Soc.*, 1949, **71**, 2703–2707.
68 E. Cielen, A. Stobiecka, A. Tahri, G. J. Hoornaert, F. C. De Schryver, J. Gallay, M. Vincent and N. Boens, *J. Chem. Soc., Perkin Trans. 2*, 2002, 1197–1206.
69 W. Qin, M. Baruah, W. M. De Borggraeve and N. Boens, *J. Photochem. Photobiol., A*, 2006, **183**, 190–197.
70 J. Han and K. Burgess, *Chem. Rev.*, 2010, **110**, 2709–2728.
71 T. Werner, C. Huber, S. Heinl, M. Kollmannsberger, J. Daub and O. S. Wolfbeis, *Fresenius' J. Anal. Chem.*, 1997, **359**, 150–154.
72 M. Kollmannsberger, T. Gareis, S. Heinl, J. Breu and J. Daub, *Angew. Chem., Int. Ed. Engl.*, 1997, **36**, 1333–1335.
73 R. Ziessel, G. Ulrich, A. Harriman, M. A. H. Alimary, B. Stewart and P. Retailleau, *Chem.–Eur. J.*, 2009, **15**, 1359–1369.
74 D. D. Perin, *Dissociation Constants of Organic Bases in Aqueous Solutions*, Butterworth, London, 1972.
75 E. P. Serjeant and B. Dempsey, *Ionisation Constants of Organic Acids in Aqueous Solution*, Pergamon Press, New York, 1979.
76 N. Isaacs, *Physical Organic Chemistry*, Longman Scientific & Technical, Harlow, England, 2nd edn, 1995.
77 T. Gareis, C. Huber, O. S. Wolbeis and J. Daub, *Chem. Commun.*, 1997, 1717–1718.
78 C. N. Baki and E. U. Akkaya, *J. Org. Chem.*, 2001, **66**, 1512–1513.
79 W. Qin, M. Baruah, A. Stefan, M. Van der Auweraer and N. Boens, *ChemPhysChem*, 2005, **6**, 2343–2351.
80 L. M. Sayre, G. Perry and M. A. Smith, *Curr. Opin. Chem. Biol.*, 1999, **3**, 220–225.
81 P. Jiang and Z. Guo, *Coord. Chem. Rev.*, 2004, **248**, 205–229.
82 K. Kikuchi, K. Komatsu and T. Nagano, *Curr. Opin. Chem. Biol.*, 2004, **8**, 182–191.
83 N. C. Lim, H. C. Freake and C. Brückner, *Chem.–Eur. J.*, 2005, **11**, 38–49.
84 P. Carol, S. Sreejith and A. Ajayaghosh, *Chem.–Asian J.*, 2007, **2**, 338–348.
85 Z. Xu, J. Yoon and D. R. Spring, *Chem. Soc. Rev.*, 2010, **39**, 1996–2006.
86 E. M. Nolan and S. J. Lippard, *Chem. Rev.*, 2008, **108**, 3443–3480.
87 E. L. Que, D. W. Domaille and C. J. Chang, *Chem. Rev.*, 2008, **108**, 1517–1549.
88 I. Móczár, O. Huszthy, Z. Maidics, M. Kádár and K. Tóth, *Tetrahedron*, 2009, **65**, 8250–8258.
89 J.-P. Malval, I. Leary and B. Valeur, *New J. Chem.*, 2005, **29**, 1089–1094.
90 W. Namkung, P. Padmawar, A. D. Mills and A. S. Verkman, *J. Am. Chem. Soc.*, 2008, **130**, 7794–7795.
91 W. Namkung, Y. Song, A. D. Mills, P. Padmawar, W. E. Finkbeiner and A. S. Verkman, *J. Biol. Chem.*, 2009, **284**, 15916–15926.
92 K. Yamada, Y. Nomura, D. Citterio, N. Iwasawa and K. Suzuki, *J. Am. Chem. Soc.*, 2005, **127**, 6956–6957.
93 V. V. Martin, A. Rothe and K. R. Gee, *Bioorg. Med. Chem. Lett.*, 2005, **15**, 1851–1855.
94 M. Kollmansberger, K. Rurack, U. Resch-Genger, W. Rettig and J. Daub, *Chem. Phys. Lett.*, 2000, **329**, 363–369.
95 K. Rurack, M. Sczepan, M. Spieles, U. Resch-Genger and W. Rettig, *Chem. Phys. Lett.*, 2000, **320**, 87–94.
96 M. Kollmannsberger, K. Rurack, U. Resch-Ginger and J. Daub, *J. Phys. Chem. A*, 1998, **102**, 10211–10220.
97 W. Qin, M. Baruah, M. Sliwa, M. Van der Auweraer, W. M. De Borggraeve, D. Beljonne, B. Van Averbeke and N. Boens, *J. Phys. Chem. A*, 2008, **112**, 6104–6114.
98 N. Basarić, M. Baruah, W. Qin, B. Metten, M. Smet, W. Dehaen and N. Boens, *Org. Biomol. Chem.*, 2005, **3**, 2755–2761.
99 N. R. Cha, S. Y. Moon and S.-K. Chang, *Tetrahedron Lett.*, 2003, **44**, 8265–8268.
100 K. R. Gee, A. Rukavishnikov and A. Rothe, *Comb. Chem. High Throughput Screening*, 2003, **6**, 363–366.
101 M. Kamiya and K. Johnsson, *Anal. Chem.*, 2010, **82**, 6472–6479.
102 J. D. Blakemore, R. Chitta and F. D'Souza, *Tetrahedron Lett.*, 2007, **48**, 1977–1982.
103 T. Kálai and K. Hideg, *Tetrahedron*, 2006, **62**, 10352–10360.
104 S. C. Dodani, Q. He and C. J. Chang, *J. Am. Chem. Soc.*, 2009, **131**, 18020–18021.
105 A. Coskun and E. U. Akkaya, *J. Am. Chem. Soc.*, 2005, **127**, 10464–10465.
106 L. Zeng, E. W. Miller, A. Pralle, E. Y. Isacoff and C. J. Chang, *J. Am. Chem. Soc.*, 2006, **128**, 10–11.
107 D. W. Domaille, L. Zeng and C. J. Chang, *J. Am. Chem. Soc.*, 2010, **132**, 1194–1195.
108 L. Jiao, J. Li, S. Zhang, C. Wei, E. Hao and M. G. H. Vicente, *New J. Chem.*, 2009, **33**, 1888–1893.
109 X. Qi, E. J. Jun, L. Xu, S.-J. Kim, J. S. J. Hong, Y. J. Yoon and J. Yoon, *J. Org. Chem.*, 2006, **71**, 2881–2884.
110 H. W. Mbatia, D. P. Kennedy, C. E. Camire, C. D. Incarvito and S. C. Burdette, *Eur. J. Inorg. Chem.*, 2010, 5069–5078.
111 Y. Mei, P. A. Bentley and W. Wang, *Tetrahedron Lett.*, 2006, **47**, 2447–2449.
112 S. Y. Moon, N. R. Cha, Y. H. Kim and S.-K. Chang, *J. Org. Chem.*, 2004, **69**, 181–183.
113 V. Csokai, M. Kádar, D. L. H. Mai, O. Varga, K. Tóth, M. Kubinyi, A. Grün and I. Bitter, *Tetrahedron*, 2008, **64**, 1058–1063.
114 S. Yin, V. Leen, S. Van Snick, N. Boens and W. Dehaen, *Chem. Commun.*, 2010, **46**, 6329–6331.
115 H. Y. Lee, H. Son, J. L. Lim, J. Oh, D. Kang, W. S. Han and J. H. Jung, *Analyst*, 2010, **135**, 2022–2027.
116 H. Y. Lee, D. R. Bae, J. C. Park, H. Song, W. S. Han and J. H. Jung, *Angew. Chem., Int. Ed.*, 2009, **48**, 1239–1243.
117 H. Son, H. Y. Lee, J. L. Lim, D. Kang, W. S. Han, S. S. Lee and J. H. Jung, *Chem.–Eur. J.*, 2010, **16**, 11549–11553.

118 X. Peng, J. Du, J. Fan, J. Wang, Y. Wu, J. Zhao, S. Sun and T. Xu, *J. Am. Chem. Soc.*, 2007, **129**, 1500–1501.
119 T. Cheng, Y. Xu, S. Zhang, W. Zhu, X. Qian and L. Duan, *J. Am. Chem. Soc.*, 2008, **130**, 16160–16161.
120 A. Coskun and E. U. Akkaya, *J. Am. Chem. Soc.*, 2006, **128**, 14474–14475.
121 M. Yuan, Y. Li, J. Li, C. Li, X. Liu, J. Lv, J. Xu, H. Liu, S. Wang and D. Zhu, *Org. Lett.*, 2007, **9**, 2313–2316.
122 A. Coskun, E. Deniz and E. U. Akkaya, *Tetrahedron Lett.*, 2007, **48**, 5359–5361.
123 A. Filarowski, M. Kluba, K. Cieślik-Boczula, A. Koll, A. Kochel, L. Pandey, W. M. De Borggraeve, M. Van der Auweraer, J. Catalán and N. Boens, *Photochem. Photobiol. Sci.*, 2010, **9**, 996–1008.
124 H. Lu, Z. Xue, J. Mack, Z. Shen, X. You and N. Kobayashi, *Chem. Commun.*, 2010, **46**, 3565–3567.
125 S. H. Choi, K. Pang, K. Kim and D. G. Churchill, *Inorg. Chem.*, 2007, **46**, 10564–10577.
126 S. H. Choi, K. Kim, J. Jeon, B. Meka, D. Bucella, K. Pang, S. Khatua, J. Lee and D. G. Churchill, *Inorg. Chem.*, 2008, **47**, 11071–11083.
127 S. Atilgan, T. Ozdemir and E. U. Akkaya, *Org. Lett.*, 2008, **10**, 4065–4067.
128 Y. Wu, X. Peng, B. Guo, J. Fan, Z. Zhang, J. Wang, A. Cui and Y. Gao, *Org. Biomol. Chem.*, 2005, **3**, 1387–1392.
129 H. Koutaka, J.-i. Kosuge, N. Fukasaku, T. Hirano, K. Kikuchi, Y. Urano, H. Kojima and T. Nagano, *Chem. Pharm. Bull.*, 2004, **52**, 700–703.
130 C. Goze, G. Ulrich, L. Charbonnière, M. Cesario, T. Prangé and R. Ziessel, *Chem.–Eur. J.*, 2003, **9**, 3748–3755.
131 K. Rurack, M. Kollmannsberger, U. Resch-Genger and J. Daub, *J. Am. Chem. Soc.*, 2000, **122**, 968–969.
132 S. Atilgan, I. Kutuk and T. Ozdemir, *Tetrahedron Lett.*, 2010, **51**, 892–894.
133 S. Atilgan, T. Ozdemir and E. U. Akkaya, *Org. Lett.*, 2010, **12**, 4792–4795.
134 A. Coskun, M. D. Yilmaz and E. U. Akkaya, *Org. Lett.*, 2007, **9**, 607–609.
135 J. Du, J. Fan, X. Peng, H. Li, J. Wang and S. Sun, *J. Fluoresc.*, 2008, **18**, 919–924.
136 J. Fan, K. Guo, X. Peng, J. Du, J. Wang, S. Sun and H. Li, *Sens. Actuators, B*, 2009, **142**, 191–196.
137 H. Lu, L. Xiong, H. Liu, M. Yu, Z. Shen, F. Li and X. You, *Org. Biomol. Chem.*, 2009, **7**, 2554–2558.
138 H. Lu, S. Zhang, H. Liu, Y. Wang, Z. Shen, C. Liu and X. You, *J. Phys. Chem. A*, 2009, **113**, 14081–14086.
139 J. Wang and X. Qian, *Org. Lett.*, 2006, **8**, 3721–3724.
140 X. Zhang, Y. Xiao and X. Qian, *Angew. Chem., Int. Ed.*, 2008, **47**, 8025–8029.
141 H. J. Kim, S. H. Kim, J. H. Kim, E.-H. Lee, K.-W. Kim and J. S. Kim, *Bull. Korean Chem. Soc.*, 2008, **29**, 1831–1834.
142 J. L. Bricks, A. Kovalchuk, C. Trieflinger, M. Nofz, M. Büschel, A. I. Tolmachev, J. Daub and K. Rurack, *J. Am. Chem. Soc.*, 2005, **127**, 13522–13529.
143 D. P. Kennedy, C. M. Kormos and S. C. Burdette, *J. Am. Chem. Soc.*, 2009, **131**, 8578–8586.
144 D. Wang, Y. Shiraishi and T. Hirai, *Tetrahedron Lett.*, 2010, **51**, 2545–2549.
145 A. Coskun and E. U. Akkaya, *Tetrahedron Lett.*, 2004, **45**, 4947–4949.
146 T. W. Hudnall and F. Gabbaï, *Chem. Commun.*, 2008, 4596–4597.
147 Y. Shiraishi, H. Maehara, T. Sugii, D. Wang and T. Hirai, *Tetrahedron Lett.*, 2009, **50**, 4293–4296.
148 M. R. Rao, S. M. Mobin and M. Ravikanth, *Tetrahedron*, 2010, **66**, 1728–1734.
149 P. G. M. Wuts and T. W. Greene, *Protective Groups in Organic Synthesis*, Wiley Interscience, Hoboken, NJ, 4th edn, 2007.
150 A. Orsini, A. Vitérisi, A. Bodlenner, J.-M. Weibel and P. Pale, *Tetrahedron Lett.*, 2005, **46**, 2259–2262.
151 O. A. Bozdemir, F. Sozmen, O. Buyukcakir, R. Guliyev, Y. Cakmak and E. U. Akkaya, *Org. Lett.*, 2010, **12**, 1400–1403.
152 Z. Ekmekci, M. D. Yilmaz and E. U. Akkaya, *Org. Lett.*, 2008, **10**, 461–464.
153 R. Guliyev, O. Buyukcakir, F. Sozmen and O. A. Bozdemir, *Tetrahedron Lett.*, 2009, **50**, 5139–5141.
154 A. Coskun, B. T. Baytekin and E. U. Akkaya, *Tetrahedron Lett.*, 2003, **44**, 5649–5651.
155 R. E. Gawley, H. Mao, M. M. Haque, J. B. Thorne and J. S. Pharr, *J. Org. Chem.*, 2007, **72**, 2187–2191.
156 A. K. Parhi, M.-P. Kung, K. Ploessl and H. F. Kung, *Tetrahedron Lett.*, 2008, **49**, 3395–3399.
157 N. W. Smith, A. Alonso, C. M. Brown and S. V. Dzyuba, *Biochem. Biophys. Res. Commun.*, 2010, **391**, 1455–1458.
158 M. Ono, M. Ishikawa, H. Kimura, S. Hayashi, K. Matsumura, H. Watanabe, Y. Shimizu, Y. Cheng, M. Cui, H. Kawashima and H. Saji, *Bioorg. Med. Chem. Lett.*, 2010, **20**, 3885–3888.
159 A. Ojida, T. Sakamoto, M.-a. Inoue, S.-h. Fujishima, G. Lippens and I. Hamachi, *J. Am. Chem. Soc.*, 2009, **131**, 6543–6548.
160 S. K. V. Vernekar, H. Y. Hallaq, G. Clarkson, A. J. Thompson, L. Silvestri, S. C. R. Lummis and M. Lochner, *J. Med. Chem.*, 2010, **53**, 2324–2328.
161 J.-S. Lee, N.-y. Kang, Y. K. Kim, A. Samanta, S. Feng, H. K. Kom, M. Vendrell, J. H. Park and Y.-T. Chang, *J. Am. Chem. Soc.*, 2009, **131**, 10077–10082.
162 X. Yang, Y. Cheng, S. Jin and B. Wang, in *Artificial Receptors for Chemical Sensors*, ed. V. Mirsky and A. Yatsimirsky, Wiley-VCH, Weinheim, Germany, 2011 and references therein.
163 N. DiCesare and J. R. Lakowicz, *Tetrahedron Lett.*, 2001, **42**, 9105–9108.
164 Z.-N. Sun, H.-L. Wang, F.-Q. Liu, Y. Chen, P. K. H. Tam and D. Yang, *Org. Lett.*, 2009, **11**, 1887–18890.
165 T. Ueno, Y. Urano, H. Kojima and T. Nagano, *J. Am. Chem. Soc.*, 2006, **128**, 10640–10641.
166 K. Teranishi, *Bioorg. Chem.*, 2007, **35**, 82–111.
167 M. Sekiya, K. Umezawa, A. Sato, D. Citterio and K. Suzuki, *Chem. Commun.*, 2009, 3047–3049.
168 R. Saito, A. Ohno and E. Ito, *Tetrahedron*, 2010, **66**, 583–590.
169 Z.-N. Sun, F.-Q. Liu, Y. Chen, P. K. H. Tam and D. Yang, *Org. Lett.*, 2008, **10**, 2171–2174.
170 P. Oleynik, Y. Ishihara and G. Cosa, *J. Am. Chem. Soc.*, 2007, **129**, 1842–1843.
171 A. Khatchadourian, K. Krumova, S. Boridy, A. T. Ngo, D. Maysinger and G. Cosa, *Biochemistry*, 2009, **48**, 5658–5668.
172 M. Li, H. Wang, X. Zhang and H.-S. Zhang, *Spectrochim. Acta, Part A*, 2004, **60**, 987–993.
173 R. M. J. Palmer, A. G. Ferrige and S. Moncada, *Nature*, 1987, **327**, 524–526.
174 J. Garthwaite, S. L. Charles and R. Chess-Williams, *Nature*, 1988, **336**, 385–388.
175 M. A. Marletta, P. S. Yoon, R. Iyengar, C. D. Leaf and J. S. Wishnok, *Biochemistry*, 1988, **27**, 8706–8711.
176 D. J. Stuehr, *Annu. Rev. Pharmacol. Toxicol.*, 1997, **37**, 339–359.
177 M. A. Marletta, A. R. Hurshman and K. M. Rusche, *Curr. Opin. Chem. Biol.*, 1998, **2**, 656–663.
178 E. W. Miller and C. J. Chang, *Curr. Opin. Chem. Biol.*, 2007, **11**, 620–625.
179 M. H. Lim, D. Xu and S. J. Lippard, *Nat. Chem. Biol.*, 2006, **2**, 375–380.
180 X. Zhang, H. Wang, J.-S. Li and H.-S. Zhang, *Anal. Chim. Acta*, 2003, **481**, 101–108.
181 Y. Gabe, Y. Urano, K. Kikuchi, H. Kojima and T. Nagano, *J. Am. Chem. Soc.*, 2004, **126**, 3357–3357.
182 J.-S. Li, H. Wang, X. Zhang and H.-S. Zhang, *Talanta*, 2003, **61**, 797–802.
183 K.-J. Huang, H. Wang, Y.-H. Guo, R.-L. Fan and H.-S. Zhang, *Talanta*, 2006, **69**, 73–78.
184 Y. Gabe, T. Ueno, Y. Urano, H. Kojima and T. Nagano, *Anal. Bioanal. Chem.*, 2006, **386**, 621–656.
185 X. Zhang, R. Chi, J. Zou and H.-S. Zhang, *Spectrochim. Acta, Part A*, 2004, **60**, 3129–3134.
186 A. C. Benniston, G. Copley, K. J. Elliott, R. W. Harrington and W. Clegg, *Eur. J. Org. Chem.*, 2008, 2705–2713.
187 Y. Yamada, Y. Tomiyama, A. Morita, M. Ikekita and S. Aoki, *ChemBioChem*, 2008, **9**, 853–856.
188 T. Ueno, Y. Urano, H. Kojima and T. Nagano, *J. Am. Chem. Soc.*, 2006, **128**, 10640–10641.
189 T. Komatsu, Y. Urano, Y. Fujikawa, T. Kobayashi, H. Kojima, T. Terai, K. Hanaoka and T. Nagano, *Chem. Commun.*, 2009, 7015–7017.

190 A. Nierth, A. Yu. Kobitski, G. U. Nienhaus and A. Jäschke, *J. Am. Chem. Soc.*, 2010, **132**, 2646–2654.
191 D. M. Jameson and J. A. Ross, *Chem. Rev.*, 2010, **110**, 2685–2708.
192 B. L. Sprague and J. G. McNally, *Trends Cell Biol.*, 2005, **15**, 84–91.
193 M. Kang, C. A. Day, K. Drake, A. K. Kenworthy and E. DiBenedetto, *Biophys. J.*, 2009, **97**, 1501–1511.
194 H. L. Kee, C. Kirmaier, L. Yu, P. Thamyongkit, W. J. Youngblood, M. E. Calder, L. Ramos, B. C. Noll, D. F. Bocian, W. R. Scheidt, R. R. Birge, J. S. Lindsey and D. Holten, *J. Phys. Chem. B*, 2005, **109**, 20433–20443.
195 M. K. Kuimova, G. Yahioglu, J. A. Levitt and K. Suhling, *J. Am. Chem. Soc.*, 2008, **130**, 6672–6673.
196 P. J. Verveer and Q. S. Hanley, *Laboratory Techniques in Biochemistry and Molecular Biology, FRET and FLIM Techniques*, ed. T. W. J. Gadella, Elsevier, 2009, vol. 33, pp. 59–94.
197 H. C. Gerritsen, A. V. Agronskaia, A. N. Bader and A. Esposito, *Laboratory Techniques in Biochemistry and Molecular Biology, FRET and FLIM Techniques*, ed. T. W. J. Gadella, Elsevier, 2009, vol. 33, pp. 95–132.
198 M. A. H. Alamiry, A. C. Benniston, G. Copley, K. J. Elliott, A. Harriman, B. Stewart and Y.-G. Zhi, *Chem. Mater.*, 2008, **20**, 4024–4032.
199 X. Yin, Y. Li, Y. Zhu, X. Jing, Y. Li and D. Zhu, *Dalton Trans.*, 2010, **39**, 9929–9935.
200 G. Ulrich, S. Goeb, A. De Nicola, P. Retailleau and R. Ziessel, *Synlett*, 2007, 1517–1520.
201 R. Ziessel, G. Ulrich and A. Harriman, *New J. Chem.*, 2007, **31**, 496–501.
202 *Artificial Receptors for Chemical Sensors*, ed. V. Mirsky and A. Yatsimirsky, Wiley-VCH, Weinheim, Germany, 2011.
203 R. D. Carpenter and A. S. Verkman, *Org. Lett.*, 2010, **12**, 1160–1163.
204 K. Umezawa, Y. Nakamura, H. Makino, D. Citterio and K. Suzuki, *J. Am. Chem. Soc.*, 2008, **130**, 1550–1551.
205 K. Umezawa, A. Matsui, Y. Nakamura, D. Citterio and K. Suzuki, *Chem.–Eur. J.*, 2009, **15**, 1096–1106.
206 O. Buyukcakir, O. A. Bozdemir, S. Kolemen, S. Erbas and E. U. Akkaya, *Org. Lett.*, 2009, **11**, 4644–4647.

